Refrigerated Warehouse Operation under Real-time Pricing

by

Ronald Stoeckle

A thesis submitted in partial fulfillment
of the requirements for the degree of

Master of Science

(Mechanical Engineering)

at the
University of Wisconsin-Madison
2001

Abstract

Refrigerated warehouses play an essential role in the food delivery chain. The construction and operation of refrigerated storage is growing. Because of the relatively high energy intensity associated with the operation cold storage warehouses, controlling energy consumption and the cost of energy is often an important operational concern. Under standard electricity rates, refrigerated warehouses are usually operated continuously to keep the products in storage at a constant temperature.

Deregulation of the electricity markets over the past years has lead to new electricity pricing approaches, one of which is called real-time pricing (RTP). Under real-time pricing, the electricity price varies hourly. The hourly changing electricity price offers the possibility of cost savings for the customer if demand can be reduced during hours of high prices and shifted to hours of lower prices.

This study investigates the possibility to utilize product stored in a refrigerated warehouse as a thermal energy storage media to minimize energy costs under real-time pricing rate structures. Demand shifting, i.e. precooling the warehouse during hours of low electricity prices to a lower temperature and shutting down the refrigeration equipment during high price hours, can yield operating cost savings. The increase in product temperature during equipment shutdown limits the possible floating duration.

A computer model of a representative refrigerated warehouse was developed. The model includes the building envelope, the refrigeration systems and a model of the stored product. A thermally massive and a lightweight wall construction were investigated.

From the results of the simulation runs, a method was developed that allows determining if demand shifting on the next day is likely to offer operating cost savings. The method includes forecasting the allowable floating duration based on the outside air temperatures for the next day and deciding on the best shutdown period. A simple criterion based on a price ratio was found to be a good indicator if demand shifting offers savings.

The simulation results indicate that operating cost savings through demand shifting are relatively small compared to the yearly operating cost. Installation of additional refrigeration capacity results in projected savings of about 7-11 % of the yearly electricity cost. Considerably increased energy demand during the precooling period is the reason for the small projected savings. Only high real-time peak prices can compensate for the cost penalty paid during precooling.

Acknowledgements

I would like to thank my two advisers, Douglas Reindl and John Mitchell, for all their support throughout this project. Without their guidance, I would never have accomplished this project in the given time. Douglas Reindl especially impressed me how he could find the time to answer my questions in-depth all his other obligations given. John Mitchell always surprised me with his good ideas in situations when I was not expecting any good idea at all. From both of them I learned what commitment for a project means.

I also would like to thank David Bradley for supporting me with TRNSYS and Sandy Klein for supporting me with EES. It is a privilege of the Solar Energy Lab to have the programmers of the computer programs I was using right next door.

This project was supported in part by ASHRAE under research project RP-1154 and I would like to thank ASHRAE for their support.

Part of the funding for my stay in the US was provided by the German Academic Exchange service (DAAD). I would like to thank the DAAD and the program coordinators at the University of the Stuttgart, Prof. Heisel, Mrs. Peyk-Stenzel and Dr. Michaelis for having given me the opportunity to study abroad. The 16 months I spent in Madison were such a rewarding experience for me that I will never want to miss it. I did not only learn very much about engineering, but I learned even more about myself, my views and my own cultural background. It will take more time for me to realize what I have all learned, experienced, done and seen during my time in Madison and the US.

I am very grateful to my parents who supported me throughout my stay. They were probably thinking more of me while I was abroad than I was thinking of myself.

Last but not least I want to thank all the friends I made in Madison and who became a part of my life in Madison.

We, and those who share our attitude, will hope to make new discoveries; and we shall hope to be helped in this by a newly erected scientific system. Thus we shall take the greatest interest in the falsifying experiment. We shall hail it as a success, for it has opened up new vistas into a world of new experiences. And we shall hail it even if these new experiences should furnish us with new arguments against our own most recent theories.

Karl R. Popper,
The Logic Of Scientific Discovery

Table of Contents

List of Figures

List of Tables

Chapter 1 Introduction

1.1 Background

Refrigeration plays an important role in many applications throughout the world. These range from heat removal in many industrial process applications, space conditioning to preservation and storage in the food sector. Refrigerated warehouses play an essential role in the food delivery chain. For example, demand for produce is high throughout the year, while the supply is only seasonal. In many cases, producer and consumer locations are far apart. Storage in refrigerated warehouses balances supply and demand over the year.

Modern food distribution chains would not be possible without refrigerated storage. Food preservation issues require certain products to be kept at or below a critical temperature throughout the distribution and sales process and refrigerated storage makes this distribution chain possible.

The construction and operation of refrigerated storage is growing. From 1997 to 1999, refrigerated storage capacity increased by 6% to 82 million m^3 (2.9 billion ft^3) (USDA, 2000). Most refrigerated storage capacity is located in states where agriculture plays an important role. California leads the nation in cold storage warehouse capacity, followed by Florida, Washington, and Wisconsin.

Because of the relatively high energy intensity associated with the operation of refrigeration systems connected with cold storage warehouses, controlling energy consumption and the cost of energy is often an important operational concern. An uncontrolled element in the energy costs for a cold storage warehouse is the electric rates. In the past, electricity prices represented the average production cost plus guaranteed revenues for the utility. In reality, production cost of electricity varies greatly depending on the time of the day, the day of the week and the time of the year. The average price had to cover the average cost.

Deregulation of the electricity markets over the past years has lead to new electricity pricing approaches, one of which is called real-time pricing (RTP). Under real-time pricing, the electricity price varies hourly, depending on the projected electricity production cost made by the utility the day before. The customer is usually notified of the next day prices on the day before. Because electricity production or market cost can vary greatly, real-time prices vary also greatly. The hourly changing electricity price offers the possibility of cost savings for the customer if demand can be reduced during hours of high prices and shifted to hours of lower prices.

The variable nature of electricity prices under RTP rate structures has created a need to evaluate this rate structure in the context of cold storage warehouse operations. Under standard electricity rates, refrigerated warehouses are usually operated on an "as needed" basis. The refrigeration system is operated continuously to keep the products in storage at a constant temperature. The advent of real-time pricing has created the possibility that alternative operating strategies can take advantage of "soft-spots" in the daily price profiles, thereby, allowing warehouse operators to minimize energy costs.

1.2 Research Objective

The primary objective of the research is to develop and evaluate appropriate refrigeration system control strategies that utilize stored products as a thermal energy storage media to minimize energy costs for refrigerated warehouses operating under real-time pricing rate structures.

In order to develop operation strategies under real-time pricing, the nature, variability and temporal character of real-time pricing structures needs to be understood. Three different real-time price rate structures from three different utilities in the US were included in the present analysis. A comparative analysis of the three price profiles was conducted and the results are presented in the study.

As part of the present research project, a computer model of a representative refrigerated warehouse was developed. The model includes the following major refrigerated

warehouse components: the building envelope (walls, roof, heated floor, and conditioned dock) and the required refrigeration systems to serve the freezer and dock. Because the cooling load also depends on the thermal coupling to the stored product, a product computer model was included in the analysis and subsequent simulations.

The computer models of the stored product, warehouse envelope and refrigeration systems, combined with the real-time pricing structures serve as a basis for developing and assessing alternative operating scenarios to minimize energy costs while constraining the warehouse operation to protect stored products. An essential phase of the analysis is identifying critical variables and parameters for the warehouse and the pricing structures to allow simple but reliable operating strategies to be established. General recommendations derived from the simulations conclude the research.

1.3 Literature

Numerous literature can be found in the fields related to this study, but literature related to the specific aspect of refrigerated warehouse operation strategies is rather sparse. Mankse (1999) did a study on performance optimization of industrial refrigeration systems. He developed a detailed model of a vapor compression refrigeration system, including subcomponents. Modeling assumptions from Manske (1999) were used in this study. Jekel (2000) modeled infiltration into a loading dock of a large refrigerated warehouse. The focus there was on the comparison of a desiccant infiltration air dehumidification system compared to hot gas defrost which is normally used. Insight into infiltration load calculation was gained from this study. Cleland (1990) presents a general overview of the food refrigeration process. Requirements for correct modeling are presented and many references to certain aspects in food refrigeration are given. Altwies (1998) did a study on electrical demand reduction in refrigerated warehouses through demand shifting. A model of a refrigerated warehouse was developed, which also included a refrigerated product model to consider thermal storage in the refrigerated product. Food quality issues resulting from product temperature changes were part of the study. Altwies (1998) concluded that no negative impact on the product quality should result from using the product as thermal storage medium as long as the product

temperature does not exceed a critical value based on food quality. Altwies (1998) predicted potential savings of 53% through full demand shifting under a time-of-use electricity rate compared to normal operation.

The building structure was modeled using the transfer-function method. The transfer-function method for heat transfer calculations was developed by Stephenson and Mitalas (1967) and Mitalas and Stephenson (1967). Pawelski (1976) used this method to calculate heat transfer through building walls and compared the results to finite-difference solutions. He concluded that both methods lead to similar results. Sanz (1986) used a transfer-function to calculate heat flow into and out of a model refrigerated product and verified the results experimentally. Good agreement was reported. On the other hand, the model product he used was very small compared to the dimensions of a block of frozen product in a refrigerated warehouse. Seem (1987) developed another transfer-function approach based on the state space representation of a heat transfer problem. Braun (2000) employed this method in a simulation of a large office building to evaluate demand-shifting strategies for the air conditioning system using the building thermal mass as storage medium. Depending on the electricity rate structure and the demand shifting strategy implemented, Braun (2000) projects potential savings of up to 40% in operation cost compared to a reference case.

Literature related to real-time pricing is frequent and in most cases related to building air conditioning. Gabel (1998) describes the installation of a controller for the energy management system of a large New York hotel in response to real-time pricing. Overall, the hotel energy demand could be reduced significantly and the operating cost under a real-time pricing structure could be decreased even more. Henze (1997) developed a predictive optimal controller for thermal energy storage systems, which is based on dynamic programming. The controller offered significant performance benefits over a conventional controller under complex rate structures. EPRI (1995) presented a general survey of real-time pricing programs from US utilities. Characteristics of real-time pricing structures from different utilities are discussed and compared. EPRI (1995) states

that the implementation of real-time pricing rate structures offers large potential benefits for electric utilities and their customers.

1.4 Thesis Organization

The thesis is basically organized in 5 chapters. The introductory Chapter 1 gives a brief background on the topic of the study and identifies research objectives. A short literature review is included. Chapter 2 describes the TRNSYS refrigerated warehouse model in detail. The component models are presented and different modeling options for the components are evaluated. The real-time pricing structures are analyzed and compared in Chapter 3. Chapter 4 shows the results from the simulation runs. Different options of demand shifting are compared and the impact on the yearly operation cost is estimated. From these results, a criterion is developed that indicates if demand shifting offers savings compared to constant warehouse operation. The criterion developed is then implemented into the simulation and the achieved savings compared to constant operation are presented. Chapter 5 summarizes the study and recommendations for refrigerated warehouse operation under real-time pricing are given. Future work recommendations conclude the study.

1.5 Software

During the process of research mainly two computer programs were used. TRNSYS (SEL 2000) is a transient system simulation program with a modular structure. The TRNSYS library includes many of the components commonly found in thermal energy systems, as well as component routines to handle input of weather data or other time-dependent forcing functions and output of simulation results. The users can create their own components and add them to the model to represent equipment other than the standard components. A refrigerated warehouse model was built based on standard components and components were added to incorporate own modeling ideas.

The basic function provided by EES (Engineering Equation Solver) is the numerical solution of a set of algebraic equations. EES allows equations to be entered in any order with unknown variables placed anywhere in the equations. Furthermore, EES provides many built-in mathematical and thermophysical property functions. EES was used

among other things to develop models of the refrigeration equipment and the refrigerated product. Besides, many of the plots presented in this study were created with EES.

Chapter 2 Model of Refrigerated Warehouse

In order to simulate the effects resulting from different operating strategies under real-time pricing, a model of a refrigerated warehouse was created in TRNSYS. This chapter describes the components of the warehouse considered in the model. First the components to model the warehouse structure itself are reviewed, then the warehouse equipment components are discussed. Also a detailed model of the product stored in the warehouse is presented. The end of this chapter gives an overview of the integrated warehouse envelope and the equipment.

2.1 Description of the Warehouse Facility

The distribution warehouse modeled in the simulation consists of two refrigerated spaces: A 9,204 m^2 (100,000 ft^2) freezer, in which the refrigerated product is stored, and a 1,841 m^2 (20,000 ft^2) loading dock to handle the incoming and outgoing product. Under normal operating conditions the freezer is maintained at –18 °C (0 °F) while the dock is maintained at 1 °C (34 °F). The freezer footprint is square with each sidewall having a length of 95.94 m (316.2 ft) and the freezer height is 9.6 m (31.5 ft). This leads to a freezer volume of 88,368 m^3 (3121,000 ft^3).

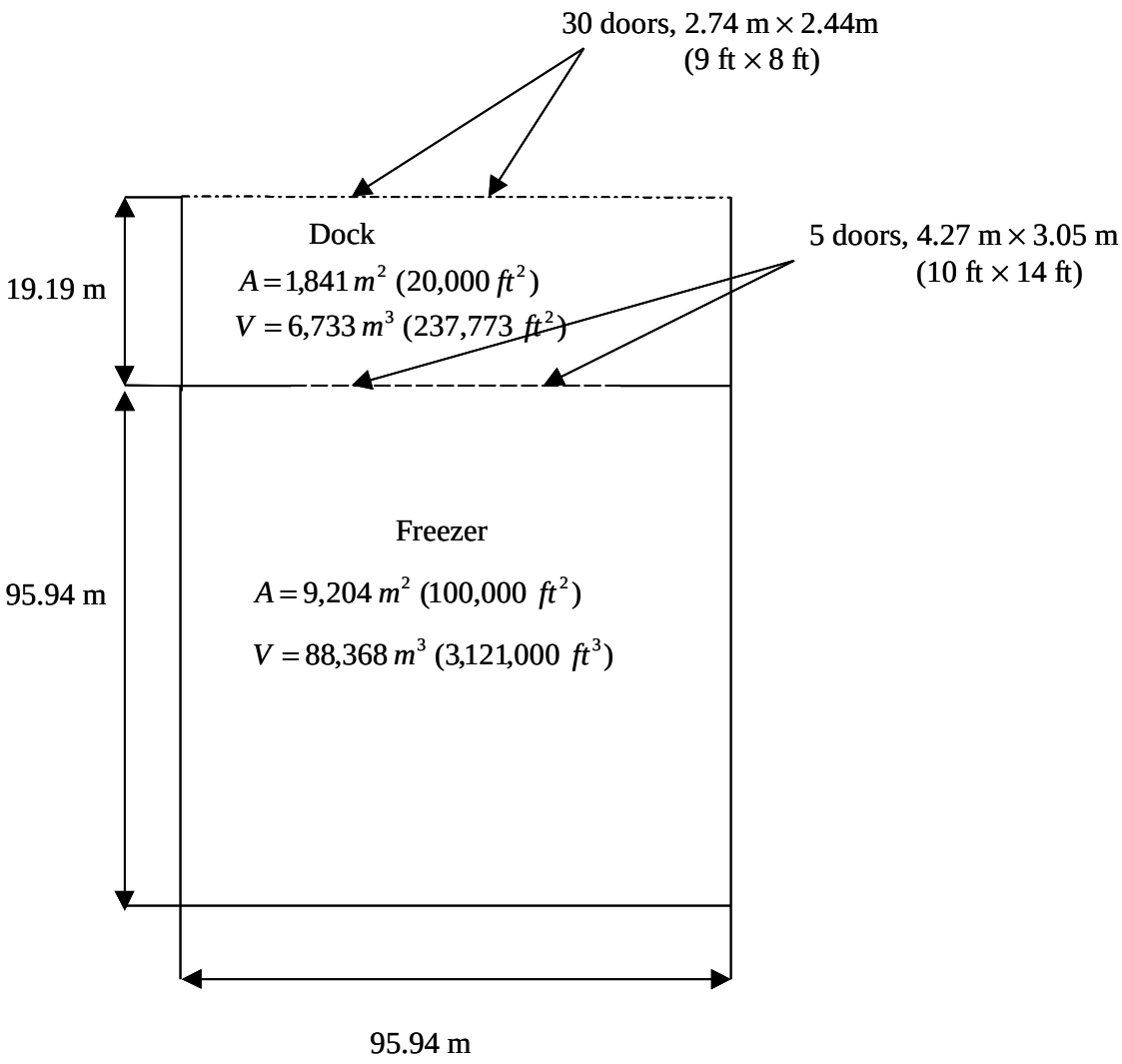

Figure 2-1: Plan view of warehouse layout.

Two different wall constructions were studied: A thermally massive wall and a thermally lighweight wall, both having the same U-value of 0.2612 W/m^2-C (0.046 BTU/hr-ft^2-F).

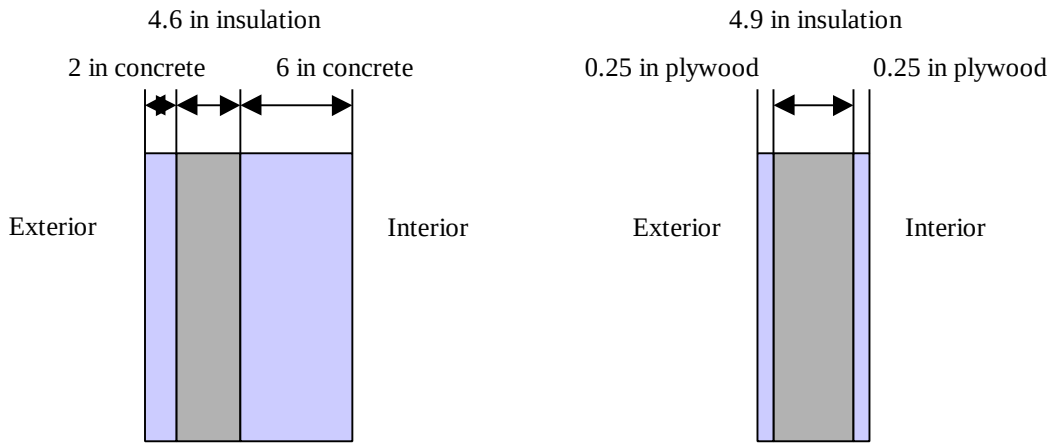

Figure 2-2: Massive and light wall construction modeled, U=0.26 W/m^2-C

The thermally massive wall is built of three layers, from outside to inside: 5.08 cm (2 in) of concrete, 11.77 cm (4.63 in) of insulation and 15.24 cm (6 in) of concrete. The thermally lightweight wall is built of 0.64 cm (0.25 in) of plywood, 12.42 cm (4.89 in) of insulation and 0.64 cm (0.25 in) of plywood. The freezer roof is assumed to have the same respective construction as the walls. The freezer is connected to dock by five doors, 4.27 m × 3.05 m (14 ft × 10 ft) each.

The dock adjoins the freezer to the north wall over the whole length. Therefore the long side of the dock is 95.94 m (316.22 ft), parallel to the freezer, and the short sides of the dock are 19.19 m (62.96 ft). The dock is 3.66 m (12 ft) high, which leads to a dock volume of 6,733 m^3 (237,773 ft^3). The dynamic nature of the dock walls is not modeled in detail but an overall U-Value of 0.54 W/m2-C (0.095 BTU/hr-ft^2-F) is assumed for the dock. This value corresponds to the recommendations from ASHRAE (1998) for minimum insulation for a dock (Jekel, 2000). The dock has thirty truck bays, 2.74 m × 2.44 m (9 ft × 8 ft) each, opening to the outdoor environment.

The analysis assumes that on average 43% of the freezer area is covered with product. The 43% inventory estimate is based on assuming a typical static pallet rack installation from Dellino (1997).

The warehouse is assumed to be a distribution type where product is constantly shipped from and received in the warehouse, i.e. the warehouse is operated 24 hours, 7 days a week. The entering product is assumed to arrive "at-temperature". There are no additional gains or losses to the conditioned space associated with thermal energy storage in the shipped and received product.

2.2 Warehouse components

2.2.1 Walls/ Roof

The freezer operation is not steady state as ambient conditions and conditions in the freezer change constantly. In order to account for the transient behavior, the heat transfer and energy storage in the walls and the roof has to be modeled. Two possible methods of modeling were investigated and are compared: a finite-difference model and a transfer-function model.

2.2.1.1 Finite-difference model

The finite-difference model divides the wall into nodes and the temporal heat transfer process is divided into discrete time steps. An energy balance is performed for every node to calculate the node temperatures and heat flows at every time step. Figure 2-3 shows the finite-difference model for one node.

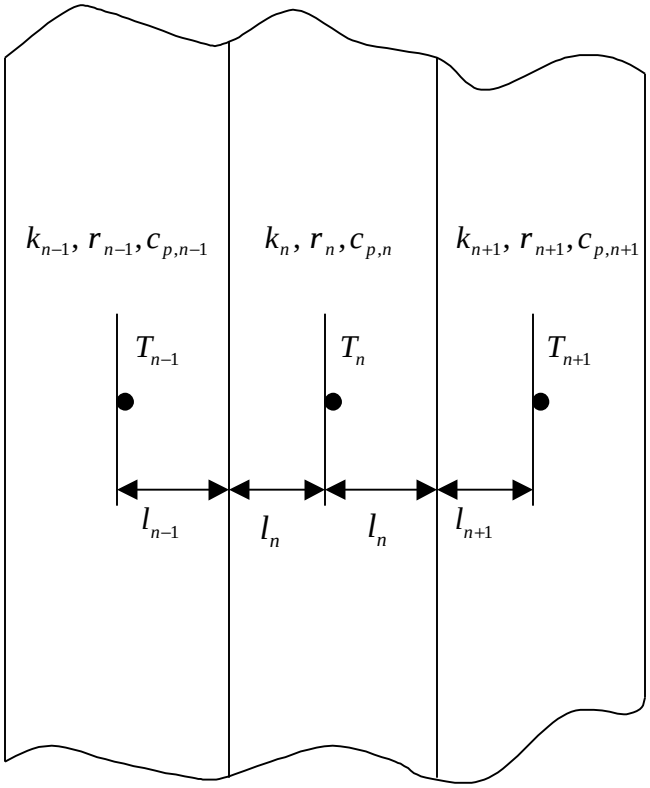

Figure 2-3: Finite-difference model.

The change in internal energy of node n per time step must equal the heat flows into node n from nodes n-1 and n+1. Equation (2-1) shows the energy balance for a node between two other interior nodes.

$$rc_p dxdy\frac{T_n^+ - T_n}{\Delta t} = \frac{T_{n-1} - T_n}{R}dy + \frac{T_{n+1} - T_n}{R}dy = \frac{T_{n-1} - T_n}{\frac{l_{n-1}}{k_{n-1}} + \frac{l_n}{k_n}}dy + \frac{T_{n+1} - T_n}{\frac{l_n}{k_n} + \frac{l_{n+1}}{k_{n+1}}}dy \qquad (2\text{-}1)$$

r	Density	T_n	Temperature of node at time step
c_p	Specific heat	Dt	Time step
dx	Dimension of node in x-direction	R	Resistance between nodes
dy	Dimension of node in y-direction	k	Thermal conductivity
T_n^+	Temperature of node at next time step	l_n	Distance in node n

If one neighbor node, i.e. node n-1 is an exterior node, the resistance changes:

$$rc_p dxdy \frac{T_n^+ - T_n}{\Delta t} = \frac{T_{n-1} - T_n}{R'} dy + \frac{T_{n+1} - T_n}{R} dy = \frac{T_{n-1} - T_n}{\frac{1}{h} + \frac{l_n}{k_n}} dy + \frac{T_{n+1} - T_n}{\frac{l_n}{k_n} + \frac{l_{n+1}}{k_{n+1}}} dy \qquad (2\text{-}2)$$

h *Surface heat transfer coeffcient*

Using an implicit Crank-Nicholson scheme, the average of the actual and the future temperatures is taken:

$$r_n \cdot c_{p,n} \cdot dx \cdot \frac{T_n^+ - T_n}{\Delta t} = 0.5 \frac{T_{n-1} - T_n + T_{n-1}^+ - T_n^+}{\frac{l_{n-1}}{k_{n-1}} + \frac{l_n}{k_n}} + 0.5 \frac{T_{n+1} - T_n + T_{n+1}^+ - T_n^+}{\frac{l_n}{k_n} + \frac{l_{n+1}}{k_{n+1}}} \qquad (2\text{-}3)$$

To model the walls in a refrigerated warehouse Altwies (1998) used this scheme with three interior nodes in the wall to calculate the node temperatures T_n^+ at the next time step. The system of equations consists of three energy balances for the three interior nodes with their unknown temperatures.

The heat flux at the inside of the wall can then be calculated from the temperature of the exterior node 1:

$$q`` = 0.5 \frac{T_1 - T_{zone} + T_1^+ - T_{zone}^+}{\frac{1}{h} + \frac{dx}{2k}} \qquad (2\text{-}4)$$

Using EES, the system of equations for the wall can be solved for the unknown temperatures and the heat flux.

Finite-difference methods are easy to use and by decreasing the node spacing and the time step accuracy can be improved until the finite-difference solution approaches the real solution. An advantage of finite-difference methods lies in their ability to model relatively complicated geometries for which no analytical solution exists. Unfortunately, finite-difference methods require some computational effort, especially when large

numbers of nodes are considered or a small time step is used. Therefore, other methods have been developed, one of which is the transfer-function method.

2.2.1.2 Transfer-function models

In general a transfer-function model in heat transfer assumes that an output variable can be calculated as a function of certain input variables including previous values of the output variable. For example the heat flow through a wall can be calculated as a function of the current and previous temperatures on both sides of the wall and the previous heat flows through the wall (Stephenson and Mitalas, 1967):

$$q''_0 = \sum_{n=0}^{\infty} a_n T_{out,n} - \sum_{n=0}^{\infty} b_n T_{in,n} - \sum_{n=1}^{\infty} c_n q''_n \qquad (2\text{-}5)$$

$q``_0$ heat flow at time step zero

a_n n^{th} transfer coefficient for outside temperature

$T_{out,n}$ Outside temperature at n^{th} time increment before

b_n n^{th} transfer coefficient for inside temperature

$T_{in,n}$ Inside temperature at n^{th} time increment before

c_n n^{th} transfer coefficient for heat flow

q_n Heat flow at n^{th} time increment before

Theoretically an infinite number of coefficients and previous temperatures and heat flows would be needed to determine the heat flow. Practically the value of the coefficients a_n, b_n and c_n approaches zero for n increasing, so only a limited history of previous values of temperatures and heat flows are required. Compared to a finite-difference method, the calculation effort for a transfer-function is considerably less. The transfer-function equation is explicit in heat flow and only a limited number of previous temperatures and heat flows need to be stored. Besides, the transfer function approach allows a larger time step for the calculation to be used compared to a finite-difference calculation (which can be limited in accuracy and stability if using a too large time step). The drawback of transfer-functions is that before applying the method the transfer function coefficients

have to be obtained. For different wall constructions, the coefficients will be different. Several methods of calculating transfer-function coefficients exist:

Mitalas and Stephenson (1967) and Stephenson and Mitalas (1967) developed a method to analytically calculate transfer-function coefficients. Their approach is based on Laplace transforms of the heat conduction equation. They first developed the response-factor method, which is similar to the transfer-function method, but does not use the previous heat flows as input. Therefore more previous temperatures are needed to obtain accurate results. The transfer-function method is an extension of the response factor method. For details on the mathematical method to calculate the coefficients see Stephenson and Mitalas (1967), Mitalas and Stephenson (1967) and Pawelski (1976).

A computer program based on this approach was developed by Mitalas and Arsenault (1970) to facilitate the rather complicated task of calculating transfer. This code is included in TRNSYS package as PREP. Providing the number of layers in a wall and the thermal properties of each layer to the program, PREP computes the transfer-function coefficients for that wall. The TYPE 19 Single-Zone Building Model in TRNSYS, which is used to model the freezer in the simulation, requires transfer-function coefficients for the heat transfer calculations through walls and roof. PREP was used in this study to compute the coefficients for the different wall constructions.

Seem (1987) presents a method to calculate transfer-function coefficients based on the state space representation of a heat transfer problem, which results in a similar relation for the heat flow than equation (2-5).

$$q`` = \sum_{n=0}^{k} S_n^{'T} \begin{bmatrix} T_{out,t-n\Delta t} \\ T_{in,t-n\Delta t} \end{bmatrix} - \sum_{n=1}^{k} e_n q``_{t-n\Delta t} \quad (2\text{-}6)$$

k	number of transfer coefficients and previous temperatures and heat flows
$S_n^{'T}$	vector of transfer coefficients for temperatures at time step n prior to current time
e_n	transfer coefficient for heat flow at time step n prior to current time
Δt	time step

For the method of calculation to obtain $S_n^{'T}$ and e_n see Seem (1987).

Braun (2000) uses this method to compute transfer coefficients for exterior and interior walls of a building for simulation purposes.

Seem (1987) also compares the resulting transfer coefficients using his method of calculation and the one from Stephenson and Mitalas (1967). He concludes that if using enough interior nodes in the state space representation in his method, the results of the two methods become identical.

2.2.1.3 Comparison

To verify that the transfer-coefficients obtained from PREP are realistic, the cooling load resulting from heat transfer through the walls and roof to a refrigerated space was compared using the two methods. The implicit Crank-Nicholson scheme from Altwies (1998) with three interior nodes and the PREP-coefficients for the same wall constructions were both included in the same EES-Model. Two wall types were compared: A thermally massive wall and a thermally lightweight wall. Both walls have the same U-value of 0.26 W/m^2-C (0.046 BTU/hr-ft^2-F) but differ in their construction: One wall has a thick layer of concrete around the insulation while the other wall only has a thin layer of plywood. Figure 2-4 and Figure 2-5 show the resulting heat flows through the walls and roof of a warehouse for a hot summer day.

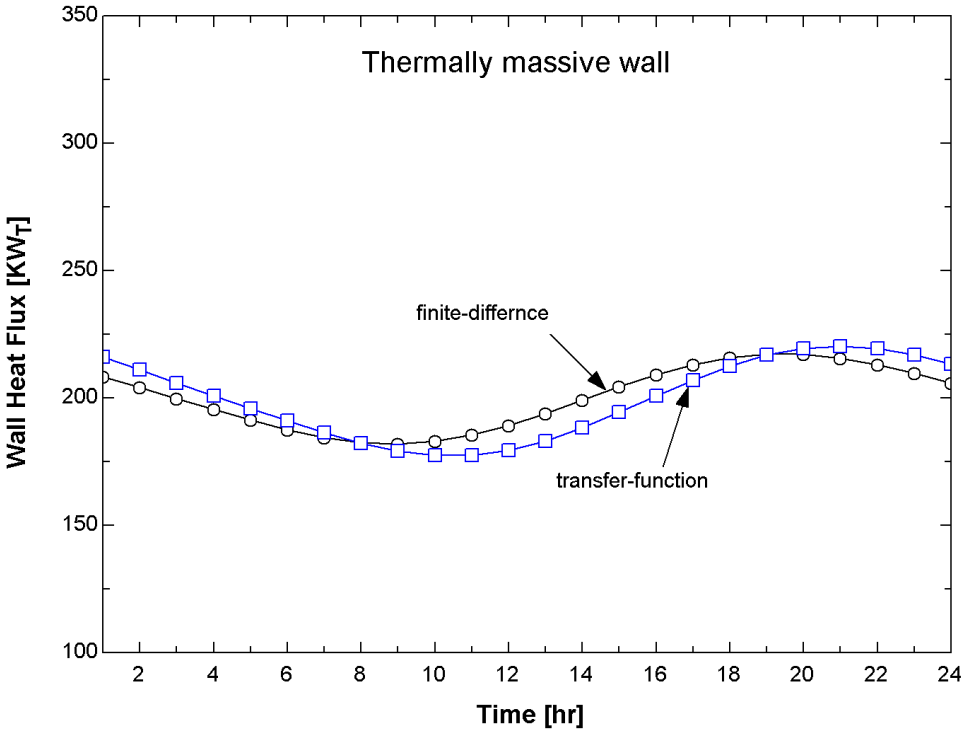

Figure 2-4: Comparison of heat flux calculated by finite-difference and transfer function methods for massive wall.

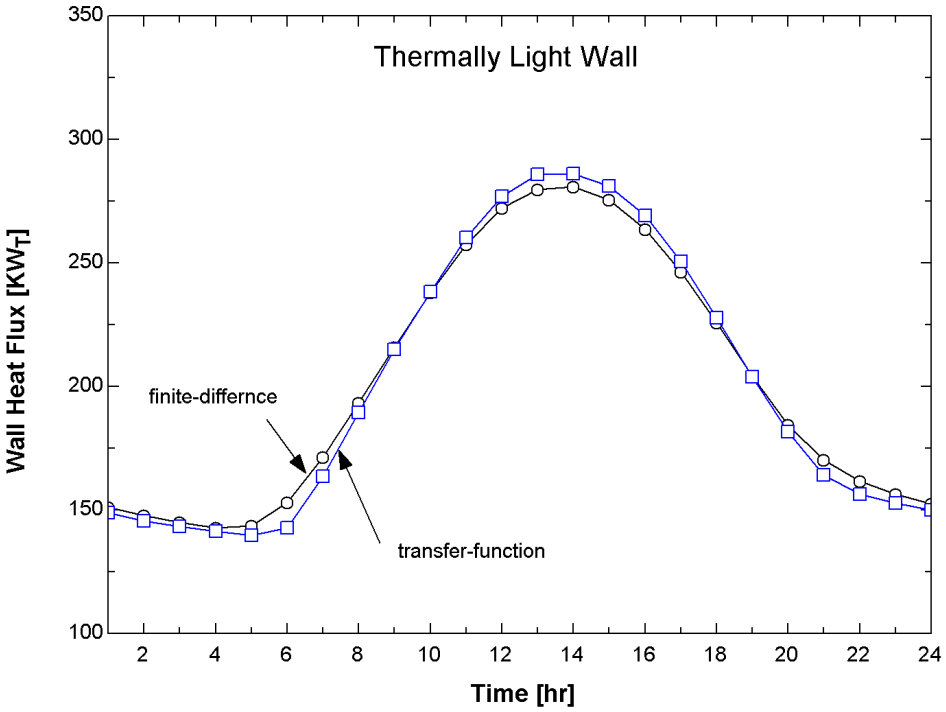

Figure 2-5: Comparison of heat flux calculated by finite-difference and transfer function methods for lightweight wall.

The results for the two methods of calculation are not identical, but are in good agreement. The results obtained from the finite-difference scheme were verified by increasing the number of nodes and decreasing the time step to values far less than the one hour shown in the plots. Decreasing the node spacing and the time step did not change the finite-difference results. Therefore it can be assumed that the 3-node-solution is a reasonable approximation to the true solution. Still the small discrepancy between the methods of calculation persisted.

One possible explanation for the discrepancy is found by considering an additional constraint the transfer coefficients have to satisfy.
The wall transfer function has the form

$$q``_0 = \sum_{n=0} a_n T_{out,n} - \sum_{n=0} b_n T_{in,n} - \sum_{n=1} c_n q``_n \tag{2-7}$$

Assuming steady state, i.e. T_{out} and T_{in} are constant, the heat flux through the wall, q``, approaches a constant value (the coefficient c_0 is always 1). In this case

$$q`` \sum_{n=0} c_n = T_{out} \sum_{n=0} a_n - T_{in} \sum_{n=0} b_n \tag{2-8}$$

If $T_{out}=T_{in}$ the heat flux q`` is zero. Then

$$0 = T \sum_{n=0} a_n + T \sum_{n=0} b_n \tag{2-9}$$

or

$$\sum_{n=0} a_n = \sum_{n=0} b_n \tag{2-10}$$

The sum of the a-coefficients must equal the sum of the b-coefficients. Therefore, for steady state:

$$q`` \sum_{n=0} c_n = (T_{out} - T_{in}) \sum_{n=0} a_n = (T_{out} - T_{in}) \sum_{n=0} b_n \tag{2-11}$$

At the same time, the following relation employing the U-value explains the wall heat flux at steady state:

$$q`` = U_{wall}(T_{out} - T_{in}) \tag{2-12}$$

Comparing equation (2-11) and equation (2-12) yields

$$\frac{\sum_{n=0} a_n}{\sum_{n=0} c_n} = \frac{\sum_{n=0} b_n}{\sum_{n=0} c_n} = U_{wall} \tag{2-13}$$

If applying the relation on the coefficients calculated with PREP it can be observed that the sum of the a-coefficients is not exactly identical to the sum of the b-coefficients. For the wall properties given, PREP calculates only a certain number of coefficients until convergence limits are reached, but the sums of the coefficients are still not identical to the last digit. Table 2-1 compares the coefficients and the resulting U-Values to the U-value calculated from the wall properties. Inside and outside surface resistances are included.

Table 2-1: Transfer coefficients and U-Values

	$\sum_{n=0}^{6} a_n$	$\sum_{n=0}^{6} b_n$	$\sum_{n=0}^{6} c_n$	$U = \frac{\sum_{n=0}^{6} a_n}{\sum_{n=0}^{6} c_n}$	$U = \frac{\sum_{n=0}^{6} b_n}{\sum_{n=0}^{6} c_n}$	$U = \frac{1}{\sum R}$
	KJ/hr-m2-C	KJ/hr-m2-C	-	W/m2-C	W/m2-C	W/m2-C
Massive wall	0.02126730	0.02126540	0.2381350	0.24807709	0.24805493	0.2495
Light wall	0.74939960	0.74939930	0.82040360	0.25373679	0.25373668	0.2495

The difference in the sums of the coefficients and the resulting different U-values is the likely reason for the slightly different results in the comparison between transfer function and finite-difference.

2.2.2 Floor

Heat is also transmitted into the zone through the floor of the freezer. Because the temperature of the freezer is far below the freezing point, freezing of the ground below

the warehouse will occur and eventually damage its foundation. Freezing is usually prevented through a heating loop embedded in the foundation. Additional heat gain is associated with this heating loop. Altwies (1998) created a finite-difference model to calculate the heat gain through the floor. Altwies (1998) assumed a constant temperature of the earth adjoining to the floor of 19.72 °C (67.5 °F). With the floor built of 30 cm (12 in) of concrete and 5.1 cm (2 in) of insulation the resulting heat flow was 7.82 W/m^2 (2.48 BTU/hr-ft^2). Jekel (2000) on the other hand suggests a value of 11.36 W/m^2 (3.6 BTU/hr^2). Finally the value of Jekel was chosen, which results in an additional transmission load through the floor of 106 KW$_t$ (30 tons).

2.2.3 Doors

Two types of doors exist in the model: freezer doors and dock doors. Five doors, 14 ft × 10 ft each, provide access from the freezer to the dock. The 30 truck bay doors between the dock and outdoors are 9 ft × 8 ft each. Realistic modeling of the doors of the warehouse is important because for a well-built refrigerated warehouse nearly all infiltration loads are associated with infiltration through the doorways. The infiltration loads through the doors are calculated using the following formula for infiltration loads to a refrigerated space through an opening based on the approach of Downing and Meffert (1993):

$$Q_{\inf} = \left[2491.47 A r_{in} \sqrt{1 - \frac{r_{out}}{r_{in}}} \sqrt{z} F_m (1 - E) \right] (h_{out} - h_{in}) = \dot{m}_{\inf} \Delta h \qquad (2\text{-}14)$$

$$F_m = \left[\frac{2}{(1 + \frac{r_{in}}{r_{out}})^{\frac{1}{3}}} \right]^{\frac{3}{2}}$$

A	Door area in m^2
E	Effectiveness of door protective device or opening fraction of door
Z	Height of doors in m
Q_{inf}	Infiltration gain to space in kJ/hr
r	Density of air in Kg/m^3
h	Enthalpy of air in kJ/Kg
F_m	Density factor

The formula was converted from English units to SI units for use in TRNSYS. A component was created that performs the calculations for the infiltration load to the freezer and dock. For the dock two sources of infiltration exchange exist: freezer and outdoors. Infiltration from the freezer results in a sensible and latent cooling credit. Infiltration from the outdoors leads to a cooling load. Furthermore, in winter the ambient temperature might be colder than the dock temperature, which is always kept above 0 °C. In that case, the dock is not gaining heat from the ambient, but losing heat to it. The analysis conducted accounts for heating requirements of the dock to maintain its temperature at or above 0 °C (32 °F).

An important parameter in the Downing-Meffert infiltration calculations is E, the fraction of time a door is open. In the simulation it was assumed that the freezer doors are open 4 min/hr and the dock doors are open 2 min/hr. This results in efficiencies of 0.933 and 0.966 for the freezer and the dock doors, respectively.

2.3 Refrigeration Equipment

The TRNSYS TYPE 19 single-zone building offers two modes of operation. Energy rate control and temperature level control. In energy rate control, the zone temperature is set to a constant value and TRNSYS calculates the cooling load of the structure. This mode of operation is convenient if the goal of the simulation is to calculate cooling loads and for the purpose of sizing the refrigeration equipment. For a warehouse operated at a constant temperature, for example at -18 °C (0 °F), energy rate control would work well

because it could be assumed that sufficient refrigeration capacity is installed. In this study however, the zone temperature is not kept constant, but the warehouse is precooled to a lower temperature during low cost periods, e.g. over night. During the day, ideally, the equipment is turned off, and the warehouse temperature floats back to -18 °C (0 °F). In a standard warehouse, which was designed for a freezer temperature of -18 °C (0 °F), there may not be enough refrigeration capacity installed to precool the freezer over night on a design day to the lowest desired temperature. In this case, the refrigeration capacity will be the limiting factor for precooling the warehouse to the desired set point. Therefore energy rate control cannot be used as mode of operation, temperature level control has to be used instead. In temperature level control, the airflow rate and supply air temperature has to be specified for the zone. These two inputs determine the amount of cooling that can be supplied by the equipment. They also determine to what temperature the given zone can be cooled. Integration of a model of the refrigeration equipment with the warehouse model is necessary to compute the maximum available cooling capacity.

The scope of the study is to determine operating strategies under real-time pricing that minimize operating costs. Operating costs are strongly influenced by the operation of the equipment. Therefore, the equipment has to be modeled in sufficient detail to allow reasonable estimate of the utility cost associated with different operating strategies. Refrigeration and component models are discussed next.

2.3.1 Compressor

Different types of compressors are used for refrigeration. For larger applications, like the 100,000 ft^2 freezer simulated in this study, mainly two types are used: reciprocating compressors and screw compressors. Screw compressors have less moving parts than reciprocating compressors, an advantage that results in less maintenance required and a longer lifetime. Screw compressors have won market share over reciprocating compressors for large refrigeration applications in recent years.

Manufacturers usually rate the performance of their compressors (refrigeration capacity and required power) as a function of two parameters: saturated suction temperature (SST)

and saturated discharge temperature (SDT). SST is the saturation temperature of the refrigerant vapor entering the compressor at the suction pressure. In the same way, SDT is the saturation temperature that belongs to the discharge pressure of the compressor. The manufacturer's ratings include the maximum cooling capacity a compressor can deliver for a given SST and SDT and the resulting brake horsepower for these conditions. Brownell (1998) performed a regression analysis on manufacturer's data and showed that the manufacturer's data can be best represented by second order polynomials including cross terms. Equations (2-15) and (2-16) show the relations for cooling capacity and brake horse power:

$$CAP = c_1 + c_2 \cdot SDT + c_3 \cdot SDT^2 + c_4 \cdot SST + c_5 \cdot SST^2 + c_6 \cdot SDT \cdot SST \quad (2\text{-}15)$$

$$BHP = p_1 + p_2 \cdot SDT + p_3 \cdot SDT^2 + p_4 \cdot SST + p_5 \cdot SST^2 + p_6 \cdot SDT \cdot SST \quad (2\text{-}16)$$

CAP	Maximum available cooling capacity per compressor [tons]
BHP	Maximum brake horse power [KW]
c	Regression coefficient for cooling capacity
p	Regression coefficient for brake horse power
SDT	Saturated discharge temperature [C]
SST	Saturated suction temperature [C]

Manske (1999) calculated regression coefficients for several compressors from manufacturer's data in English units. His results were taken and new coefficients were calculated in SI-units. In the simulation, Vilter VSS-451 high stage screw compressors are used; the calculated coefficients for this model are shown in Table 2-2.

Table 2-2: regression coefficients for conditioning equipment

n	1	2	3	4	5	6
c_n	279.6	-1.0101	-0.00468	9.5125	0.089808	-0.023317
p_n	21.634	3.7262	0.0014765	-1.3623	0.019687	0.063796

The available cooling capacity per compressor depends strongly on the suction temperature. The discharge temperature also plays a role, but the influence of the suction

temperature is much stronger. Figure 2-6 shows the available cooling capacity as a function of the suction temperature. A second parameter is the discharge temperature.

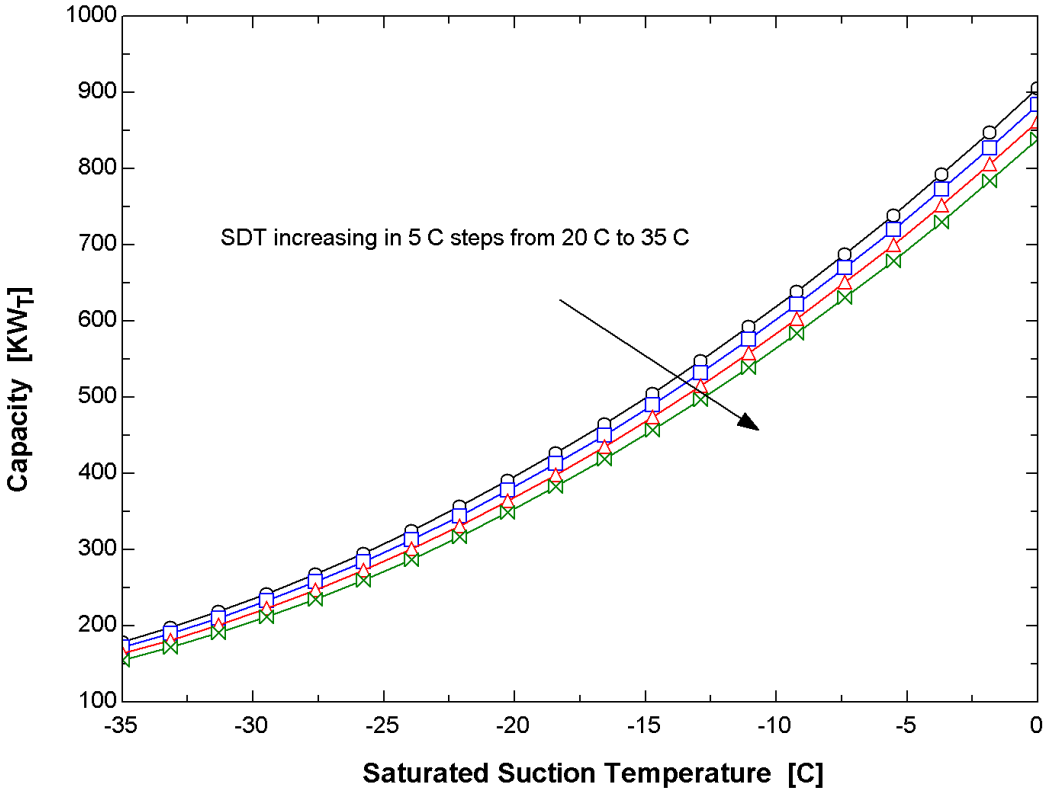

Figure 2-6: Available cooling capacity as a function of SST and SDT for Vilter VSS-451 high stage screw compressor.

As a refrigerated warehouse is precooled to a lower temperature, the drop in compressor saturated suction temperature results in decreased compressor performance. For the selected compressor, the cooling capacity would drop from around 300 KW_t at a suction temperature of –22 °C to less than 250 KW_t at –27 °C, a drop of more than 15 %, or 3 % per °C drop of suction temperature. Simultaneously to the warehouse temperature decreasing, the cooling load on the warehouse increases. Both effects together limit the possibilities to precool the freezer to temperatures much lower than the design temperature.

During most times of normal equipment operation, the cooling load is less than the maximum available cooling capacity of the equipment. The equipment is operated at part-load. Most reciprocating compressors are built with several cylinders. Part-load operation is achieved by charging only the number of cylinders needed. The part load behavior of a reciprocating compressor can therefore be best described by a straight line: the fraction of full load power (FLP) required is proportional to the fraction of full load capacity (FLC) needed.

$$FLP = \frac{power}{power\ at\ \ full\ load} \tag{2-17}$$

$$FLC = \frac{capacity}{available\ capacity} \tag{2-18}$$

Part load behavior of a screw compressor is different from the behavior of a reciprocating compressor. Two slide valves along the screw allow regulating the mass flow rate and the discharge pressure of a screw compressor continuously. Part load efficiency of a screw compressor is slightly lower than full load efficiency. Manske (1999) presents an equation to model the part load behavior of a screw compressor:

$$\begin{aligned} \%FLP = {} & 21.5733 + 0.465983 \cdot \%FLC + 0.00544201 \cdot \%FLC^2 \\ & - 5.55343 \cdot \%FLC^3 + 7.40075 \cdot 10^{-8} \cdot \%FLC^4 - 2.43589 \cdot 10^{-9} \cdot \%FLC^5 \end{aligned} \tag{2-19}$$

Figure 2-7 shows the part load behavior for a reciprocating and screw compressor:

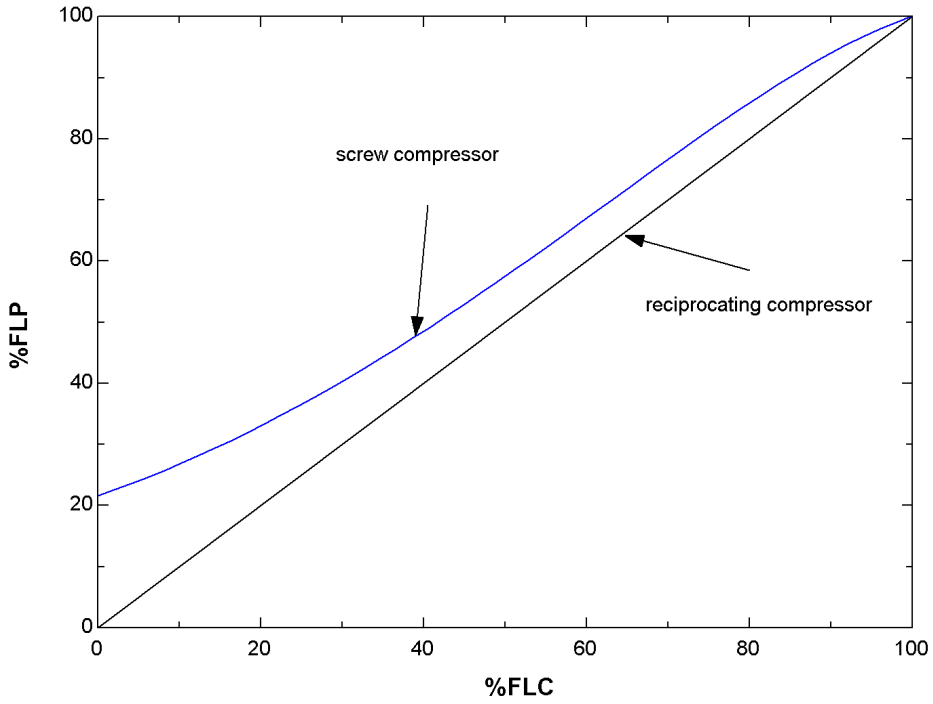

Figure 2-7: Part load behavior for screw and reciprocating compressors.

For the 100,000 ft^2 freezer modeled in the simulation, the design cooling load is much higher than the maximum available cooling capacity of one VSS-451 screw compressor. Depending on the warehouse construction and the design weather data, 3 or 4 of the compressors have to be used.

At part load, the same problem arises for the equipment operation than for the single compressor. Several strategies of operation are possible. Two of them were investigated: In the first strategy, all compressors are always in operation and operate at part load when less cooling is needed than the full load capacity. In the second strategy, compressor use is staged. Only one compressor is operated until it operates at full load, than a second compressor is started and operates at part load. In this strategy, only the last compressor started operates at part load, all others in use operate at full load. This strategy should result in a higher efficiency for the equipment operation. Figure 2-8 shows the ambient dry bulb temperature and the resulting cooling load, and Figure 2-9 shows a comparison of the power consumption of the equipment under the different operating strategies during a week in March.

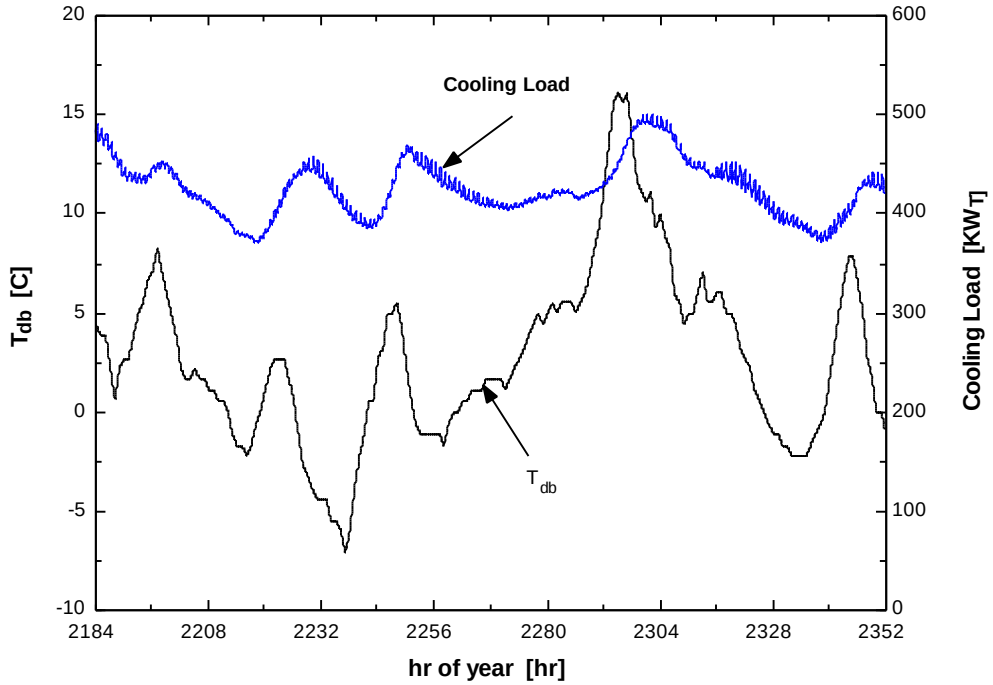

Figure 2-8: Outside dry bulb temperature and cooling load during March week

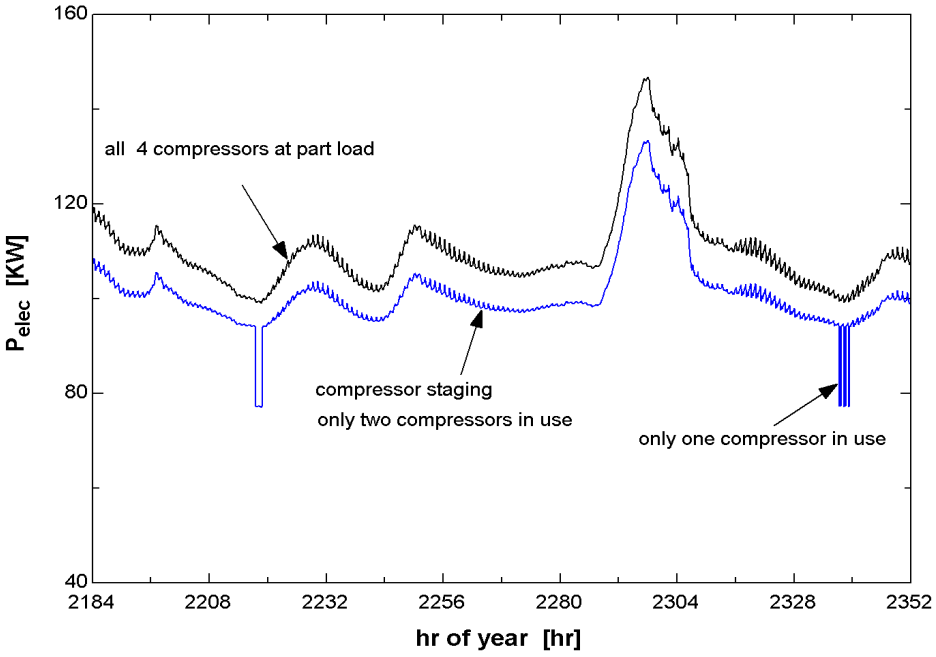

Figure 2-9: Compressor power consumption during a March week for compressor staging and without staging.

The figure shows the higher power consumption if all four of the installed compressors are in use. During the March week, the warehouse load is much lower than the design

load. Only two of the four installed compressors need to be in operation. At the fifth and sixth day of the week, when the cooling load is even smaller, even the second compressor can be turned off, which results in additional power savings.

2.3.2 Evaporator

2.3.2.1 Evaporator model

The zone air enters the evaporators, is cooled down to a lower temperature and leaves the evaporators at a colder temperature than the zone temperature. At the same time, the liquid refrigerant enters the evaporators at the evaporating temperature, is evaporated and possibly superheated. In order to allow heat transfer from the air to the refrigerant, the refrigerant has to be at a temperature colder than the air leaving the evaporators.

The evaporator model basically consists of two temperature differences:

- The air leaving the evaporator at T_{vent} is assumed to be 3 °C colder than air entering the evaporator at $T_{zone,}$ i.e. $\Delta T_{evap,air}$=3 °C:

$$T_{vent} = T_{zone} - \Delta T_{evap,air} \tag{2-20}$$

- The refrigerant temperature, which is the saturated suction temperature in the compressor model, is assumed to be 1.5 °C colder than the air leaving the evaporator, i.e. $\Delta T_{evap,ref}$=-1.5 °C:

$$SST = T_{vent} - \Delta T_{evap,ref} \tag{2-21}$$

Overall, the refrigerant in freezer and dock evaporator is 4.5 °C colder than the respective zone temperatures of freezer and dock.

2.3.2.2 Evaporator fan loads

The power consumed by the electric motors of the evaporator fans is converted into heat, which is an additional load on the freezer and the dock.
If the evaporators operate at rated capacity, the heat gain can be explained in terms of volumetric flow rate through the evaporators, the rated pressure drop across the fans and the efficiencies of motors and fan:

$$Q_{rated} = \frac{\dot{V}_{max} \cdot \Delta P}{\eta_{motor}\eta_{fan}} = \frac{\dot{m}_{max} \cdot \Delta P}{\rho\eta_{motor}\eta_{fan}} \tag{2-22}$$

The part load behavior of an evaporator can be explained by equation (2-23) (Manske, 1999):

$$PLR = \frac{cap_{actual}}{cap_{rated}} = \left(\frac{FanSpeed_{actual}}{FanSpeed_{rated}} \right)^{0.65} \tag{2-23}$$

where PLR is the part load ratio.

The power consumption and therefore the heat generation of an electric motor is proportional to the 3rd power of fan speed:

$$Q = FanPower \sim FanSpeed^3 \tag{2-24}$$

Therefore

$$PLR^{\frac{1}{0.65}} = \sqrt[3]{\frac{FanPower_{actual}}{FanPower_{rated}}} = \sqrt[3]{\frac{Q_{actual}}{Q_{rated}}} \tag{2-25}$$

From equation (2-25), the heat generation associated with the evaporator fans is calculated:

$$Q_{actual} = Q_{rated} \cdot PLR^{\frac{3}{0.65}} \tag{2-26}$$

A TRNSYS component was created, which does the fan power calculations for the freezer and the dock. The rated pressure drop is set to 0.5 in H_2O, the motor efficiency to 0.65, the fan efficiency to 0.3 and the rated mass flow rate to 1,700,000 Kg/hr

2.3.3 Condenser

A simplified condenser model is used in the simulation. The condensing temperature of the refrigerant is linked to ambient wet bulb temperature. The minimum temperature difference between condensing refrigerant and wet bulb temperature, ΔT_{cond}, is set to 10 °C. Depending on the wet bulb temperature, the condensing temperature is calculated:

$$T_{wb} \geq 5\ ^{\circ}\text{C}: T_{cond} = T_{wb} + \Delta T_{cond}$$
$$T_{wb} < 5\ ^{\circ}\text{C}: T_{cond} = 5\ ^{\circ}C + \Delta T_{cond} \qquad (2\text{-}27)$$

2.3.4 Defrost

The air in the freezer will balance out at a humidity level that depends on the latent infiltration load, the total sensible warehouse load and the coil selection and operation. The freezer air enters the evaporators at the freezer temperature, is cooled down and leaves the evaporators at a colder temperature. If the air temperature in the evaporator falls below the dew point, condensation and freezing of the excess humidity occurs on the evaporators. The frost that is building up worsens the heat transfer from evaporators to air, which increases the load on the equipment. Therefore, the evaporators have to be defrosted from time to time. Manske (1999) lists as possible defrost options: hot gas, hot water, electric heat and warm air. Defrosting improves the heat transfer from the evaporators to the air, but at the same time, only a fraction of the energy intended to melt frost really melts frost. A much larger fraction is released into the freezer air, directly contributing to the load. The defrost efficiency can be defined as:

$$h_{defrost} = \frac{energy\ to\ melt\ the\ frost}{total\ energy\ of\ defrost} \qquad (2\text{-}28)$$

Jekel (2000) uses a value of 20% for the defrost efficiency.

The latent load associated with the frost formation can be calculated as

$$Q_{lat,ice} = \dot{m}_{vent} \cdot \Delta h_{freeze} \cdot (w_{freezer} - w_{vent}) \qquad (2\text{-}29)$$

$\dot{m}_{vent}$	mass flow rate of air through evaporator
Δh_{freeze}	latent heat of freezing for water
$w_{freezer}$	humidity ratio of freezer air
w_{vent}	humidity ratio of air leaving the evaporators

The defrost load can then be determined as

$$Q_{defrost} = \frac{1}{h_{defrost}}(1 - h_{defrost}) \cdot Q_{lat,ice} \qquad (2\text{-}30)$$

The second multiplier (1-$\eta_{defrost}$) can be explained be the fact that only a fraction of the excess defrost heat goes into the space, the fraction $h_{defrost} \cdot Q_{lat,ice}$ is absorbed by the melting ice.

2.3.5 Dock equipment

The dock equipment is similar to the one of the freezer. As the dock temperature is set to a value of 1 °C (34 °F), much more cooling capacity is available from the equipment. Only one Vilter VSS-451 compressor is needed for the dock. The dock equipment is modeled in a similar way to the freezer equipment. Again, the regression curves to manufacturer's data are used. The dock equipment discharge temperature is the same than for the freezer equipment. The suction temperature is determined as a function of the dock temperature. As the scope of this study is more on the freezer than on the dock, no part load efficiencies are calculated for the dock equipment.
With the dock temperature around freezing, the proportion of the defrost load of the total dock load is very small and therefore not calculated. The loads from the dock evaporators are modeled in the same way than the ones for the freezer.

2.3.6 Internal Loads (lights, fork trucks, people)

Lights, fork trucks, people and other miscellaneous heat source contribute to additional loads on the freezer. The following assumptions were made for these loads:

- Lights: For the freezer, a value of 4.84 W/m^2 (0.45 W/ft^2) is assumed, which corresponds to an additional load for the 100,000 ft^2 freezer of 44.5 KW (12.8 tons). For the dock, the power density from lights is higher, 26.91 W/m^2 (2.5 W/ft^2).
- Fork trucks: Equipment used to transport the refrigerated product in the warehouse also causes additional loads. The value from Manske (1999) was taken and converted for the use in the 100,000 ft^2 freezer, which is an additional load of 63.89 KW (18.17 tons).

- People: The people working in the warehouse also cause loads on the space, but compared to the loads from lights and fork trucks, the loads are rather small. For people the additional load input is 7.92 KW (2.25 tons).

2.4 Product Modeling

The frozen product stored in the freezer is an important component in the warehouse model. As long as the freezer temperature is kept constant and product is brought into the freezer at the freezer temperature, the freezer-product interaction can be neglected. But if the freezer is precooled over a certain period and the refrigeration equipment is turned off at other times, the freezer temperature is no longer constant. The resulting temperature difference between freezer and product leads to a heat flow into or out of the product. Consequently, the thermal mass of the frozen product can be used as storage medium for the additional cooling provided at times of precooling and as an additional source of cooling at times when the equipment is turned off. Two approaches were developed to represent the frozen product in the warehouse model: a finite-difference model and a transfer-function model.

2.4.1 Finite-difference model

2.4.1.1 Model description

A new component in TRNSYS was created to model the frozen product. A block of frozen product is modeled as a two-dimensional model. The heat flow is calculated for the 2-D model per unit of depth. Multiplication with the product depth gives the heat flow into bottom, front and top of the product. The 3-D heat flow is finally obtained by assuming the same heat flow per unit area into the sides of the product than through the front.

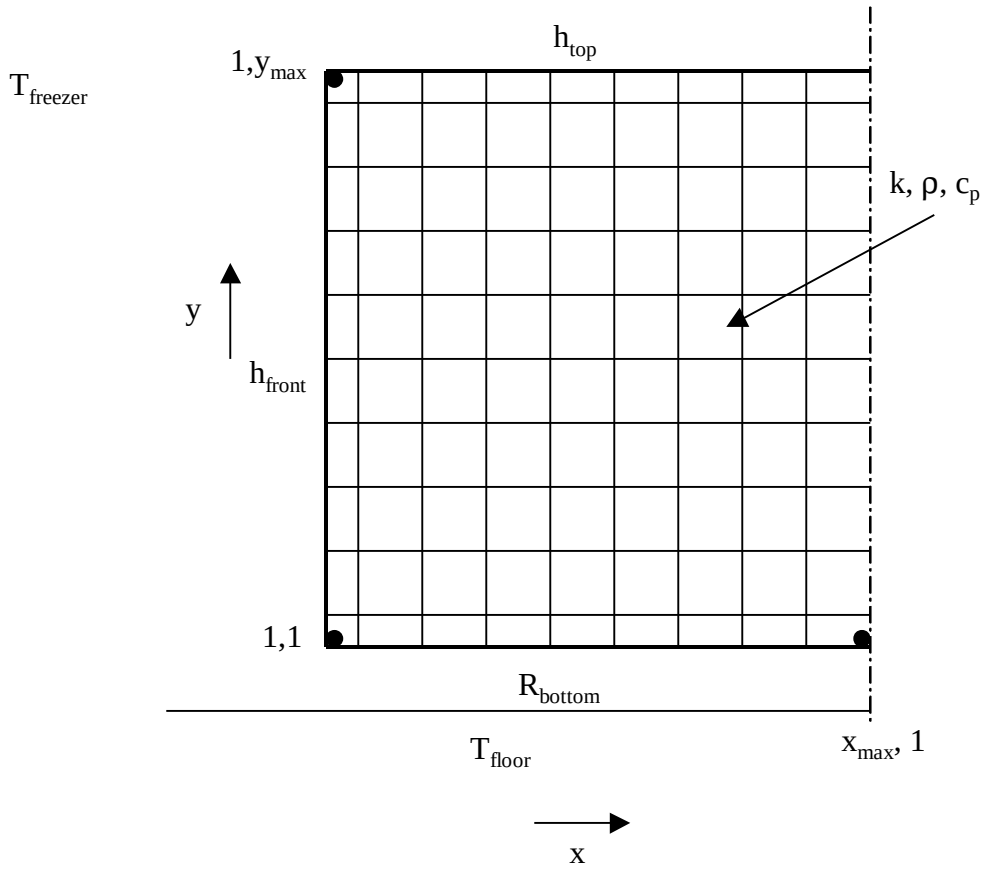

Figure 2-10: 2-D product model.

The block is modeled assuming a symmetry line in the middle of the block. Parameters supplied to the component are the height y, the width x and the depth of the block, its initial temperature and the calculation time step. An important parameter is also the node spacing in the 2-D model. Close to the surface, a very fine spacing would be ideal to resolve the temperature distribution within the block accurately due to the high temperature gradients. The temperature in the surface layers of the product is very important because it determines the rate of heat transfer into and out of the frozen block. On the other hand, the grid spacing in the block interior could be coarser because calculations showed that in the middle of the block short-term temperature fluctuations are negligible. Only over longer periods of time the core temperature changes if the medium core temperature is below or above the long-term average temperature of the freezer. But as an explicit method of calculation is used and this scheme of calculation

proceeds fast, the fine grid spacing, which is needed for the surface nodes, is also used for the interior nodes, even if such accuracy would not be necessary in the core.

Boundary conditions for the product model are the following: the upper and the front surface are in contact with the freezer air, the bottom of the block is on a palette. A surface heat transfer coefficient represents the heat transfer between product surface and freezer air. The package of the product is included in the surface heat transfer coefficient. The bottom of the product is on a palette. A corresponding resistance represents the palette. The palette is on the freezer floor, which is assumed to be at constant temperature. Inputs to the component representing the boundary conditions are the freezer air temperature, the product properties, the air surface heat transfer coefficients and the bottom surface resistance.

Equation (2-31) shows the relation for the new temperature of an interior node obtained by performing an energy balance on the node in the previous time step. Equation (2-32) shows the relation for an upper surface node as an example. Similar equations are used for the front surface, the bottom surface and the corner nodes.

$$T^{+}_{x,y} = a\Delta t \cdot \frac{\left(T_{x-1,y} - 2T_{x,y} + T_{x+1,y}\right)}{\Delta x^2} + a\Delta t \frac{\left(T_{x,y-1} - 2T_{x,y} + T_{x,y+1}\right)}{\Delta y^2} + T_{x,y} \tag{2-31}$$

$$\begin{aligned} T^{+}_{x,y_{\max}} = {} & 2a\Delta t \frac{T_{x-1,y_{\max}} - T_{x,y_{\max}}}{\Delta x^2} + 2a\Delta t \frac{T_{x+1,y_{\max}} - T_{x,y_{\max}}}{\Delta x^2} \\ & + 2h_{top}\Delta t r c_p \frac{T_{freezer} - T_{x,y_{\max}}}{\Delta y} + 2a\Delta t \frac{T_{x,y-1} - T_{x,y_{\max}}}{\Delta y^2} \end{aligned} \tag{2-32}$$

$T^{+}_{x,y}$	Temperature in node x,y in next time step of simulation	Dt	Time step
$T_{x,y}$	Temperature in node x,y in actual time step	r	Density of product
a	Thermal diffusivity of product	c_p	Specific heat of product
Dx	Node spacing in x-direction	h	Surface heat transfer coefficient
Dy	Node spacing in y-direction		

The heat flows are then calculated based on the updated estimates of the product surface temperatures. Equation (2-33) shows the relation for a top surface node, corresponding heat flow calculations are performed for the top and bottom nodes and the corner nodes:

$$q_{node,top} = h_{top} \cdot \left(T_{freezer} - T_{x,y_{top}}\right) \cdot dx \tag{2-33}$$

The overall heat flow is then obtained by summing up the heat flows into the surface nodes and multiplying by the depth. For the top row of nodes as example:

$$q_{top} = \sum_{3}^{x_{max}} q_{node,top} \cdot depth \tag{2-34}$$

$$q_{total} = q_{top} + q_{front} + q_{bottom} + q_{corners} + q_{sides} \tag{2-35}$$

An important output of the product component is also the corner temperature. As the corner of the frozen product has the biggest surface to volume ratio, the product corner is most sensitive to changes in the freezer temperature. If the freezer temperature increases it is most likely that the corner has the highest temperature of the whole block. Therefore the corner temperature is monitored as indicator if the product temperature gets above a critical temperature for long-term storage.

Figure 2-11 and Figure 2-12 compare the product heat flow and the temperature of the upper product corner for one block of frozen product for a different number of nodes, ranging from only 10×20 nodes up to 50×100 nodes. The calculations were performed with a step function temperature profile for the zone air temperature. The plots are the results for the last two days out of a seven-day series; initial effects should therefore be negligible.

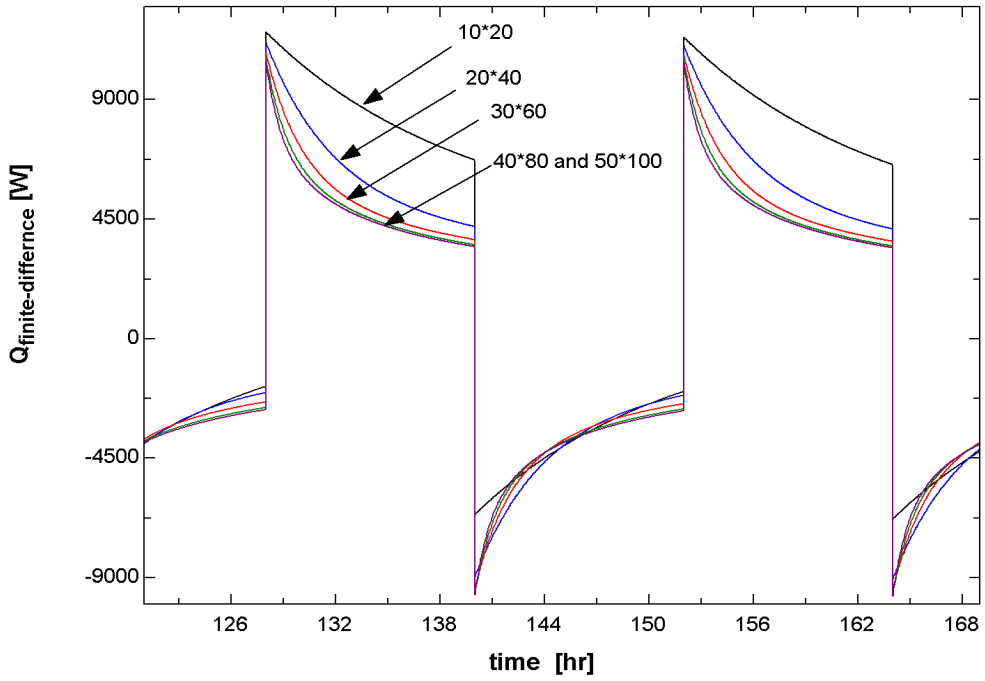

Figure 2-11: Product heat flow for different grid spacing.

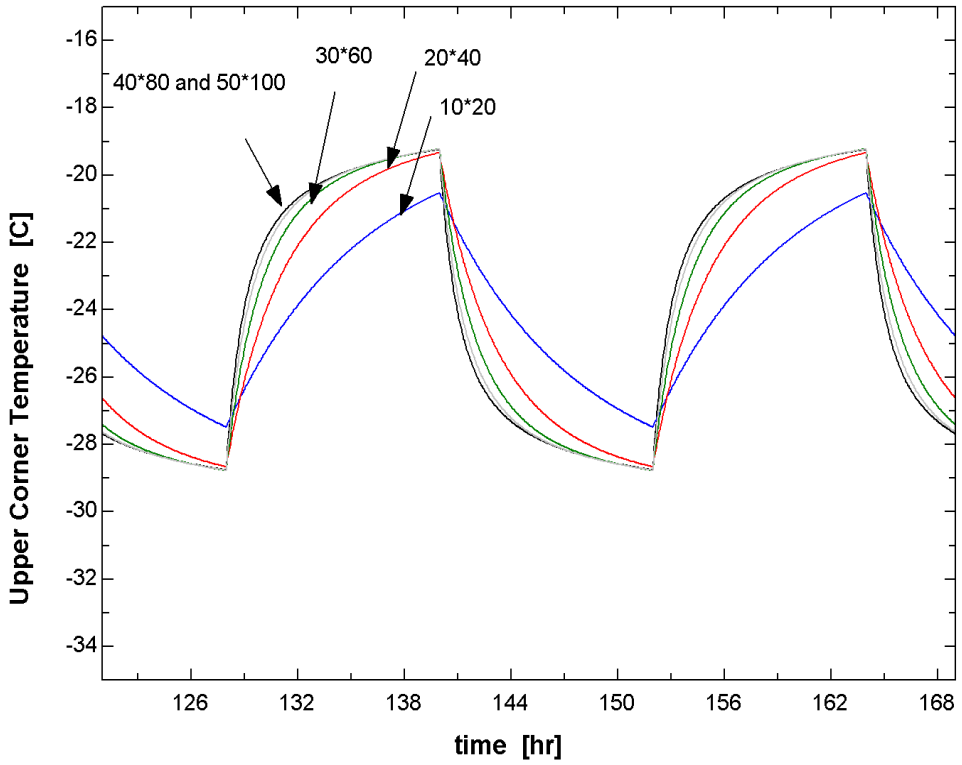

Figure 2-12: Product upper corner temperature for different grid spacing.

As a compromise between accuracy and speed of calculation, a grid spacing of 30×60 nodes is used in the simulation.

With an explicit scheme for the finite-difference calculation used for the product, care has to be taken of the critical time step of the simulation. Incropera (1996) gives as criterion for stability that the coefficient associated with the node of interest in the finite-difference scheme is greater than or equal zero. For the block of frozen product, the critical nodes are the corner nodes: These nodes have the least thermal mass because their dimensions are only half in the x- and the y-direction compared to an interior node.

$$T^{+}_{x_{\max},y_{\max}} = 2\frac{h_{front}}{rc_p\Delta x}\Delta t(T_{freezer} - T_{x,y}) + 2a\Delta t\frac{T_{x+1,y} - T_{x,y}}{\Delta x^2} + 2\frac{h_{top}}{rc_p\Delta y}\Delta t(T_{freezer} - T_{x,y}) + 2a\Delta t\frac{T_{x,y-1} - T_{x,y}}{\Delta y^2} + T_{x,y} \tag{2-36}$$

Equation (2-36) shows the relation for the new temperature for the top corner node. The coefficient associated with the node temperature must be greater than zero:

$$1 - (2\frac{h_{front}}{rc_p\Delta x} + \frac{2a}{\Delta x^2} + 2\frac{h_{top}}{rc_p\Delta y} + \frac{2a}{\Delta y^2})\Delta t_{crit} \geq 0 \tag{2-37}$$

$$\Delta t_{crit} \geq \frac{1}{2\frac{h_{front}}{rc_p\Delta x} + \frac{2a}{\Delta x^2} + 2\frac{h_{top}}{rc_p\Delta y} + \frac{2a}{\Delta y^2}} \tag{2-38}$$

For the product properties (see Table 2-3) used in the simulation, Δt_{crit} is more than one hour, while the time step used in the simulation is always less. Therefore no stability problems should originate from the explicit formulation used to model the stored products.

At the first call of the simulation, the temperature of all nodes is set to the initial value. From then on, the component calculates the heat flow into and out of one block of frozen product including the temperature distributions in the product. In order to obtain the total

heat flow into and out of all products that is stored in the freezer, the output of the component has to be multiplied by the number of blocks that is actually in the freezer. In the simulation it was assumed that the block measures 7.62 m (25 ft) in height, 7.62 m (25 ft) in depth and 6.10 m (20 ft) in width. Assuming coverage of 43 % of the warehouse floor area with product (see section 2.1) results in 85 blocks of product stored in the warehouse.

Altwies (1998) did previous work on the properties of frozen product. She recommended using the properties of frozen peas, which would represent a good median value for the different kind of vegetables stored in a refrigerated warehouse. Consequently, the values shown in Table 2-3 for a bulk of frozen peas are used.

Table 2-3: Average properties for bulk of frozen peas used in the simulation

Property	SI units	English units
Specific heat	1.851 KJ/Kg-C	0.442 BTU/lb-F
Thermal conductivity	0.55 W/m-C	0.3178 BTU/hr-ft-F
Density	700 Kg/m^3	43.7 lb/ft^3

For the surface heat transfer coefficient, Altwies (1998) wrote an EES-program to include the thermal resistance of the product packaging. This heat transfer coefficient is linearized to include effects of free convection, forced convection and radiation. Originally, two coefficients were computed, one for increased forced convection due to the evaporator fans running and one for reduced forced convection with the evaporator fans off. Altwies (1998) concluded that using an average value of 4.26 W/m^2-C (0.75 BTU/hr-ft^2-F) does not affect the results significantly. Therefore, this average value is used in the simulation. The resistance representing the wooden palette between freezer floor and product is set to 0.1656 m^2-°C/W (0.9403 ft^2-F-hr/BTU).

2.4.2 Transfer-function approach

Before modeling the refrigerated product with the explicit finite-difference scheme, the product was modeled by a transfer-function approach. It was assumed that the product heat flow could be represented by a transfer function of the following from:

$$q_{product} = \sum_{n=0}^{k} a_n (T_{n_{freezer}} - T_{n_{core}}) + \sum_{n=1}^{k} b_n q_{n_{product}} = \sum_{n=0}^{k} a_n T_{n_{diff}} + \sum_{n=1}^{k} b_n q_{n_{product}} \quad (2\text{-}39)$$

$q_{product}$	Product heat flow	$T_{n,freezer}$	Temperature of freezer air at n^{th} time step before calculation
a_n	n^{th} transfer coefficient for actual and previous temperatures	$T_{n,core}$	Core Temperature of product at n^{th} time step before calculation
b_n	n^{th} transfer coefficient for previous heat flow	$T_{n,diff}$	Temperature difference between freezer and core
		k	Number of previous time steps considered

In EES, a finite-difference model of a block of frozen product was created using an implicit Crank-Nicholson scheme. 20×40 nodes were used for the finite-difference calculations as the implicit scheme was much slower than if using 30×60 nodes in an explicit scheme. This model was run over a series of days with the daily freezer temperature profile as the forcing input. Different freezer temperature profiles were used as forcing functions. Figure 2-13 shows a triangular, a step, a pulse and a profile representing a temperature variation that might actually occur in a freezer during a precooling and floating cycle, enough cooling capacity provided.

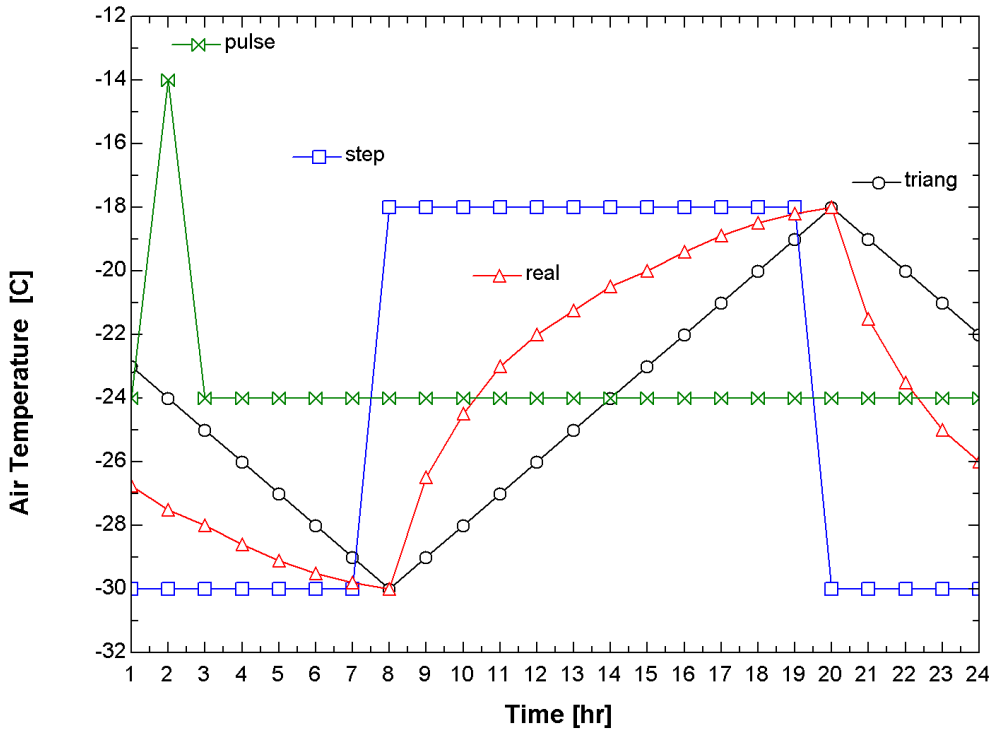

Figure 2-13: Forcing temperature profiles used to calculate product heat flow.

The step, real, and triangular temperature profiles have in common that the daily average freezer temperature is -24 °C (-11.2 °F). Ideally, the core temperature of the product should remain at this value over repeated daily cycles.

From the finite-difference calculations for the miscellaneous freezer temperatures, the hourly heat flow into and out of the product was obtained. A linear regression analysis was performed on the results, assuming that the product heat flow at each time step is a function of the difference between freezer and product core temperature, T_{diff}, at the time step and the previous time steps as well as the previous heat flows, $q_{product}$. Different numbers of previous inputs were used ranging from the values of the two previous time steps up to values of the 10 previous time steps. A one-hour time step is used.

The results from the linear regression analysis showed that using more coefficients for previous values leads to better agreement between the finite-difference model and regression model. Figure 2-14 shows the product heat flow over one day computed from the finite-difference model (20×40 nodes) compared to the results from the regression

analysis for the step temperature forcing profile. No appreciable difference can be seen between the curves.

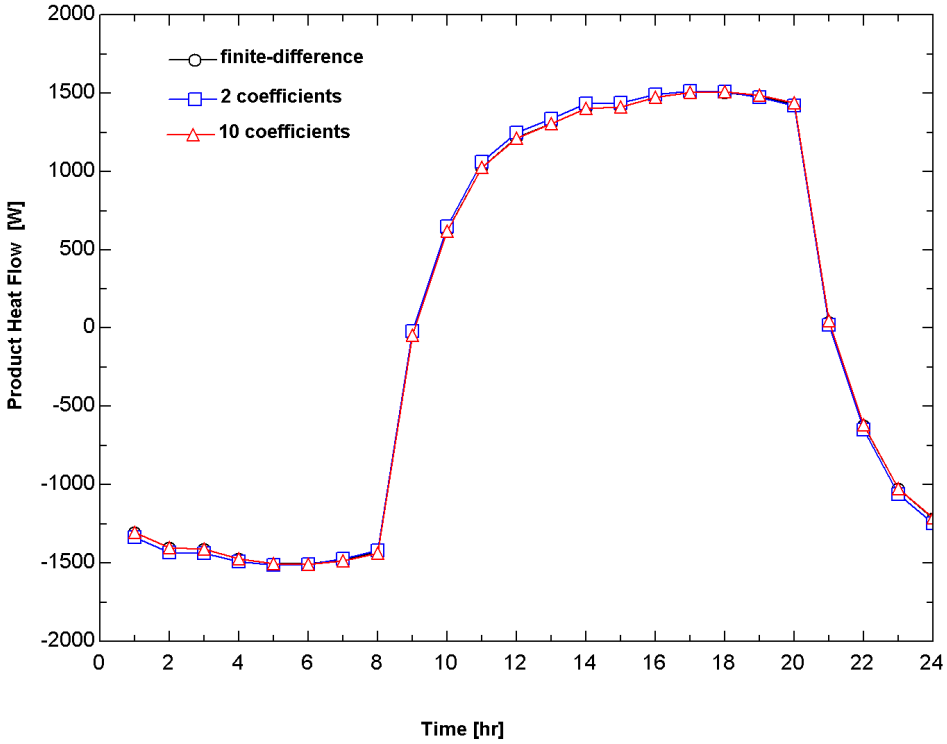

Figure 2-14: Comparison of product heat flow from finite-difference calculation and linear regression analysis for realistic temperature profile.

The goal of the regression approach was to obtain coefficients in order to calculate heat flows for forcing temperature profiles different from the ones used to obtain the coefficients. Figure 2-15 shows the product heat flow for the step forcing temperature profile, but the regression coefficients obtained from the triangular temperature profile.

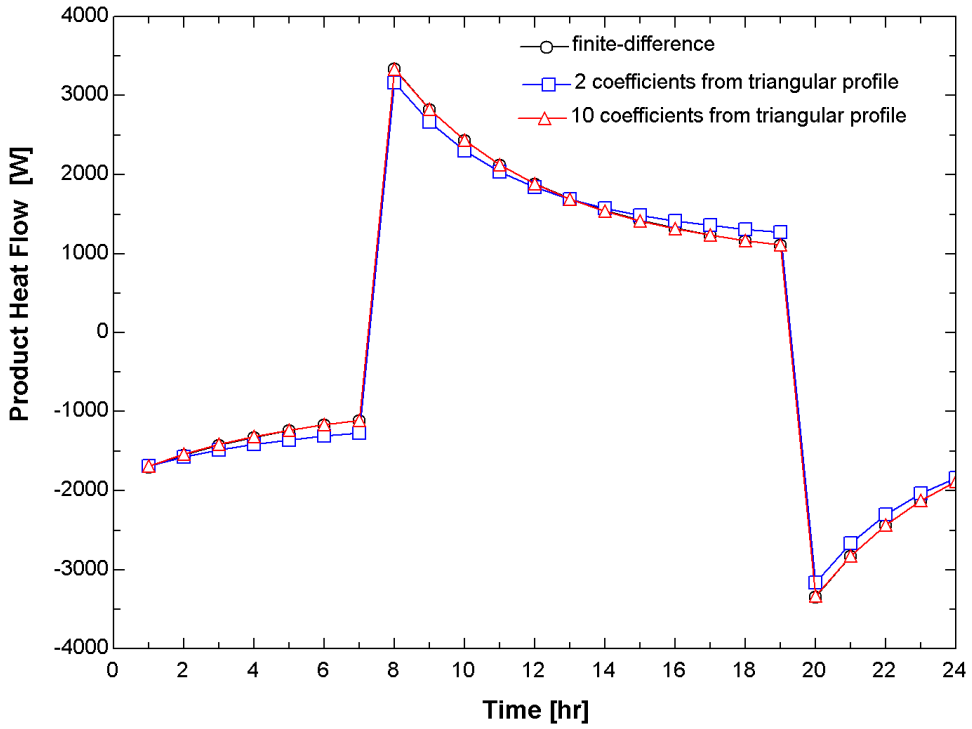

Figure 2-15: Product heat flow for step forcing temperature profile and with regression coefficients obtained from triangular profile.

For only two coefficients, the regression model tends to under and over predict the heat flow, but for ten coefficients, the finite-difference model and the regression model are in very good agreement. Similar plots could be generated for other combinations of forcing temperature profiles and regression coefficients from different profiles, for example for the triangular forcing temperature profile with the coefficients from the realistic. In general, the agreement between finite-difference solution and regression solution is very good for 10 coefficients.

Pawelski (1976) did a regression analysis to compute transfer coefficients for a wall. Considering steady state, he derived a relation similar to equation (2-13) (see section 2.2.1.3):

$$\frac{\sum_{n=0} a_n}{\sum_{n=0} c_n} = \frac{\sum_{n=0} b_n}{\sum_{n=0} c_n} = U_{wall} \qquad (2\text{-}13)$$

He used an equation of this from as an additional constraint on the coefficients of the transfer-function.

Unfortunately, no such additional constraint on the transfer coefficients can be derived for the product transfer function. If a constant core temperature of the frozen product is assumed, the long-term sum of the heat flow into and out of the product must equal zero. If the product heat flow is positive over a given time period, it has to be negative over another time period. Therefore, no such steady state assumption with the heat flow being constant can be made. This missing additional constraint can also be seen in the values for the transfer-function coefficients computed in the regression analysis. Table 2-4 shows the values of the temperature coefficient a_n and the heat flux coefficient b_n for the different temperature forcing profiles.

Table 2-4: Regression coefficients for different temperature profiles for the product transfer function $q``_{product} = \sum_{n=0}^{k} a_n T_{n_{diff}} + \sum_{n=1}^{k} b_n q_{n_{product}}$

	Triangular profile		Step profile		Realistic profile		Pulse profile	
n	a_n	b_n	a_n	b_n	a_n	b_n	a_n	b_n
0	366.478	1	366.600	1	366.562	1	366.633	1
1	-133.06	0.23758	-212.21	0.45334	-161.87	0.31592	-120.27	0.20271
2	-98.62	0.20034	-57.20	0.11477	-34.90	0.03659	-90.84	0.17498
3	-50.33	0.10809	-48.24	0.11313	-100.59	0.23226	-51.10	0.10392
4	-44.30	0.11062	-5.76	0.01473	-37.94	0.09899	-36.50	0.08400
5	-77.24	0.21557	-65.32	017848	-29.99	0.08960	233.88	-0.64060
6	-26.81	0.10295	31.87	-0.06503	-71.30	0.21086	-96.96	0.18100
7	-38.94	0.14163	-13.40	0.04501	-53.78	0.18513	-282.48	0.72710
8	16.52	-0.00018	-20.56	0.06791	60.80	-0.11298	-79.98	0.2742
9	33.81	-0.05749	-39.75	0.12580	18.04	-0.02272	-86.51	0.31260
10	52.82	-0.12423	76.64	-0.17992	47.76	-0.11239	260.20	-0.61124

The table shows that the values of the regression coefficients seem to be distributed arbitrarily among n. Transfer function theory would require the coefficients to decrease with n increasing and finally converge to zero. With the additional U-value constraint,

the coefficients Pawelski (1976) calculated from the regression analysis were similar to the coefficients calculated from transfer function theory (see section 2.2.1.2). But the missing constraint in the regression analysis for the product coefficients leads to this deliberate distribution where temperatures and heat fluxes of former time steps can be much more influential than recent ones. Never the less, surprisingly good agreement exists between the results for the heat flux for coefficients derived from different forcing temperature profiles shown in Figure 2-15. This good agreement can be explained by the relative high significance of the first coefficient for the temperature (n=0), which is similar in value for all profiles.

2.4.3 Comparison

Both models for calculating the product heat flow, the finite-difference model and the transfer-function model, were included in TRNSYS. The preliminary model was run with both product models included to determine if both approaches would yield the same results. Figure 2-16 shows the results for a hot summer week. The finite-difference model consists of 20×40 nodes and the coefficients used for the transfer-function are the ones computed from the realistic temperature profile. The product core temperature is set to –24 °C (-11 °F).

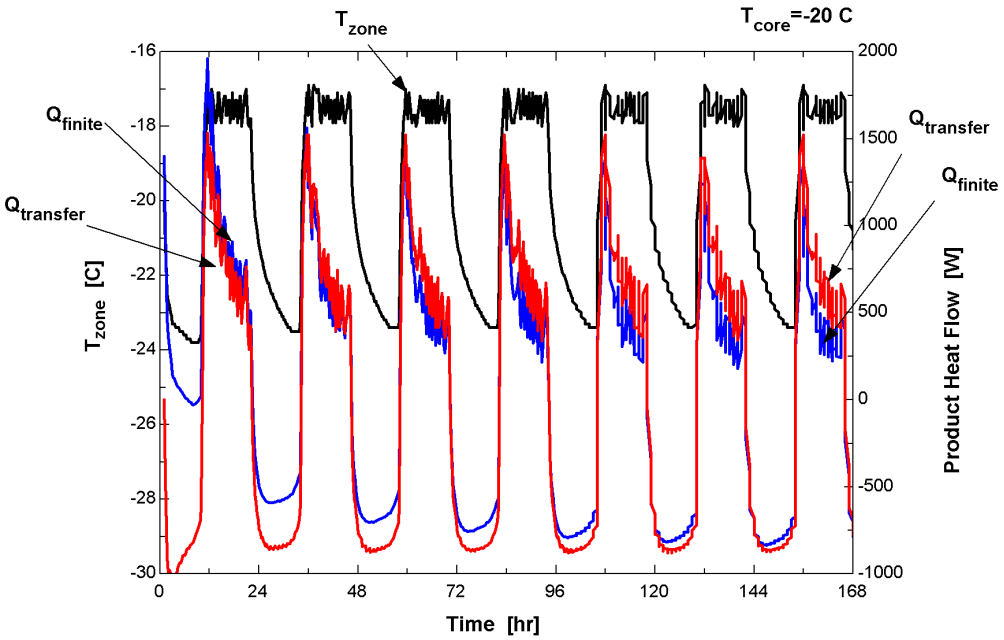

Figure 2-16: Comparison between finite-difference product model and transfer function for T_{core}=-24 °C.

In general, there is good agreement between the two methods of calculation. The transfer-function gives a slightly higher heat flow into the product at high freezer temperatures.

The freezer set point was at –30 °C (-22 °F) from 10 p.m. to 10 a.m. and at –18 °C from 10 a.m. to 10 p.m. Because of the thermal capacitance of the product and insufficient installed cooling capacity, the lower set point for the freezer temperature cannot be reached. Consequently, the average freezer temperature is above the product initial temperature of –24 °C (-11.2 °F). For the finite-difference model this results in more heat flowing out of the product than into it over the weekly run. For the transfer-function, it was still assumed that T_{core} remains at -24 °C (-11.2 °F). That assumption is obviously wrong, the core temperature increases from the initial value of –24 °C (-11.2 °F) because there is an overall heat loss for the product. But it is difficult to make long-term estimates for the average product core temperature. Figure 2-17 shows another simulation run, in which the core temperature for the transfer-function was set to a higher value of –20 °C (-4 °F).

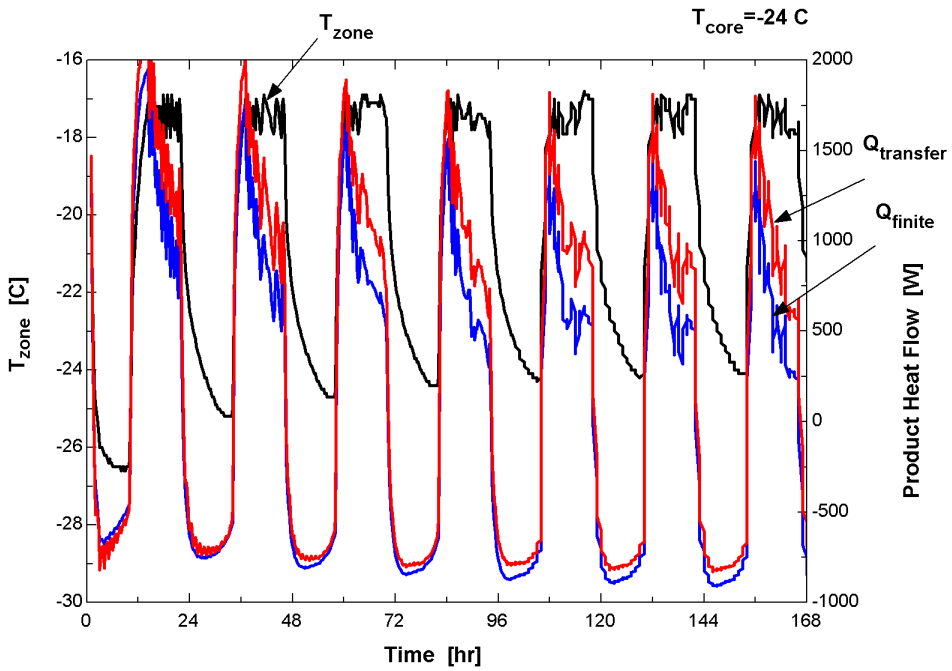

Figure 2-17: Comparison between finite-difference product model and transfer function for T_{core}=-20 °C, $T_{initial}$ for finite-difference still at –24 °C.

It can be seen very well that at the beginning of the week, when the average product temperature is still colder than the –20 °C (-4 °F) assumed for the transfer function, the finite-difference method calculates a higher product-freezer heat flux for the higher freezer temperatures at daytime. At nighttime the heat flux at lower freezer temperatures is lower for the finite-difference than the transfer function. At the end of the week, the average product temperature is warmer than the –20 °C (-4 °F) assumed for the transfer-function. The ratio of the heat flux results of transfer function and finite-difference method is changed compared to the beginning of the week

The difficulty of estimating the long-term average core temperature of the product is the main drawback of the transfer-function approach in the product modeling. For a daily or even a weekly simulation, a quick estimate still could be made by an initial run to determine the approximate average freezer temperature and then adjusting the product core temperature accordingly. But for a yearly simulation where the warehouse is precooled over night and the weekly average freezer temperature changes depending on the warehouse load and the installed refrigeration capacity, it is not possible to determine the core temperature correctly. At certain times of the year, the transfer-function will over predict the heat flow; at other times it will under predict it.

A second drawback is the need for a new regression analysis as soon as the product properties change: first, new finite-difference calculation have to be performed to obtain the corresponding heat fluxes, then the transfer coefficients can be calculated. The actual simulation might be faster with a transfer function product model because of the reduced calculation effort, but the preparation of the transfer coefficients compensates for this advantage.

Besides, if using a finite-difference method, the temperature histories of all nodes are known because they are all part of the calculation. With the transfer-function used however, only the heat flows are calculated. If temperatures of certain nodes had to be known, additional transfer-functions would have to be calculated for each node of

interest. For the warehouse simulation of this study, not only the product heat flow is of interest but also the product corner temperature. The corner is the part of the product that is most quickly affected by changes in the zone temperature. If using a transfer-function for the product-model, a second corner temperature transfer function would be necessary. Seeing this effort and the reduced accuracy of the transfer function approach, it was decided only to use the finite-difference representation of the product when adding more details to the warehouse simulation.

Nevertheless, in this section it was shown that a transfer function representation can be used to model a block of refrigerated product. The specific advantage of the transfer function method, namely the much faster speed of calculation, should always be considered, especially for cases were a more complicated geometry with more nodes has to be modeled than in this case. Even for a simulation without precooling, i.e. a constant product temperature, the transfer function would seem to be a more convenient approach.

2.5 Controllers

Two controllers are used in the simulation: one to control the freezer temperature and one to control the dock the temperature. The controllers compare the set point temperatures of freezer and dock to the actual temperatures and operate the refrigeration equipment as needed to maintain the set points.
Originally a standard on/ off controller was used. Figure 2-18 shows its control function.

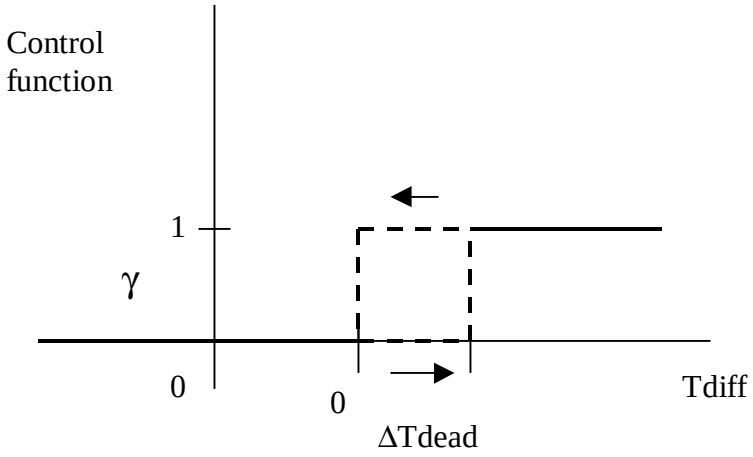

Figure 2-18: on/ off controller.

If the temperature difference $T_{diff} = T_{zone} - T_{set}$ is bigger than the dead band temperature, ΔT_{dead}, the control function is set to 1. If the set point temperature is reached, the control function is set to 0. With this control strategy, the equipment is operated part of the time at full load, part of the time it is turned off. A screw compressor, however, can also be operated at part load. Therefore the on/ off controller was replaced by a proportional controller. Figure 2-19 shows its control function.

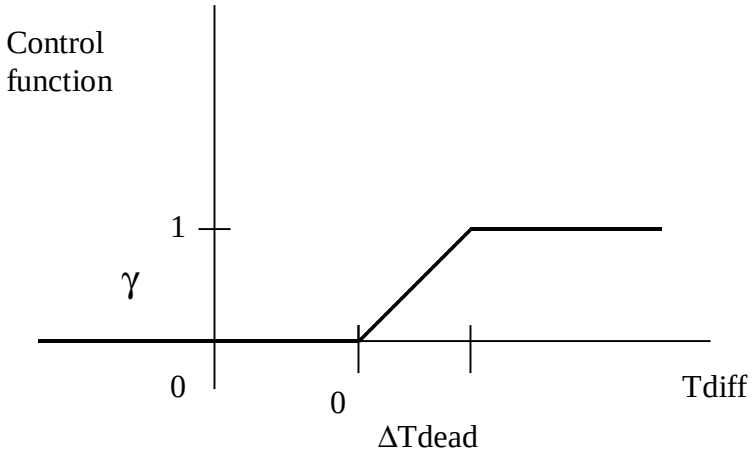

Figure 2-19: Proportional controller

If T_{diff} is between 0 and the dead band temperature, ΔT_{dead}, the controller output γ is set to $g = \frac{T_{diff}}{\Delta T_{dead}}$, i.e. the output is proportional to the input. This control strategy results in part load equipment operation. In fact, as long as cooling is necessary and enough cooling capacity is installed, the control output is between 0 and 1 and the equipment operates at part load most of the time. ΔT_{dead} is set to 2 °C (3.6 °F).

As more components were added to the TRNSYS deck, the calculations were slower and finally did not converge. Adding the variable Nstick to the proportional controller helped to promote convergence. If the controller subroutine is called more than Nstick times in a time step, the control function γ is set to the value of the last iteration: The controller output is then not changing any more and convergence occurs faster. Nstick values between 3 to 7 offered reasonable convergence promotion.

2.6 Loads

2.6.1 Types of loads

The loads on the warehouse described in the previous sections can be classified into different categories according to ASHRAE (1990):

- Transmission loads: Sensible heat gains through the walls and the roof and the floor.
- Product loads: Heat gains associated with the product. Mainly the energy needed to cool down product from the temperature at which it is received to the storage temperature. Besides, heat can also be generated by product stored. These product loads are not considered in the simulation, but a constant load from receiving product could be easily added. It is difficult to make general judgments of these loads.
- Internal loads: Additional heat generated in the warehouse, mostly from lights, motors and people. These additional loads are described in section 2.3.6.
- Infiltration loads: Loads arising from air infiltrating from conditions different to the ones in the warehouse. For a quality-built warehouse it can be assumed that infiltration through gaps in the walls is small compared to the door infiltration load. Only infiltration through the warehouse doors is considered (see section 2.2.3). For the dock, the infiltration from the freezer results in infiltration gains, the cold freezer air infiltrating reduces the loads on the dock.
- Equipment loads: Additional loads on the warehouse resulting from the equipment operation. In this simulation, equipment loads consist of loads from the evaporator fans (section 2.3.2.2) and heat gains from defrosting the evaporators (section 2.3.4).

2.6.2 Load calculation

The loads described before are imposed on the type 19 freezer model and the type 88 dock model where applicable. At the same time the refrigeration equipment provides cooling to keep both zones at the set temperature. Both TRNSYS types require an air mass flow rate and a discharge air temperature as input. From this, the corresponding cooling loads can be computed.

The cooling load is divided into sensible and latent loads. For the freezer, equations (2-40) and (2-41) show the cooling load calculation:

$$Q_{sens} = \dot{m}_{vent} \cdot c_{p,air} \cdot (T_{freezer} - T_{vent}) \quad (2\text{-}40)$$

$$Q_{lat} = \dot{m}_{vent} \cdot \Delta h_{vap,fus} \cdot (w_{freezer} - w_{vent}) \quad (2\text{-}41)$$

$$Q_{total} = Q_{sens} + Q_{lat} \quad (2\text{-}42)$$

Q_{sens}	Sensible cooling load	$T_{freezer}$	Freezer temperature
Q_{lat}	Latent cooling load	T_{vent}	Discharge air temperature
Q_{total}	Total cooling load	$Dh_{vap,fus}$	Enthalpy of evaporation and fusion of water
$\dot{m}_{vent}$	Mass flow rate of cooling air stream	$w_{freezer}$	Humidity ratio of freezer air
$c_{p,air}$	Specific heat of air	w_{vent}	Humidity ratio of cooling air

The same set of equations is valid for the dock by replacing the freezer air properties by the dock air properties.

2.7 TRNSYS Warehouse Model

2.7.1 Model description

The components and equations described in the preceding section were finally integrated into one TRNSYS model. Figure 2-20 shows the basic layout of the model and how the components and equations are linked.

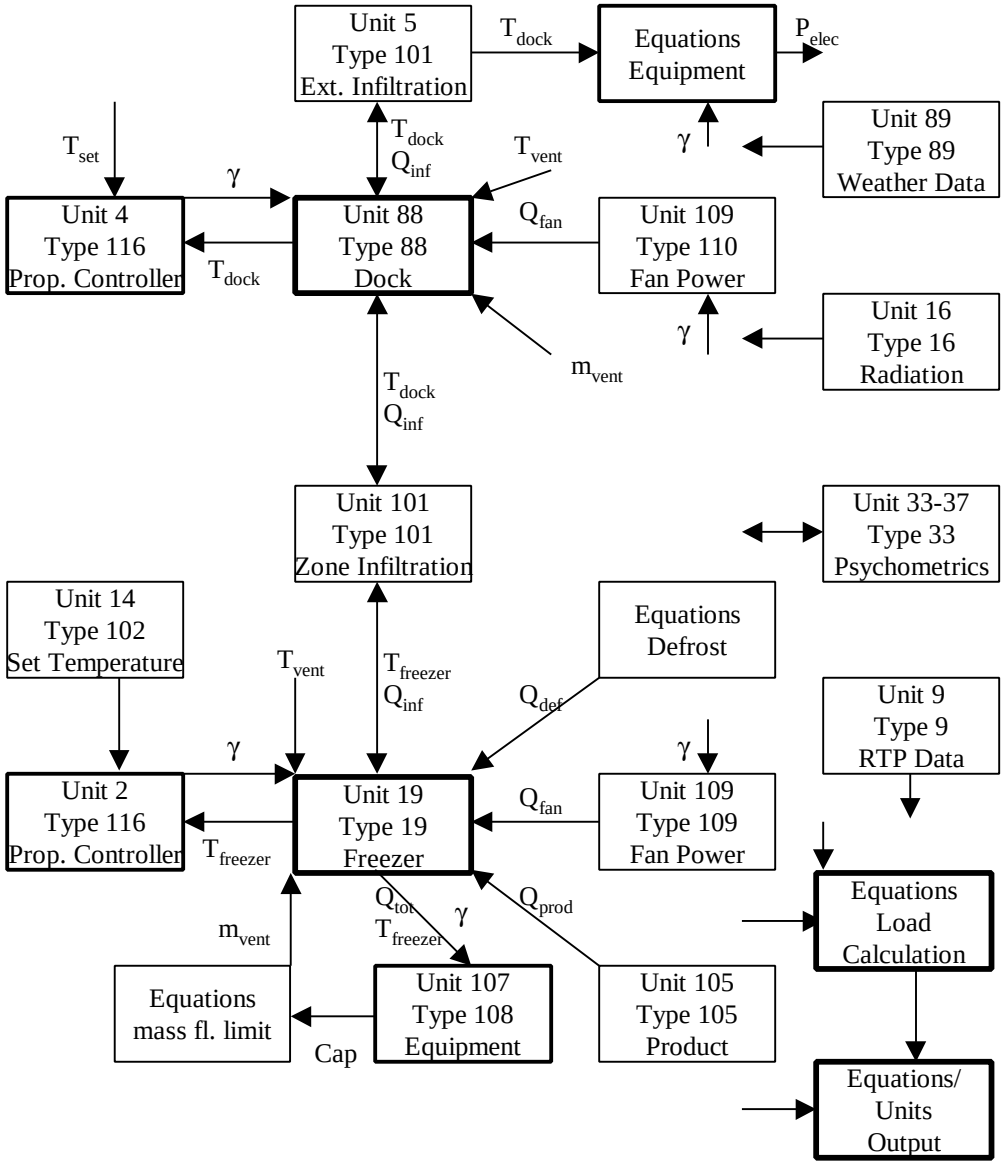

Figure 2-20: TRNSYS warehouse model.

Basically, the TRNSYS model can be divided into two parts: The Freezer model and the dock model. The two zones are linked by the infiltration air exchange between dock and freezer. The freezer and dock are linked to several components and sets of equations calculating the additional heat inputs, for example fan power and defrost. The weather data component and the radiation processor provide ambient conditions. The cooling load calculated by TYPE 19 is an input to the refrigeration equipment models, which compute the resulting electric power requirements. Several psychometric components

are needed to perform psychometric calculations and supply their outputs to other components. RTP data is read from a data file and is used to calculate the cost of operation of the warehouse. Finally, loads can be computed and output files are generated by printers and visualized by the online plotter.

2.7.2 Controlled variables

The controllers (see section 2.5) compare the respective set point temperatures to the actual temperatures of freezer and dock and give as output the control function γ, which is between 0 and 1. This control function is used to adjust the cooling air mass flow rate. For γ=1, the cooling air mass flow rates are set to their maximum value. With γ decreasing, the mass flow rates also decrease linearly. This decrease of mass flow rate can be compared to a time-averaged reduced mass flow rate through the evaporators in a real refrigerated warehouse. The discharge air temperature, which corresponds to the temperature of the air leaving the evaporators, is kept at the same value than for the maximum mass flow rate. Overall, the cooling supplied to the space decreases with the control function γ decreasing.

For the dock, sufficient cooling capacity is installed to maintain the set point over the entire year. The available compressor capacity is large enough for design ambient conditions and the dock set point of 1 °C (34 °F). For the freezer, the available cooling capacity depends on the desired freezer temperature. The design temperature for the freezer is –18 °C (-0 °F) and the equipment is sized to provide enough capacity for these conditions. If the freezer set point is colder than –18 °C (-0 °F), the maximum available cooling capacity that can be provided by the refrigeration equipment decreases. In order to cool the freezer down to the new set point, the controller will set the control function γ to 1, which would set the freezer air mass flow rate to its maximum value and supply the maximum possible cooling. With the freezer temperature decreasing, also the discharge air temperature has to decrease. The lower the discharge air temperature, the less cooling capacity is available. For the simulation this means that the cooling supplied to the space has to be adjusted to maximum available cooling capacity. A set of equations adjusts the cooling supplied to the space to the available capacity of the installed refrigeration

equipment. If the cooling provided (resulting from the cooling air mass flow and the discharge air temperature) would be more than the maximum available cooling capacity, the equations will reduce the cooling air mass flow rate to the value that corresponds to the actual available refrigeration system capacity.

2.8 Chapter Summary

A detailed model of a 100,000 ft^2 freezer with an adjoining 20,000 ft^2 loading dock was created in TRNSYS and is described in this chapter. During the model creation, different options of modeling were explored for the wall and the product modeling. Finite-difference models were compared to transfer-function approaches.

For the walls, a finite-difference model with three interior nodes and a transfer-function model give basically the same results. The results differ slightly, which is due to the way the transfer coefficients are calculated in PREP.

A transfer-function product model was also developed and compared to a finite-difference product model. The transfer-function model would offer increased calculation speed compared to the finite-difference product model. However, the transfer-function model included the assumption of a constant product core temperature. This assumption is justified for constant temperature warehouse operation, but for demand shifting associated with precooling, the constant core temperature assumption leads to different product heat flows because the long-term average freezer temperature can be different from the assumed core temperature. Furthermore, the finite-difference approach offers the possibility to easily monitor the product corner temperature, which is an important variable in demand shifting.

Chapter 3 Real-Time Pricing

3.1 Electricity Pricing

3.1.1 General considerations

In many end-use applications, the demand for energy is not constant over a given period of time. One way to balance supply of energy with the demand is to store energy when it is plentiful for use later when it is scarce. For example oil for heating a house is stored in a local tank within the house. Fluctuations in oil demand for meeting heating loads over a day do not affect the oil market; the storage tank buffers the effect. As a second example, a network of gas pipelines is also a form of storage to buffer short-term fluctuations in gas demand. For long-term storage, different types of storage are possible depending on the type of energy that has to be stored.

Unlike many sources of energy, electricity is a form of energy that is not easily (or cost-effectively) stored in large amounts. Therefore, the electricity supply has to continuously vary to meet the demand for electricity directly.

The demand for electricity can vary greatly depending on the time of the day, the day of the week and the time of the year. In order to provide electricity at all times, the generation capacity has to be sized to meet the maximum load that can occur, the peak load. Figure 3-1 shows an example electricity load profile over a day. The utility load over a 24 hour period is shown.

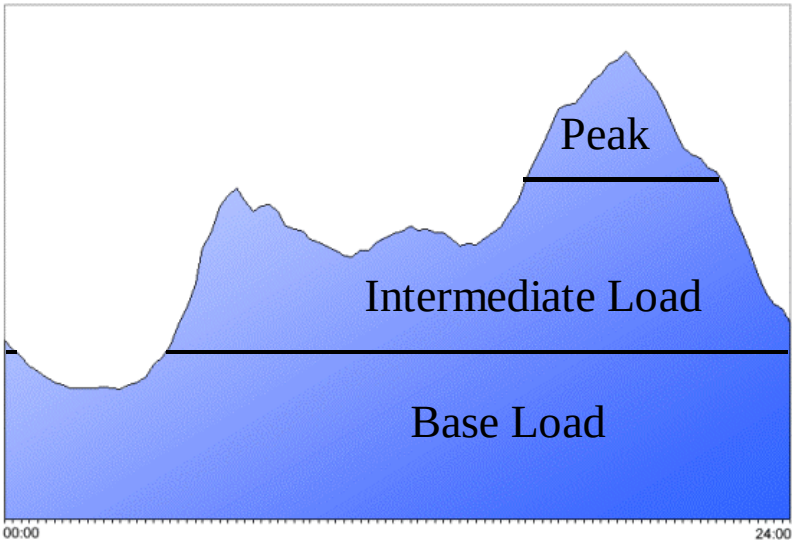

Figure 3-1: Example Load Profile

Usually, three different types of load are distinguished. The load that is relatively constant on the system most of the time is called base load. The intermediate load is present most time of the day and the peak load occurs only during a small fraction of time. Different types of power plants are used to supply the different kinds of loads economically. For the base load, power plants with a low operating cost but a higher investment cost are the most economically viable. For the medium loads, power plants might have a higher operating cost than the ones used for the base load, but a lower cost of investment. For the peak power plants, it is usually the investment cost that is low, even if the operating cost is much higher compared to a base load power plant. Another alternative for a utility to operating power plants is to buy electricity on the market if the market cost is cheaper than the cost of the power plant that would have to be run to cover the load.

From the above considerations it becomes obvious that cost of production for electricity can vary greatly. Contrary to that, the price that customers historically pay for electricity is constant compared to the strongly fluctuating production cost. The price of electricity charged to a customer is usually an average price of electricity that covers the fixed cost, variable cost and a reasonable profit.

One approach for reducing the cost of electricity production is to maximize capital utilization. This is accomplished by flattening out the aggregate demand profile. One way to accomplish demand leveling is to sell (by offering more attractive prices) more electricity at off-peak times when excess generating capacity is available. At the same time, limiting the demand at peak times can be accomplished by offering the electricity at higher prices. These concepts are grounded in basic macro economics supply/ demand principles.

In the past, many ways of giving customers incentives to shift or reduce their peak loads have been implemented. For example, larger customers often pay not only an energy charge for the electricity they consume but also a demand charge for their maximum electric demand in a given time period (usually billed based on the maximum observed demand during a 15 minute window over a month). This pricing scheme reflects the fact that the generating and transmission grid capacity has to be sized for the maximum power demand. If the customer manages to reduce his peak demand by shifting loads to off-peak times, but still uses the same amount of electric work over all, his electric bill is reduced.

3.1.2 Time-of-Use (TOU) pricing

A widely used utility rate structure is time-of-use pricing. Time-of-use pricing tariffs have been used efficiently for a long time. An on-peak and an off-peak energy charge replace the constant energy charge. In most cases, the off-peak period is during nights and weekends while the on-peak period occurs during daytime hours on weekdays. The off-peak energy price is cheaper than the price that would have to be paid on a flat rate pricing scheme while the on-peak price might be more expensive than the flat rate. In addition to energy charges, time-of-use pricing also includes demand charges. Often times, the demand, for billing purposes, is the maximum demand observed during on-peak hours only. If the customer can shift a significant share of his load to the off-peak period, cost savings can be achieved. Utilities on the other hand benefit from less peak load during the day and therefore pass on their lower off-peak production cost to the customer.

Time-of-use pricing schemes are a first step in bringing production cost and sale price of electricity closer together. The average cheaper off-peak production cost is reflected in the lower off-peak price, as is the higher production cost in the higher on-peak price. But still, time-of-use rates only reflect average trends in cost; they are still far away from assigning a price close to the production or market cost of electricity during certain times of the year. At peak times when electricity supply is short (in the United States in many states mainly on hot and humid summer days) the market cost for electricity can still be a multiple of the price the customer has to pay while at extreme off-peak times, the customer stills pays a price that is still a multiple of the actual market cost.

More recently, real-time pricing is an emerging rate structure developed in response to the trend in toward open markets and competition in the US electricity markets. It is based on the idea that the electricity price should always reflect the production cost of electricity.

3.2 Characteristics of Real-Time Pricing (RTP)

3.2.1 Basic characteristics

Real-time pricing is based on the idea that the electricity price should always reflect the current market conditions. Under a real-time pricing scheme, the electricity price is not constant but varies hour-by-hour. To give the customer time to react to the changing energy prices, he is usually notified one day in advance of the hourly electricity prices for the next day. But also schemes with hour-ahead notification are being pilot tested.

Utilities calculate electricity prices of the next day based on their own projected production costs for the next day. In some cases, neural network computer programs allow utilities to project hourly loads of the next day within a tolerance of a few percent. Based on these load projections, the utility decides which power plants will be used to meet the demand or also if it might be cheaper to buy the electricity on the market instead. Knowing the schedules for the next day for each power plant and the associated

production cost for the plants, the utility is able to project their hourly production cost and prices for the next day will be.

Ideally, in an open market the electricity price would settle at a value equal to the market marginal cost. The marginal cost can be defined as the cost of the most expensive unit that has to be operated to satisfy the demand (if the demand is not limited by the available overall capacity). Even if electricity is not traded on an open market, the real-time electricity price can be calculated based on the marginal cost of the most expensive unit. In reality, the actual electricity price is different from the marginal cost. It is adjusted to include other costs that are not marginal, for example for transmission and distribution. It also includes profits for the utility.

Figure 3-2 gives as an example the hourly real-time energy price for a warm summer day from PG&E.

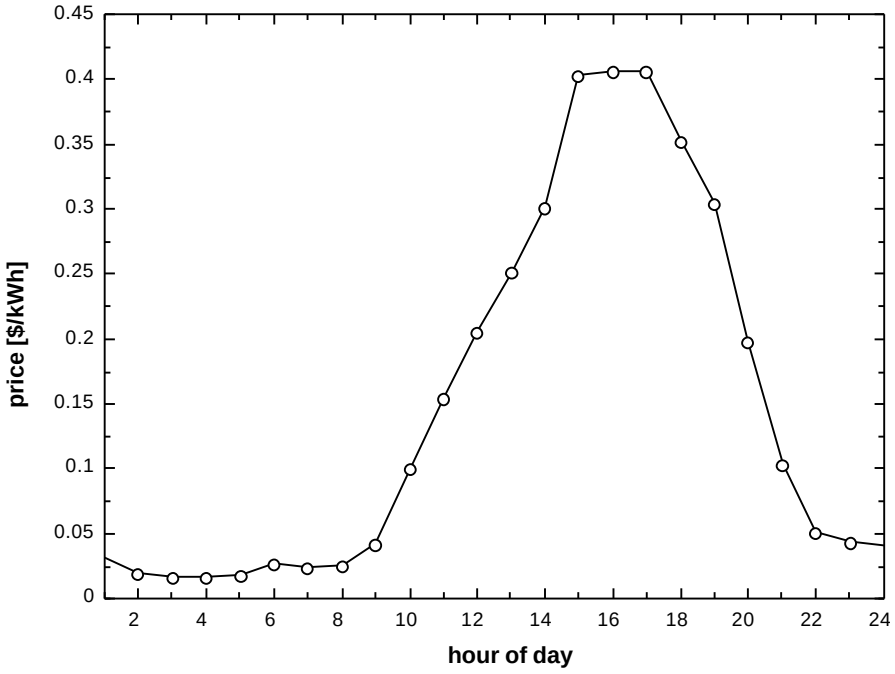

Figure 3-2: Hourly real-time energy price profile over a day.

The plot shows the great difference in electricity price over the day. At night, when demand is low and the production cost is cheap, the price is less than 0.02 $/kWh. In the afternoon hours, when demand is highest, the market cost of electricity and the production cost is much higher, the price peaks at $0.40/kWh. The above curve is for one specific day. On other days, the peak prices might be higher or lower and occur at different times of the day. Depending on the utility and the RTP scheme, the magnitude of prices and their profile over a day vary greatly.

3.2.2 One-part pricing and two-part pricing

Different RTP schemes have been developed by different utilities. Schemes can be categorized based on the number of parts the electricity bill of the customer consists of: one-part pricing and two-part pricing schemes.

- One-part pricing:
  In a one-part pricing scheme, all costs are included in the varying RTP rate. The price is based on the marginal cost. A constant factor is then applied to this marginal cost. The factor can be multiplicative or additive. This factor is determined in advance to cover all expected additional costs that are not marginal. The bill the customer receives is only dependent on how much electricity he used at a given time. For example, if the customer manages to reduce his electricity consumption at a certain hour, the price he has to pay for that hour is not only reduced by the marginal cost (which would approximately correspond to the reduction in cost for the utility), but also by the marginal cost modified by the factor.

- Two-part pricing:
  In a two-part pricing scheme, the customer bill consists of two parts. The first part is the energy cost determined from the RTP prices and the customer's load profile that occurred. The RTP prices are usually set very close to the marginal cost and do not cover any additional costs. The second part is a so-called access fee. This access fee is not constant like the factor in the one-part scheme. It is the difference between what the customer pays for the first part and what he would pay under a standard rate

with a predefined load profile, the so-called customer baseline load (CBL). This baseline load could, for example, be the customer load profile before he switched to RTP. In that case, the customer would still pay the same price under RTP than he did before if his load profile has not changed. If the customer manages to switch loads to cheaper times, his electricity bill will also be reduced, but the reduction would be smaller than under a one-part scheme

One-part and two-part pricing are only two classifications, and mixtures with elements from each category are possible.

3.2.3 Advantages and disadvantages of RTP

Each of the RTP pricing options discussed above offers advantages and disadvantages. The biggest advantage of the one-part pricing scheme is its simplicity. It is easy to understand for the customer, there is only one part in his electricity bill and the price he has to pay is directly proportional to the hourly usage. Increase or decrease in usage is directly reflected in the bill. Compared to that, the two-part scheme is more complex. Differences in usage change the first part of the customer's bill, which reflects the actual usage. But the change in the first part is then partly compensated by the changed access fee, the second part of the bill.

The greater fluctuations of prices in the one-part pricing result in more uncertainty for the customer and the utility. One might realize increased savings while the other partner realizes increased costs. The RTP prices in the one-part scheme are not as close to the marginal cost as they are set in the two-part scheme, the changes in production cost for the utility if the customer shifts loads can be significantly different from the changes in price the customer pays. Under a one-part scheme, the change in price therefore does not reflect the change in cost that actually occurs. The more complicated two-part scheme with the RTP prices close to marginal cost is much closer to change in cost that actually occurs. Besides, because of the customer baseline load idea, the two-part scheme guaranties the customer the same bill under RTP if he does not change his load profile than he would have to pay under a standard rate.

Overall, RTP is an innovative pricing approach that offers many new possibilities to customers and utilities in a liberalized electricity market. For the first time in the history of electricity pricing, prices reflect costs as they really occur. Prices that represent real costs and not just averages of costs offer incentives to market participants to adjust their behavior in response to the cost. Therefore, RTP is a means to balance supply of and demand for electricity in a manner that is economically more efficient than with standard rates.

Ideally, RTP offers the possibility of cost savings for both the customer and the utility. For the customer, shifting loads to cheaper hours can save money, while the utility is able to operate more efficiently due to their flattened aggregate demand profile. In addition, real-time pricing offers the possibility for the utility to shift its operational risk to the customer. Instead of having to estimate their average production cost over a longer period of time in advance, the pricing risk for the utility under RTP is only limited to the next 24 hours. Since the customer takes on more risk, he should be rewarded with the potential for reduced energy costs. In reality, it is reasonable to question whether or not the additional risk for the customer is justified by the reduced energy costs being offered.

RTP introduces new problems of control for the customer: What is the most efficient way for the customer to react to the prices? Simple solutions usually do not exist and finding the "optimal" solution might be impossible with too many variables involved in the problem. Introducing RTP rate structures adds a new dimension of complexity to electricity consumption. On the other hand, introducing RTP rates also brings back energy pricing into focus of the customer. The customer might no longer see his energy cost as a fixed cost that cannot be changed. Besides reacting to the RTP rates, the customer might also become aware of other possibilities of energy and cost savings. For the utility, the new awareness of the customer for his energy needs offers new possibilities of customer care. The utility can assist the customer in his needs for energy consulting, sell new services and enter a new state of relationship with the customer.

Typically, shifting loads is associated with additional costs for labor, for control or for energy storage. Can these additional costs (that often include initial investment costs for equipment to react to RTP) be justified with the expected future savings? It is not only the uncertainty to what extent loads can be shifted after measures have been implemented, but also the development of future RTP prices is uncertain. Utilities might change the way they determine the RTP prices. Furthermore, the more customers react to RTP and shift their loads to off-peak hours, the off-peak might no longer be a real off-peak and prices would no longer be cheap during these hours. The more RTP becomes successful, the less attractive it might become because of a smaller price differential between peak and off-peak.

3.3 RTP Pricing Structures

3.3.1 Data investigated

RTP data from three different utilities has been obtained and these provide the basis for the present pricing investigation. Data sets were obtained for the years 1997 and 1998 from Pacific Gas and Electric (PG&E) serving northern California, data sets for the same two years from the subsidiary of Southern Company, Alabama Power, and one year of data from September 1998 to August 1999 from Niagara Mohawk Power, which serves New York State. PG&E offers a one-part pricing structure, while Southern and Niagara Mohawk offer two-part pricing structures.

3.3.2 Monthly averages

The followings diagrams show the monthly average hourly real time prices for the year 1998 from PG&E and Southern, and for the period in 1998/99 considered from Niagara Mohawk.

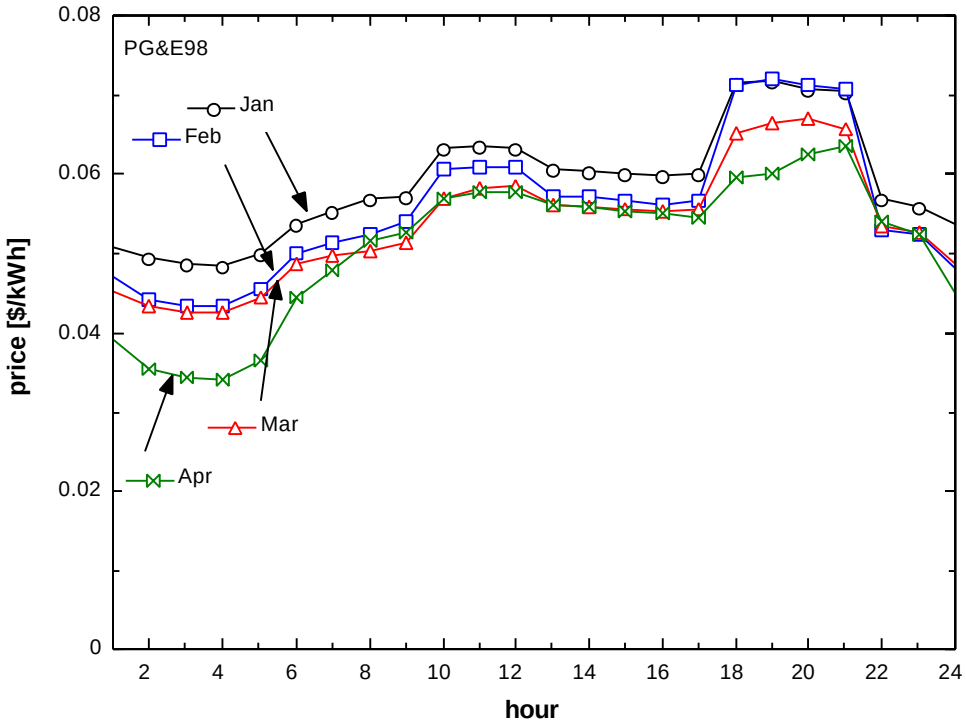

Figure 3-3: Monthly average hourly RTP prices for PG&E from January to April 1998

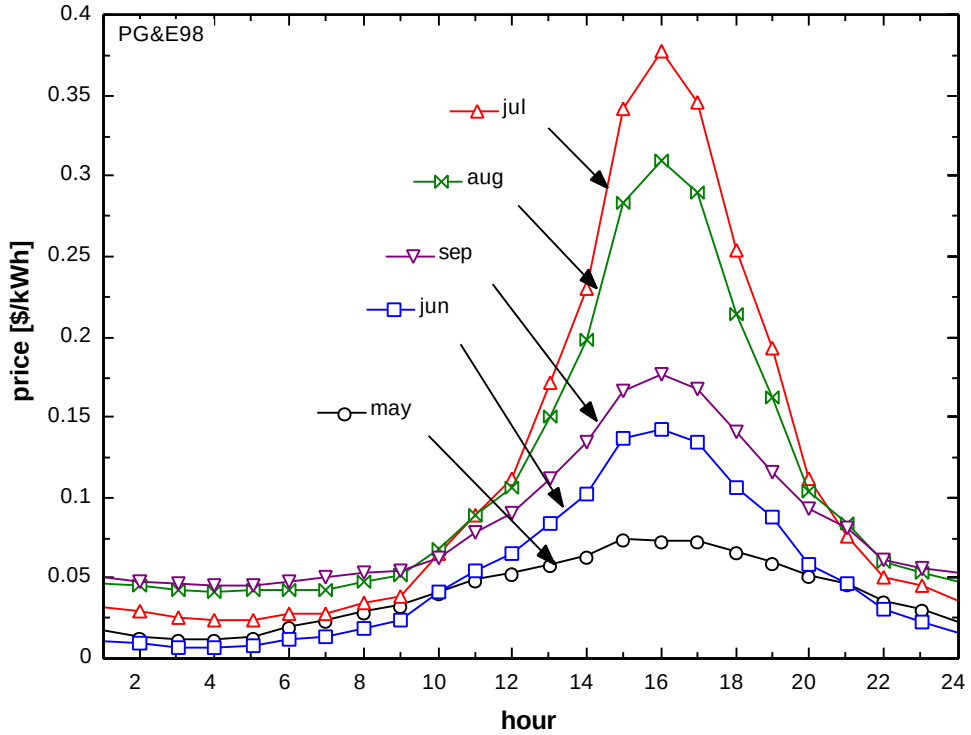

Figure 3-4: Monthly average hourly RTP prices for PG&E from May to September 1998

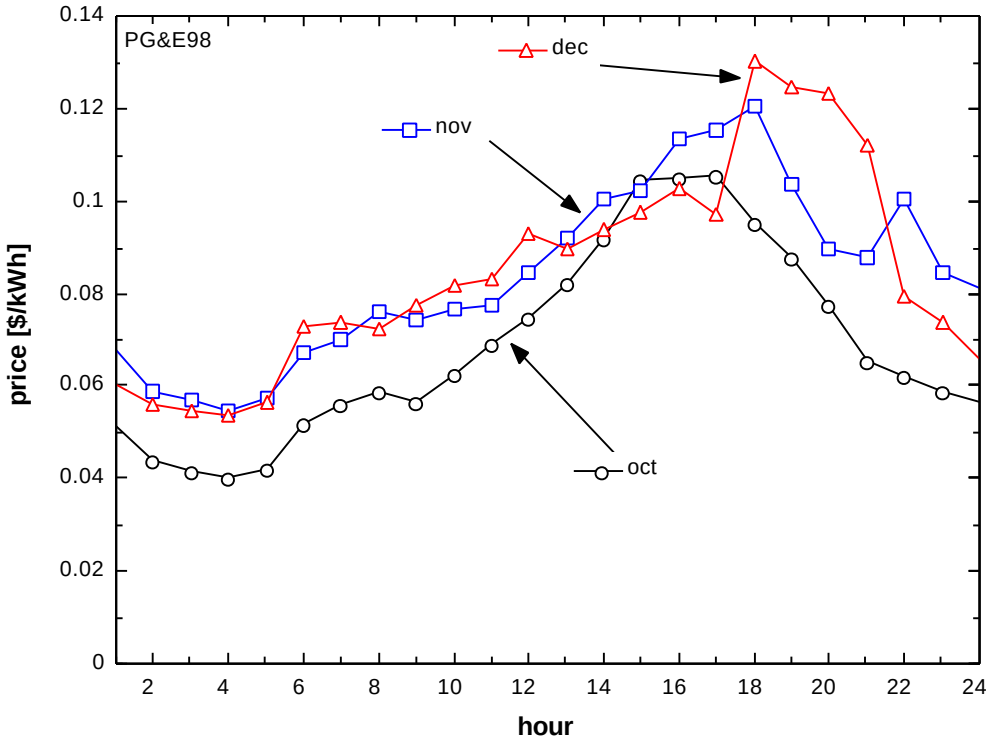

Figure 3-5: Monthly average hourly RTP prices for PG&E from October to December 1998.

The PG&E prices can be categorized depending on the month. The average price profiles for the first four months of the year are all similar in shape. A three to four hour price peak occurs after 6 p.m. A less distinct second peak can be found before noon. Nighttime prices are generally lower. The warmer climate in April with less demand for energy at night is a likely reason for the lower prices.

In contrast to the spring months, during the summer months (May – Sept) the peak prices occur around 4:30 p.m. (hour 16/ hour 17). While in May the average peak price is still 0.07 $/kWh, in July the average peak reaches 0.38 $/kWh. The nighttime prices in May and June are very low at about 0.01 to 0.02 $/kWh.

The last three months of the year illustrate the transition from the typical summer curves to the winter curves. In October the peak is still around 4:30 p.m., in November and December the peak shifts to later hours. The 1998 prices in November and December are somewhat higher than the corresponding prices in 1997, which were more similar to the

January and February prices in 1998. The change might be due to higher demand in 1998 or to changes in the method of price calculation in that year.

The next three plots show the average RTP prices of Southern Company.

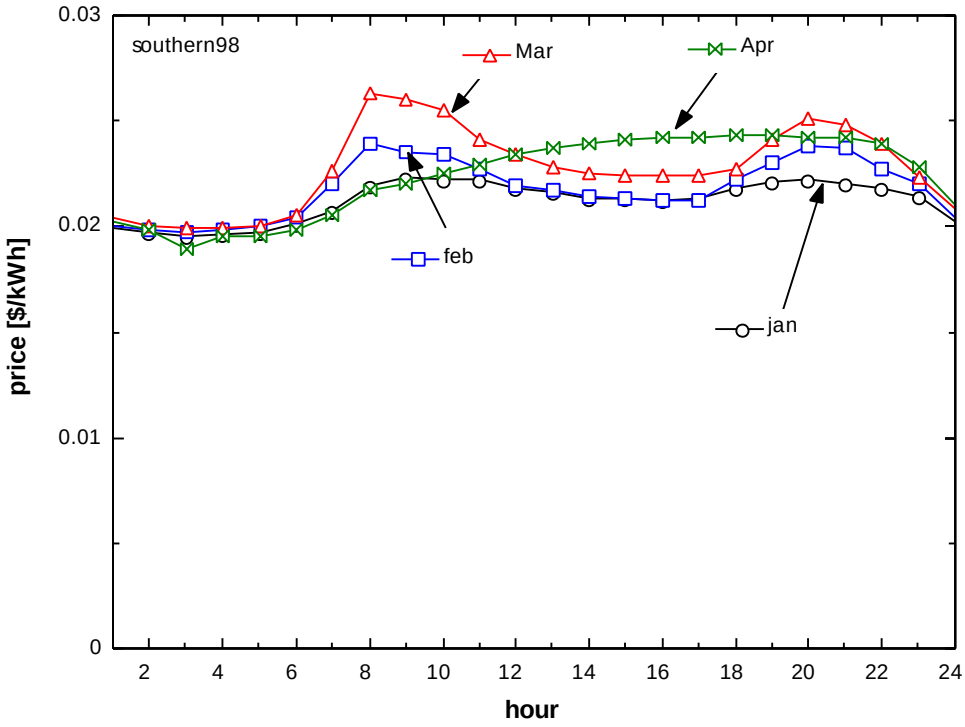

Figure 3-6: Monthly average hourly RTP prices for Southern from January to April 1998.

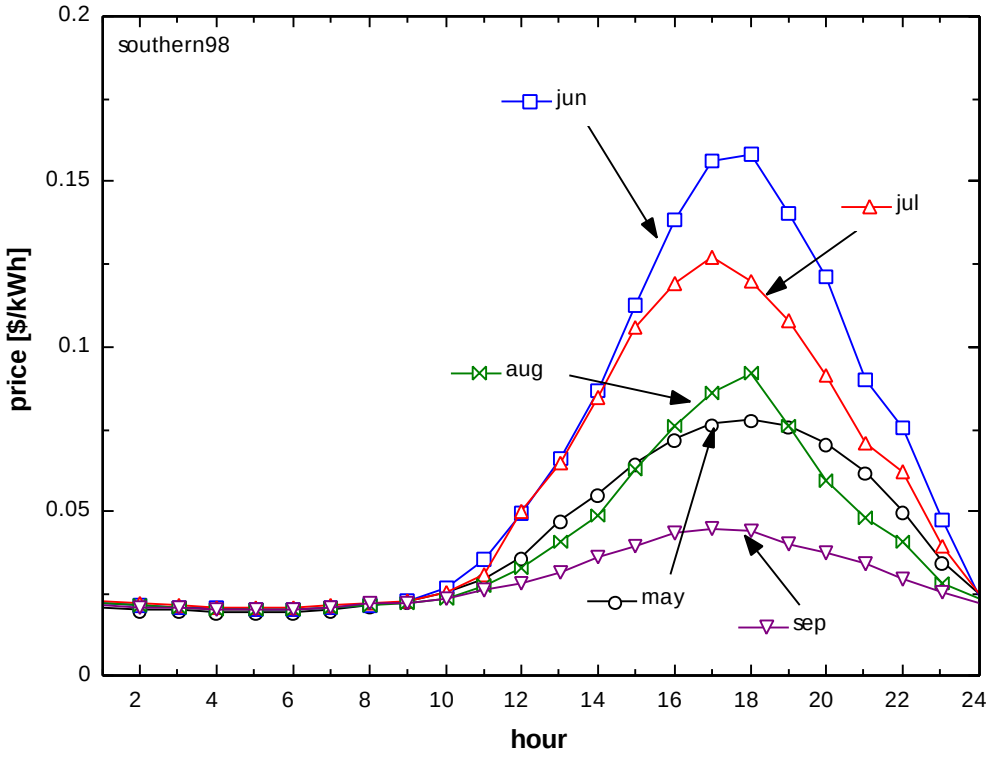

Figure 3-7: Monthly average hourly RTP prices for Southern from May to August 1998.

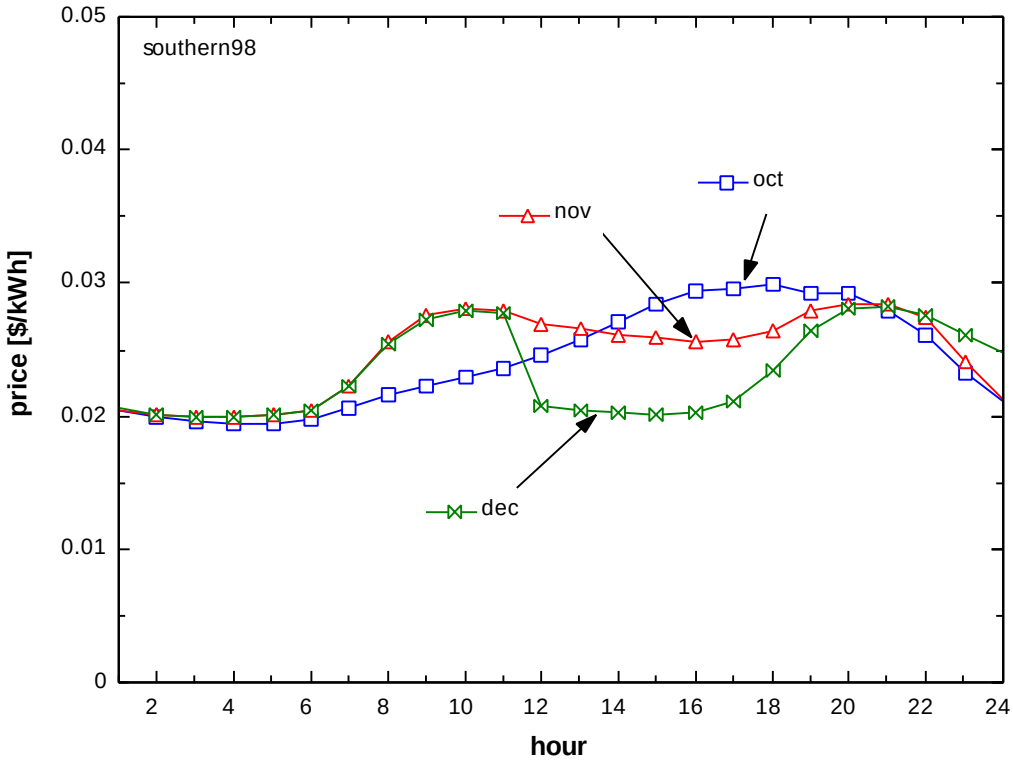

Figure 3-8: Monthly average hourly RTP prices for Southern from October to December 1998.

The difference between the one-part pricing of PG&E and the two-part pricing of Southern can be clearly seen by comparing the average prices over the year. The Southern prices vary much less than those from PG&E.

The average prices in spring are relatively constant around 0.02 to 0.025 $/kWh. For January, February and April, similar peaks to PG&E can be found. The first is before noon and the second is after 6 p.m. The difference between the average peak and the lowest price is much smaller than for PG&E. In the summer months, the peak shifts again to the later afternoon. The average nighttime price is practically constant for all summer months. The last four months of the year show again the transition to the winter pattern. October still has its peak in the afternoon; November and December show the two-peak pattern typical for the winter month. The different scaling of the plots makes the winter prices look more variable than they are compared to the summer prices, but average daily price fluctuations in winter are less than 0.01 $/kWh.

Price patterns in 1997 and 1998 are similar for most of the colder months. But an interesting change occurred from 97 to 98 for the summer months. While in 1998, peak prices in May, June, July and August reached nearly 0.5 $/kWh, peak prices during these months in 1997 reached only 0.15 $/kWh. This change in prices can hardly be explained by a change in demand between the two years, but rather by a changed method of calculation for the real-time prices.

The next plots show the prices from Niagara Mohawk Power. The data obtained starts in September 1998 and ends in August 1999. Nevertheless the plots are sorted from January to December.

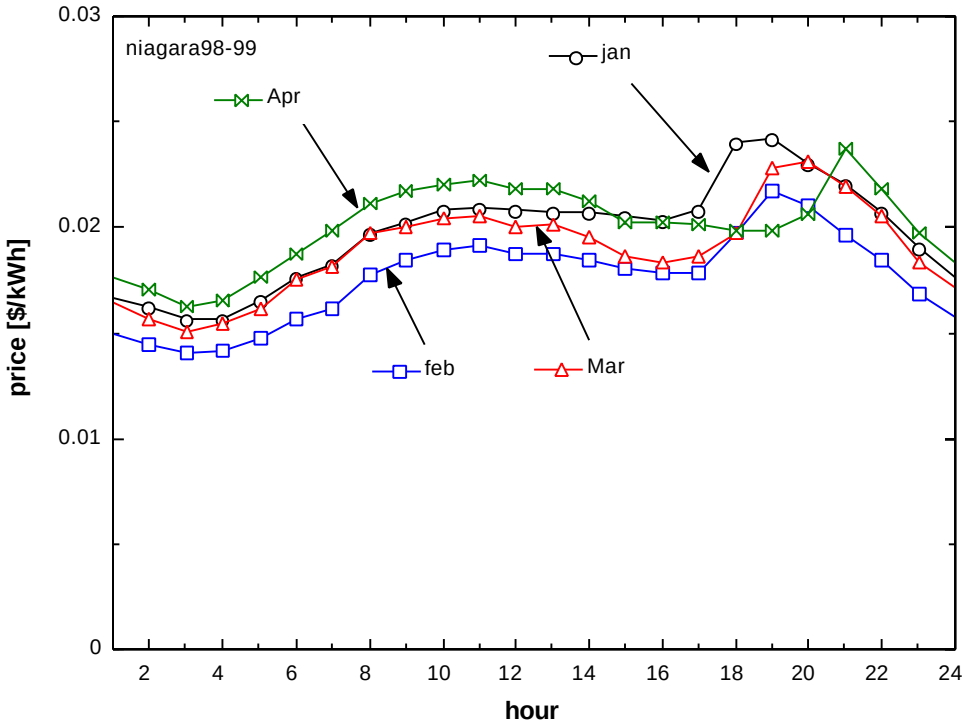

Figure 3-9: Monthly average hourly RTP prices for Niagara Mohawk from January to April 1999.

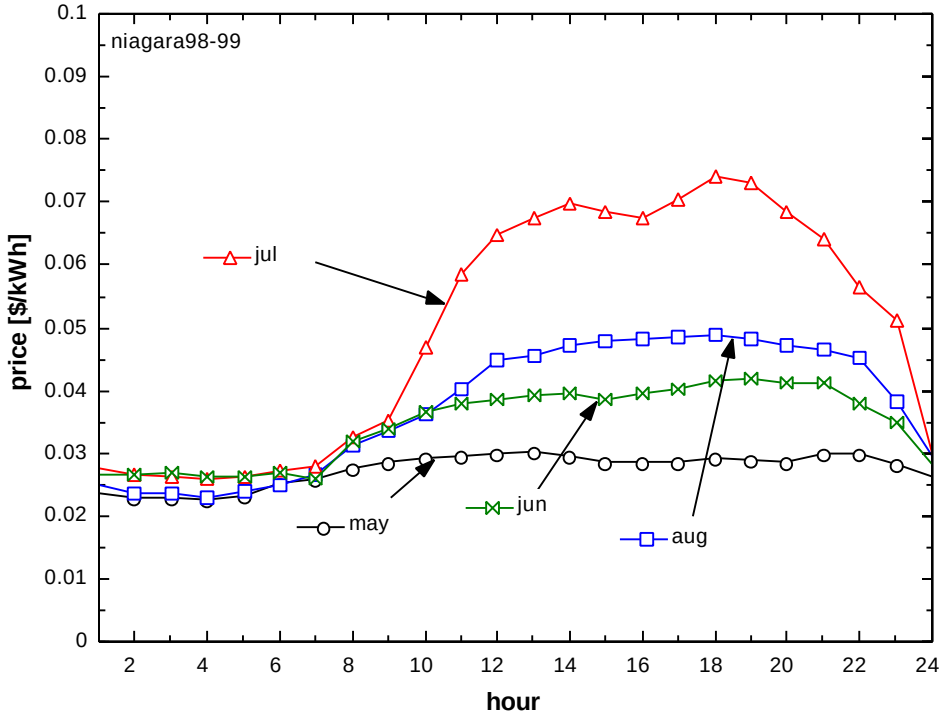

Figure 3-10: Monthly average hourly RTP prices for Niagara Mohawk from May to August 1999.

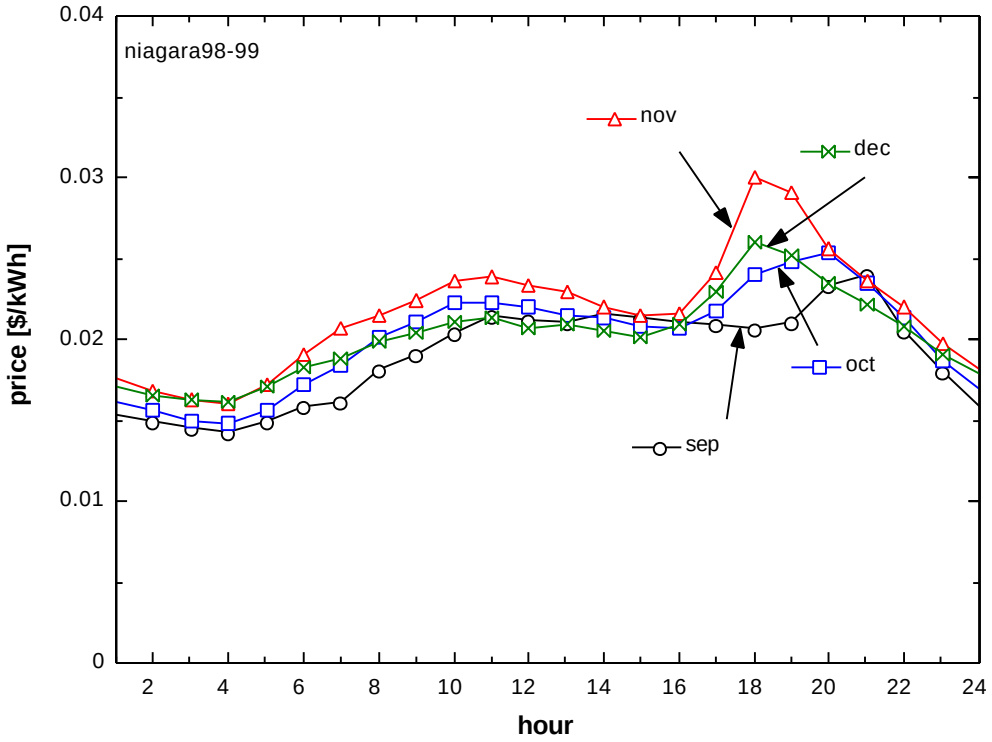

Figure 3-11: Monthly average hourly RTP prices for Niagara Mohawk from September to December 1998.

The prices in the Niagara two-part pricing scheme fluctuate even less than the Southern prices. Most times of the year, the average peak price does not exceed 0.03 $/kWh. Only during the three summer months, average prices are higher, reaching up to 0.07 $/kWh. In the winter months, the two-peak pattern exists again. For the summer months, it is difficult to recognize an explicit peak time. In general daytime prices are higher than nighttime prices, but the price curves are still relatively flat compared to the curves of the other two data sets. It becomes obvious that the Niagara pricing scheme offers much less incentive to shift loads to off-peak hours because of the much lower difference between highest and lowest price.

3.3.3 Price fluctuations in month

The average prices presented in the preceding section give a first overview of what RTP schemes have in common and also how distinct they can be. The difference between the peak price and the average daily price is a good measure of how beneficial it would be to shift electrical usage. The more concentrated the high peak prices are in a few hours, the easier it is to take measures to shift electric demand. The flatter the price curve is, the

less incentive is given to shift demand. How prices fluctuate from day to day is also an important consideration. The less that prices fluctuate from day to day, the easier it is to size equipment associated with shifting loads. The plots in this section show the price fluctuations within a month. The section after investigates day-to-day fluctuations.

PG&E

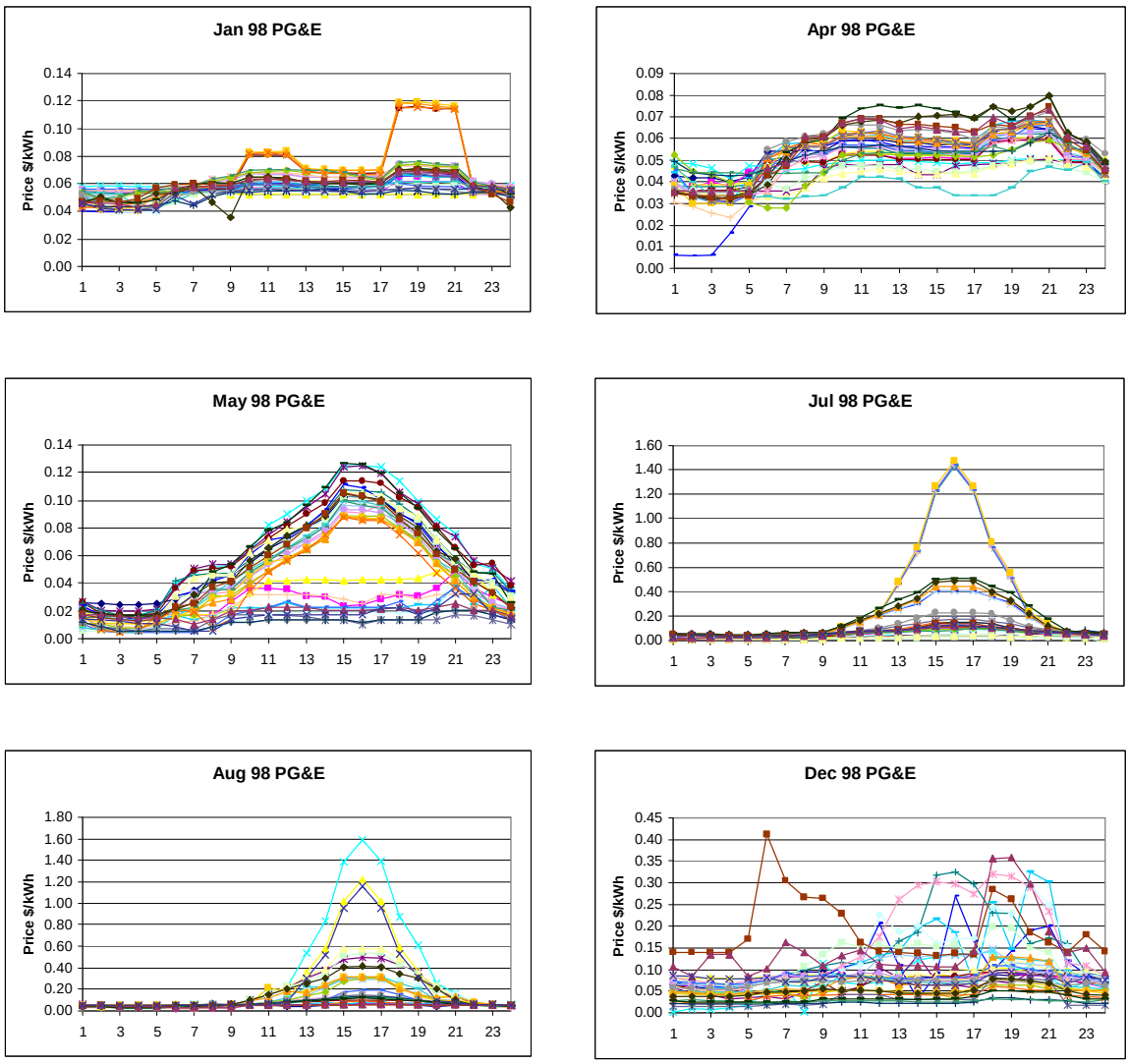

Figure 3-12: Variation in PG&E RTP daily prices for selected months.

The RTP prices of PG&E fluctuate depending on the month. Prices in January are the same for most of the days with a few exceptions where peak prices before noon and in the afternoon increase more than on the other days. Most April price curves have the

same shape, but depending on the day, prices might be up to 0.04 $/kWh higher than in other days. In May, basically two price patterns are visible: a flat price pattern with daytime prices closer to nighttime prices and many days with an explicit peak at about 0.12 $/kWh in the afternoon. The two hottest months of the year, July and August, show the most extreme real-time prices. Most of the days, the peak prices do not exceed 0.2 $/kWh, but on several days, prices reach up to 1.60 $/kWh. Facing RTP prices that high can lead to unpredictable changes in energy costs for the customer. If the customer is not able to shift loads away from the most expensive hours, the savings realized during the rest of the year will be compromised very quickly. Interestingly, the most expensive days have all peak prices at exactly $1.20, $1.40 and $1.60/kWh. These rounded up prices suggest that they are not result of a complicated computer calculation but probably set "by hand".

December is one of the least homogeneous months. Peaks occur at different times of the days and peak prices might reach levels of up to 0.4 $/kWh.

Overall, the PG&E prices seem to follow a pattern depending on the time of the year most days. Depending on the time of the year, many days are in the same price range. But days exist that are far off the average. Days with extreme prices, mainly during the summer months, have to be considered because their high prices can strongly influence the yearly energy cost.

Southern

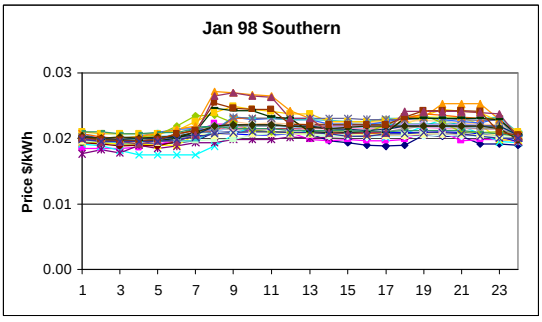

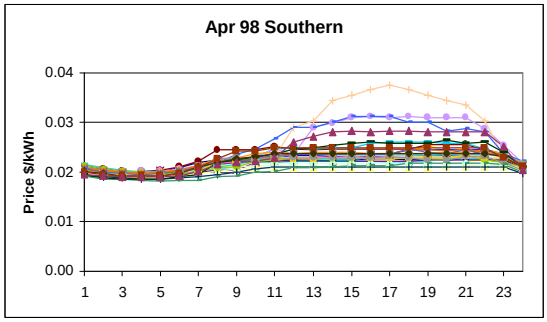

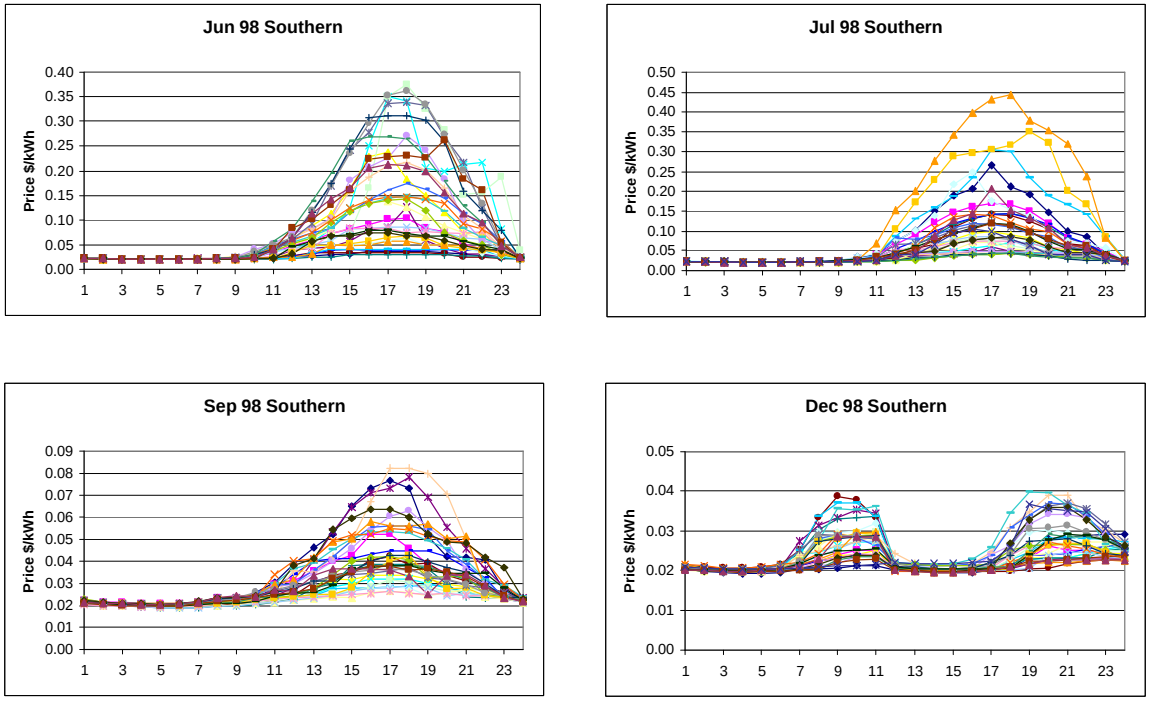

Figure 3-13: Variation in Southern daily RTP prices for selected months.

Compared to PG&E, the prices of Southern are more homogenous. Extreme days that are far off the average like in the PG&E pricing scheme are not common.

January and April are two very homogenous months. Prices are between 0.02 and 0.03 $/kWh nearly all days. In summer, prices peak at 0.45 $/kWh, which is far below the $1.60/kWh from PG&E. June has a relatively homogenous price distribution, peak prices are evenly distributed between 0.02 and 0.37 $/kWh. In July, many peak prices are around 0.2 $/kWh. The September price distribution looks similar to the one in June, but the peak prices are generally lower, which means that price variations are much smaller. The December plot shows very constant prices at off peak times and two peaks located before noon and at night. Around the peaks, prices vary between 0.02 and 0.04 $/kWh.

Niagara

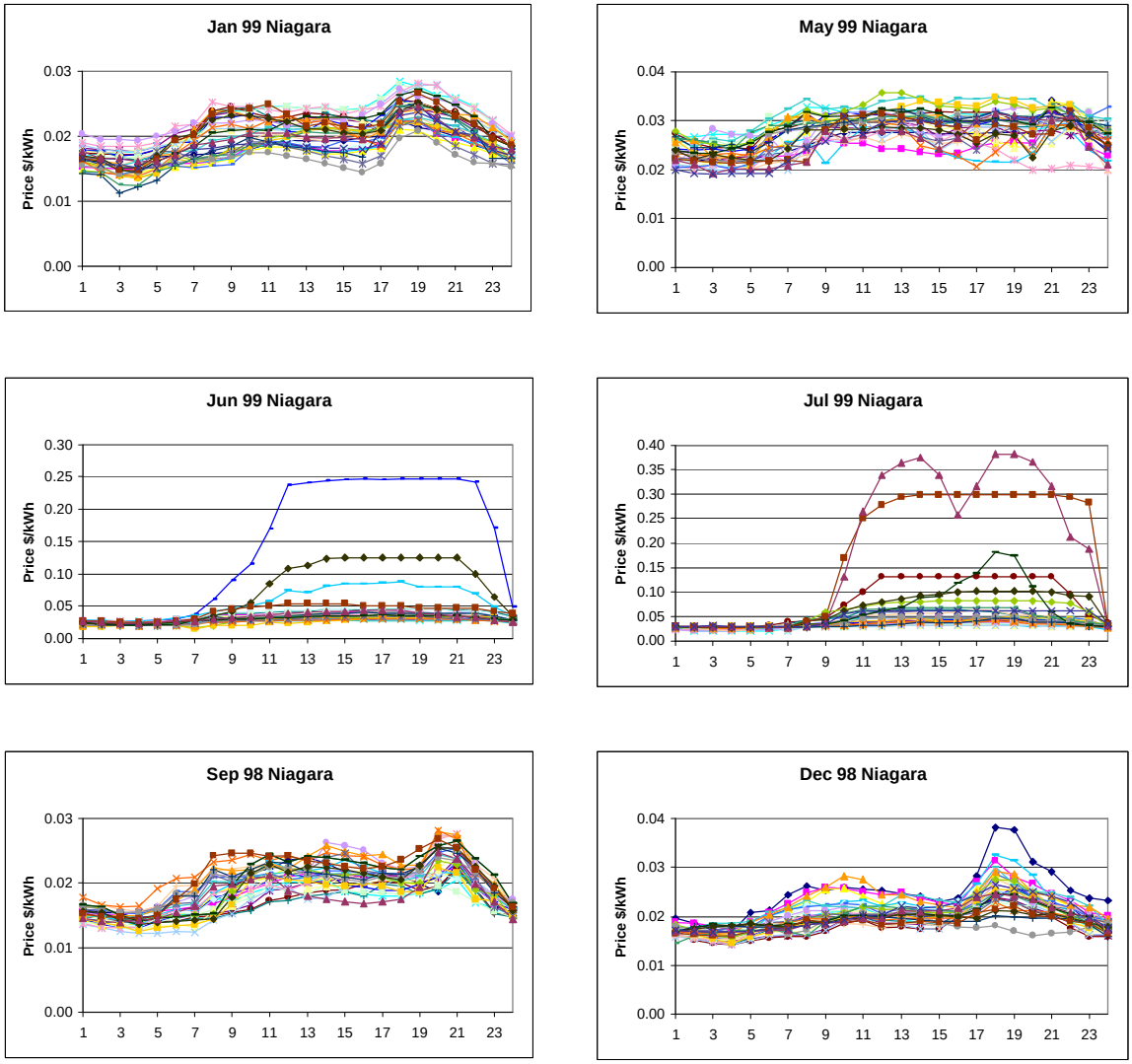

Figure 3-14: Variation in Niagara Mohawk daily RTP prices for selected months.

Comparing the prices of Niagara Mohawk within a month to the other sets of data, it can be observed that they are the least fluctuating. In January, May and September, price fluctuations are less than 0.01 $/kWh from day to day. Only on a few days in the months of June and July, prices reach a much higher level than average. Still, peak prices are low compared to the other utility prices.

3.3.4 Daily price fluctuations

Besides looking at the distribution of the RTP prices in a month, it is interesting to investigate a series of RTP prices over consecutive days. The first series of plots shows the prices from May 7th to May 12th from PG&E in 1998.

PG&E

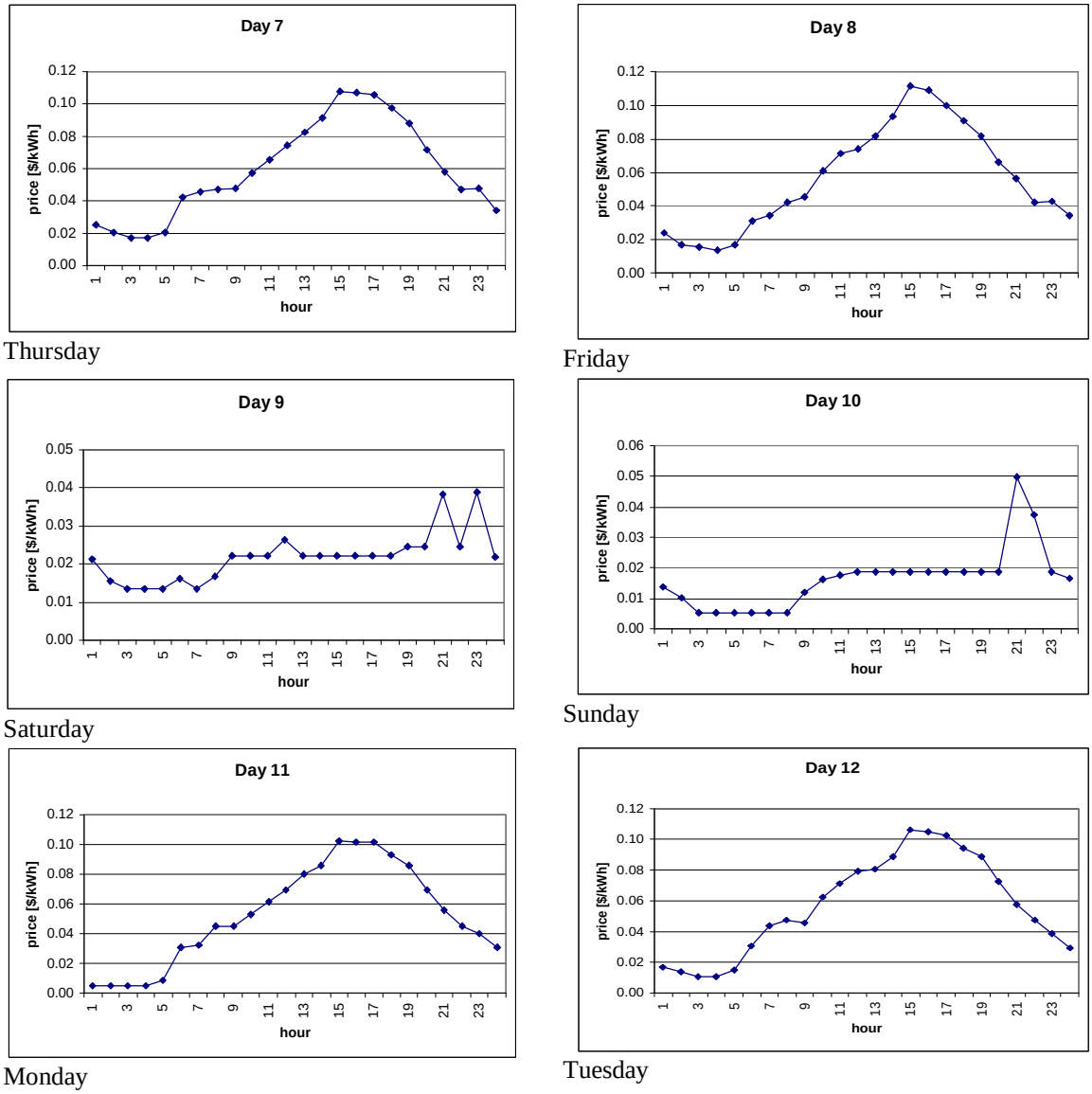

Figure 3-15: PG&E prices from May 7th to May 12th 1998

In Figure 3-15, weekdays can be clearly distinguished from weekends. Days 9 and 10 are weekends. The lower aggregate utility loads on the weekends are also reflected in the

prices. While weekend prices rarely exceed 0.04 $/kWh and the short peak is located in the late evening, during the week prices reach over 0.1 $/kWh and the much longer peak is centered around 4:30 p.m.

The next series in Figure 3-16 shows probably the most expensive series of days from PG&E in July 1998.

PG&E

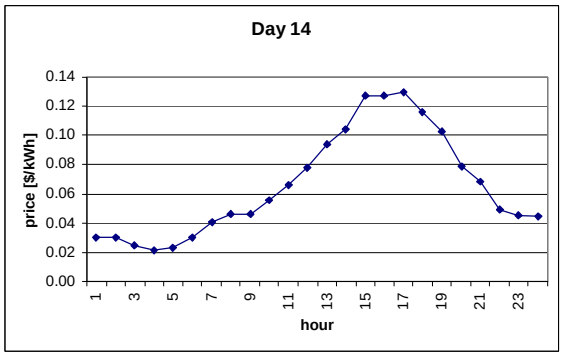

Tuesday

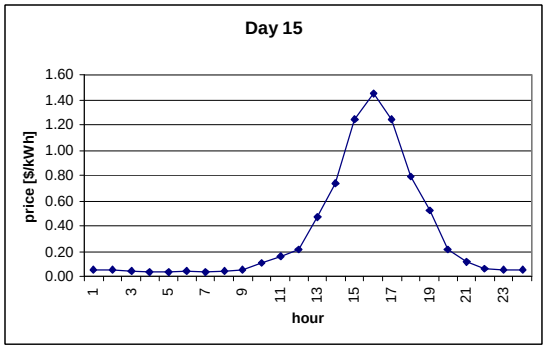

Wednesday

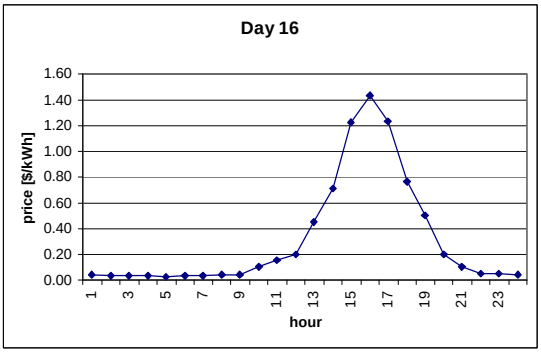

Thursday

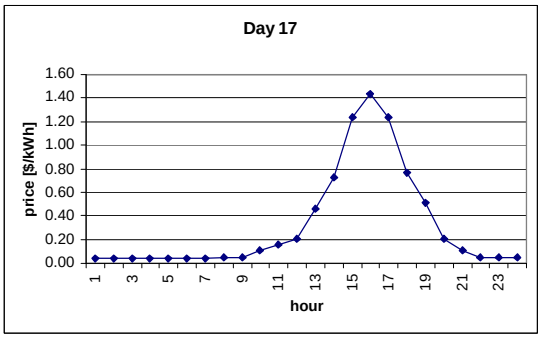

Friday

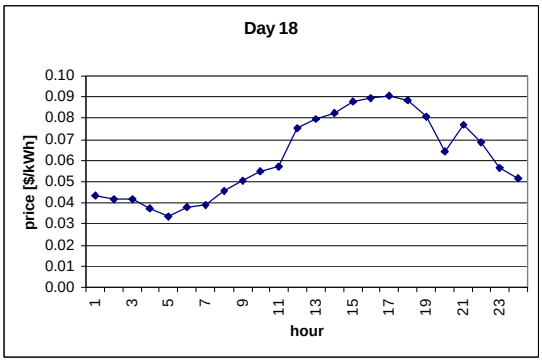

Saturday

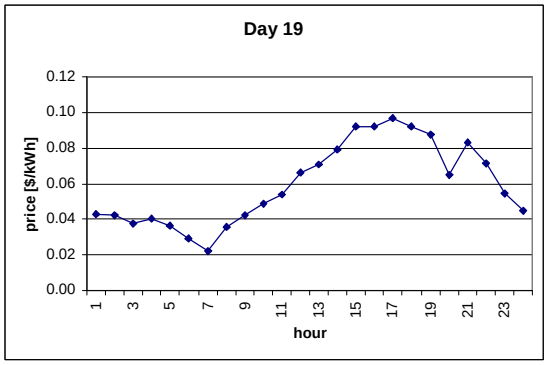

Sunday

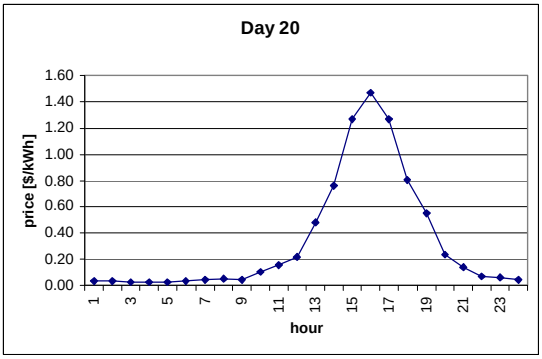

Monday

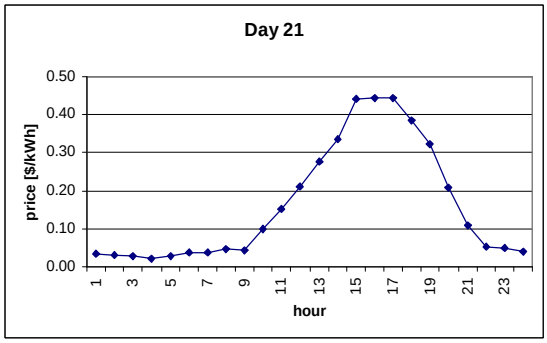

Tuesday

Figure 3-16: PG&E prices from July 14th to July 21st 1998

From one day to another, peak prices change from 0.12 $/kWh to 1.40$/kWh. This change in price can hardly be explained by a change in demand from one day to another. Reasons for explanation must found besides pure consideration of production cost. The peak price of up to 1.60 $/kWh is more probably close to the price that has to be paid on the electricity market at a day when electricity is short in a larger region. The very high prices might also be seen as a very clear signal to the customer to shift loads on these days.

In December 1998, shown in the next figure, the PG&E RTP prices are again very fluctuating. On one day, the peak is at a different time and of a different length than on another day. The prices during the week are higher than the weekend prices.

PG&E

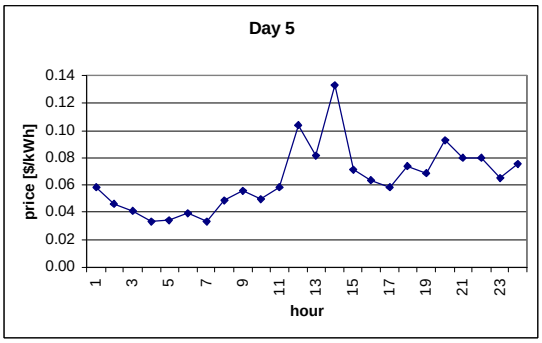

Saturday

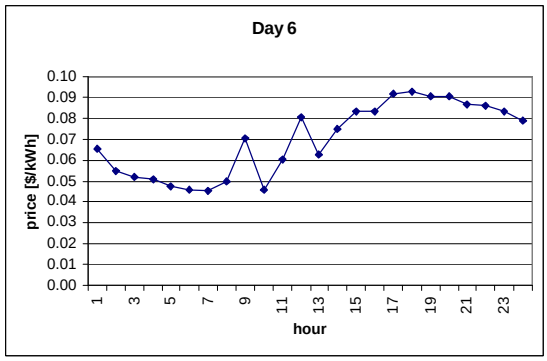

Sunday

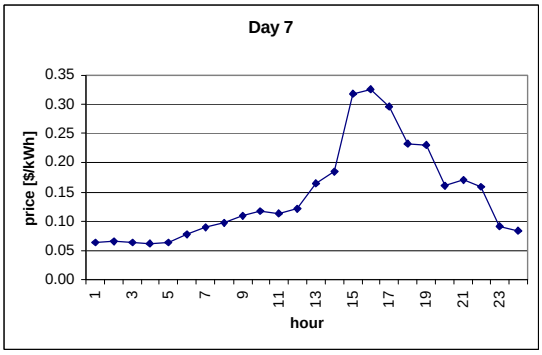

Monday

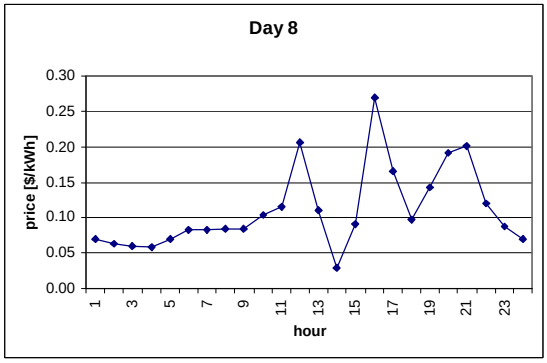

Tuesday

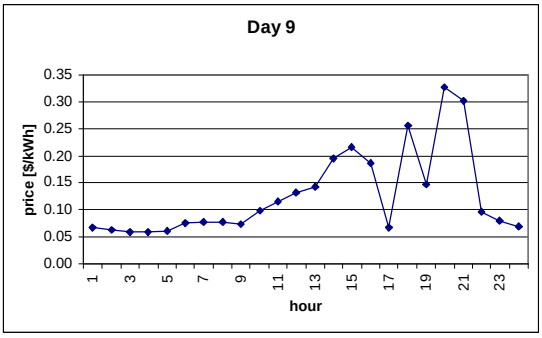

Wednesday

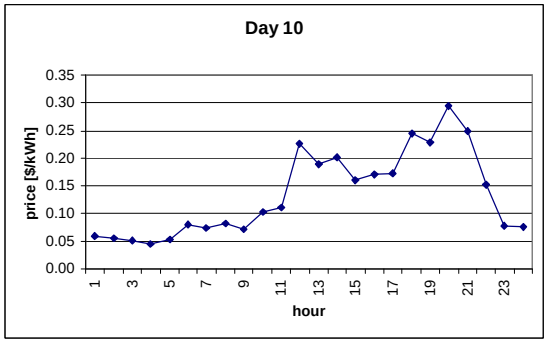

Thursday

Figure 3-17: PG&E prices from December 5th to December 10th 1998

The Southern prices are much less variable than the PG&E prices. For example, for the month of January shown in Figure 3-18, the price curves hardly change from day to day and even the weekend curves have the same shape as workday curves. Only in the summer months are differences between the single days significant. The following Southern price curves are for a series of days in June 1998.

Southern

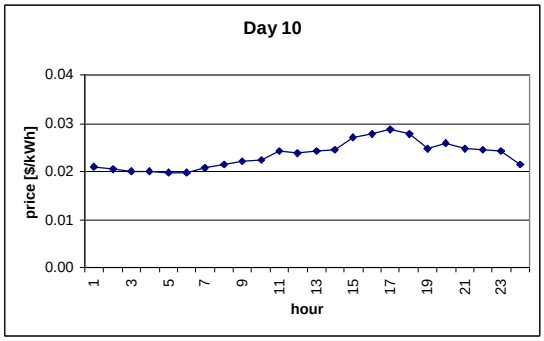

Wednesday

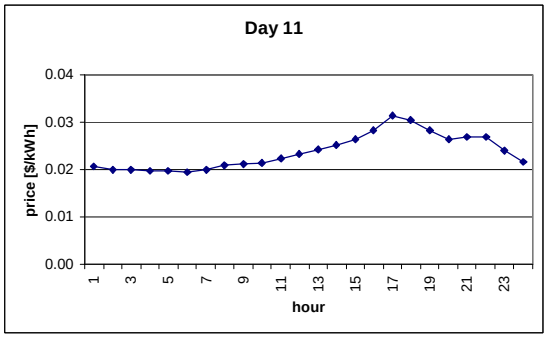

Thursday

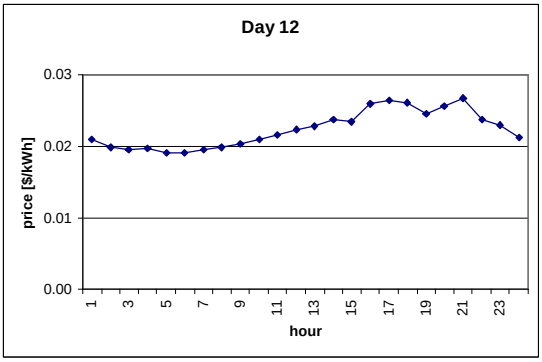

Friday

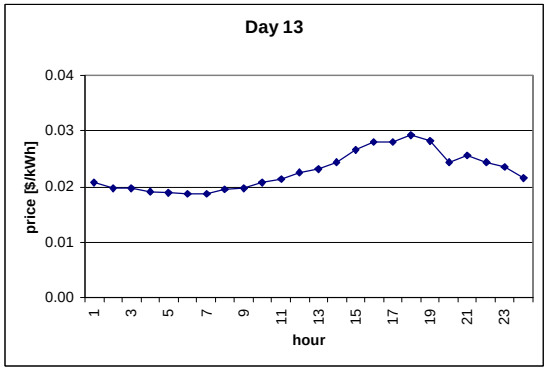

Saturday

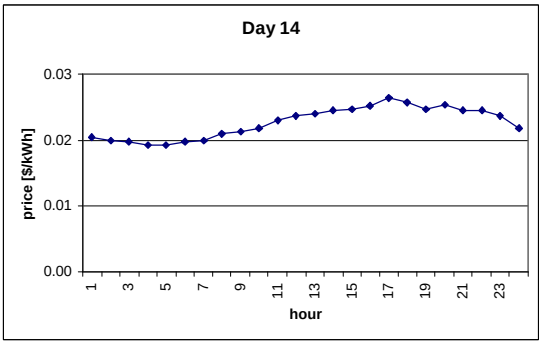

Sunday

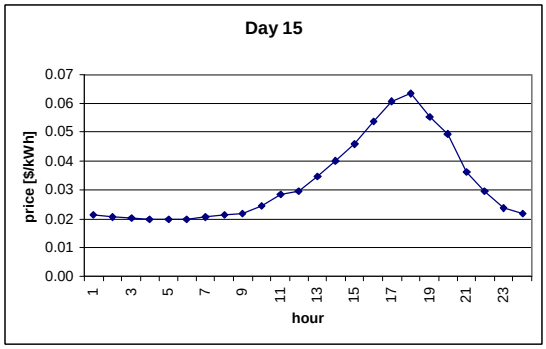

Monday

Figure 3-18: Southern prices from June 10th to June 15th

The first five out of the six days shown are all of the same daily price profile. Prices are relatively constant over the day and a flat peak is in the afternoon. Only Monday, June 15th is of a different type: The peak price is much higher and more clearly distinguishable. The weekend prices (Day 13 and 14) are the same than the weekday prices.

In December, the price curves between weekdays and weekend are relatively similar as shown in Figure 3-19.

Southern

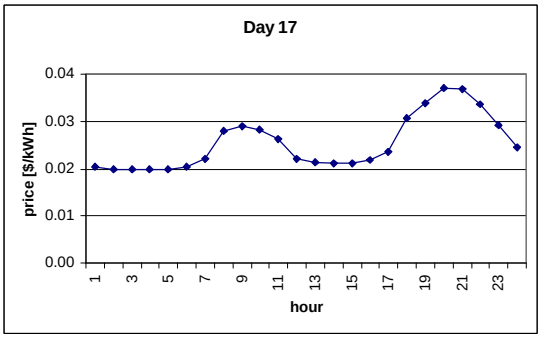

Thursday

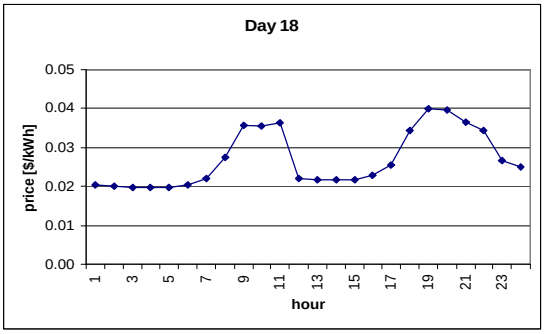

Friday

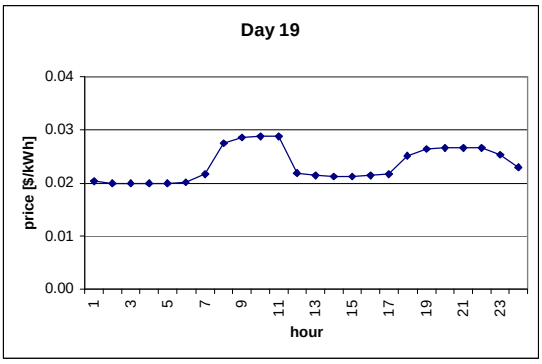

Saturday

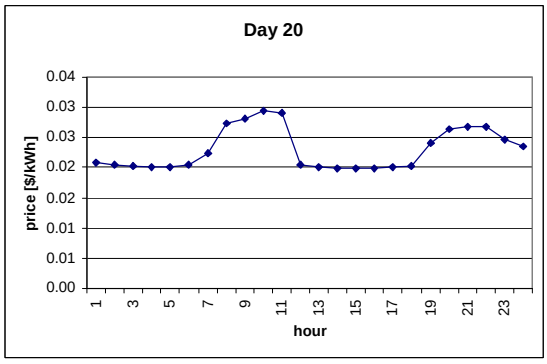

Sunday

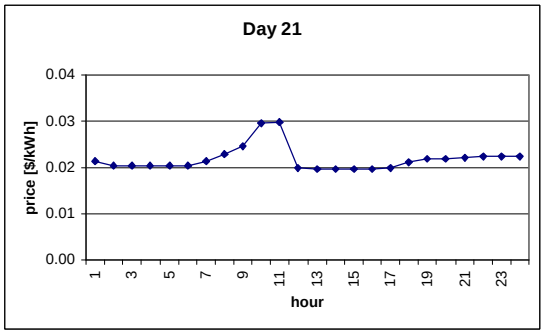

Monday

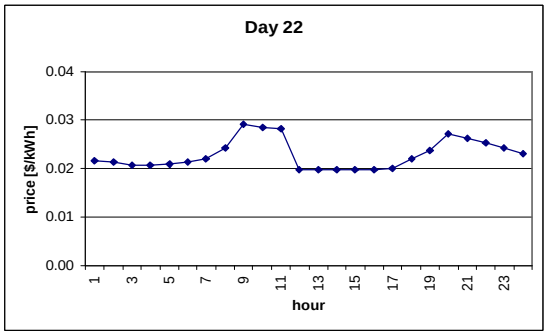

Tuesday

Figure 3-19: Southern prices from December 17th to December 22nd 1998.

The two peaks before noon and in the evening continue throughout the week, only Monday 21st is somehow different from the other days shown. Overall, the Southern prices are much more predictable on a day-to-day basis than the PG&E prices. A few days are still far from the average, but as prices are not as high as they are under the PG&E pricing scheme, the customer is not obliged to shut all operation down in order to avoid the extraordinary costs.

Similar to the Southern prices, the Niagara Mohawk RTP prices hardly show any sensitivity to the day of the week in winter and early summer. The following series (Figure 3-20) is from May 1999:

Niagara

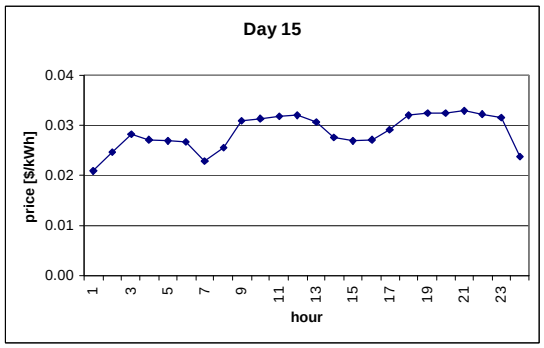

Friday

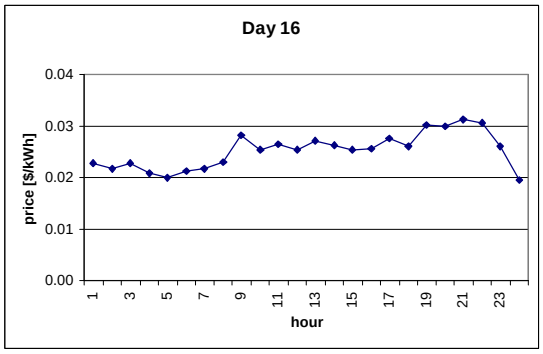

Saturday

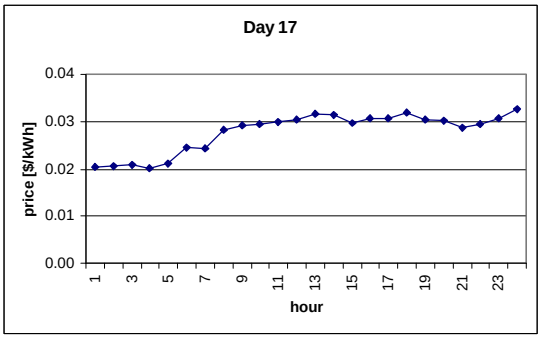

Sunday

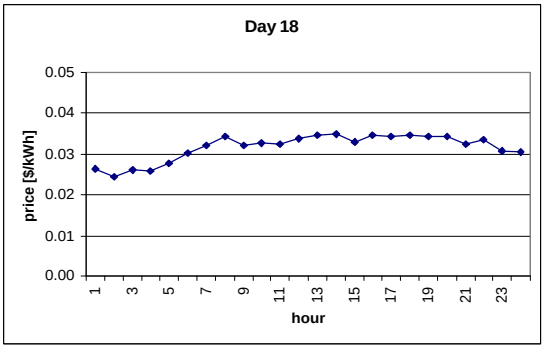

Monday

Figure 3-20: Niagara Mohawk prices from May 15th to May 18th 1999.

In summer the prices change more depending on the day, but it is still hard to distinguish between workdays and weekends. The July 1999 series in the following figure shows this:

Niagara

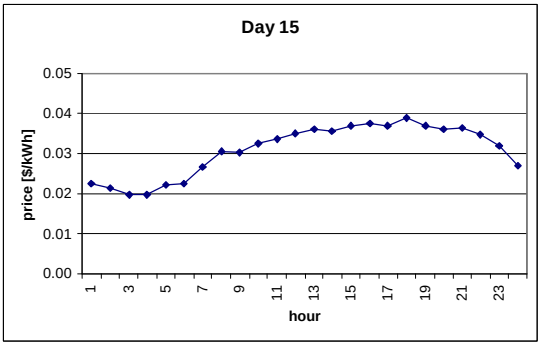

Thursday

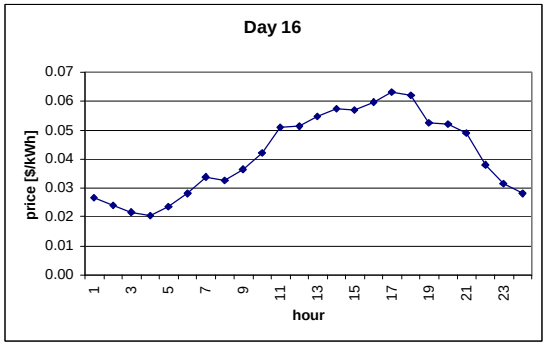

Friday

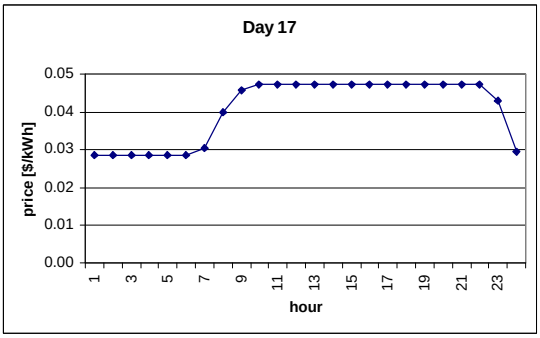

Saturday

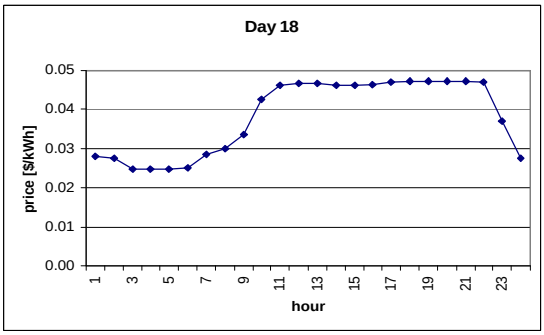

Sunday

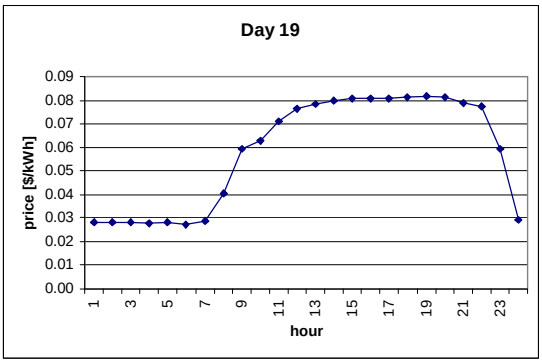

Monday

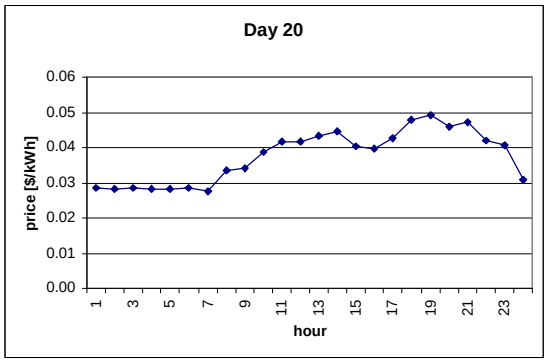

Tuesday

Figure 3-21: Niagara Mohawk prices from July 15th to July 20th.

The pricing curves on most of the days resemble a pricing profile under time-of-use pricing. The daytime price is higher and the nighttime price is lower. The period of transition between the two levels is very short, which makes the curves similar to time-of-use pricing. This limited variety in prices makes decisions how to shift loads easier because it limits the pricing dimension of the decision that has to be taken.

3.3.5 Statistics of price fluctuations

A statistical summary of the price fluctuations was conducted. The following table provides a statistical summary of the RTP prices expressed in terms of the monthly-average-hourly price, $\bar{y}$, the standard deviation, s, and the standard deviation of the price normalized to the monthly average hourly electric price, s/y. The standard deviation is calculated as

$$s = \sqrt{\frac{\sum_{i=1}^{n} \left(hourlyprice_i - \bar{y}\right)^2}{n-1}} \tag{3-1}$$

*Table 3-1: Average price and price standard deviation (**bold**: data shown in section 3.3.3)*

Month	PG&E			Southern			Niagara		
	$\bar{y}$	s	$s/\bar{y}$	$\bar{y}$	s	$s/\bar{y}$	$\bar{y}$	s	$s/\bar{y}$
Jan	***0.05882***	**0.01145**	**0.19466**	***0.02118***	**0.00146**	**0.06879**	***0.01971***	**0.00332**	**0.16315**
Feb	*0.05564*	0.01248	0.22430	*0.02176*	0.00238	0.10921	*0.01755*	0.00257	0.14617
Mar	*0.05366*	0.01121	0.20880	*0.02273*	0.00480	0.21113	*0.01893*	0.00293	0.15501
Apr	***0.05085***	**0.01115**	**0.21932**	***0.02237***	**0.00272**	**0.12154**	*0.02000*	0.00335	0.16770
May	***0.04060***	**0.03051**	**0.75146**	*0.04095*	0.04860	1.18687	***0.02741***	**0.00371**	**0.13528**
Jun	*0.05167*	0.10014	1.93815	***0.06306***	**0.06872**	**1.08978**	***0.03735***	**0.03025**	**0.80984**
July	***0.11506***	**0.21143**	**1.83762**	***0.05467***	**0.05983**	**1.09440**	***0.04942***	**0.05330**	**1.07850**
Aug	***0.10923***	**0.16126**	**1.47635**	*0.03957*	0.04278	1.08110	*0.03449*	0.01008	0.29229
Sep	*0.08438*	0.08364	0.99121	***0.02874***	**0.01115**	**0.38817**	***0.01898***	**0.00345**	**0.18157**
Oct	*0.06831*	0.02756	0.40343	*0.02419*	0.00521	0.21527	*0.02004*	0.00364	0.18150
Nov	*0.08388*	0.03699	0.44093	*0.02472*	0.00419	0.16937	*0.02160*	0.00408	0.18895
Dec	***0.08433***	**0.05736**	**0.68011**	***0.02330***	**0.00432**	**0.18533**	***0.02014***	**0.00334**	**0.16564**

For all months besides May, the standard deviation is biggest for PG&E. May is a relatively homogenous month for PG&E and prices for Southern vary more than usual. Dividing the standard deviation by the average price shows that even if the much higher average prices of PG&E is considered, the ratio of the standard deviation to the average

price is still higher for PG&E in all months except March and May. March is also a month where PG&E prices fluctuate little.

3.3.6 RTP and temperature

Under most RTP schemes, prices for the next day are announced before 4 p.m. of the day before. On weekends, the weekend prices are announced Friday before 4 p.m. For the customer who wants to react to the RTP prices by shifting loads to less expensive hours, the time available to take decisions that affect his electricity demand for the next day is relatively short. It would be of interest to know about the expected development of the RTP prices earlier than 4 p.m. Planning ahead more than 24 hours would allow taking additional measures to optimize reaction to RTP prices. For example working schedules could be changed in advance or thermal storage capacities could be used more efficiently.

One factor that might influence the RTP prices is ambient dry bulb and wet bulb temperature. Ambient conditions play a major role in "driving" the overall demand for electricity which is attributable to air conditioning. In the summer months, when demand is highest for most utilities and real-time prices reach their yearly peaks, air conditioning loads are the factor that increases demand the most compared to other times of the year. At the same time demand increases, the performance of power plants decreases due to the higher wet bulb temperature, which lowers the condenser performance of the plant.

This section investigates the statistical relationship between RTP prices and ambient temperature. As the RTP prices are highest in the summer month, prices in July were correlated with temperature. Weather data was obtained for two weather stations; for PG&E, data from San Francisco Airport, CA was used and for the Southern RTP data, weather data was taken for the station Montgomery Danelly Field, AL.

The first figure compares the RTP prices and ambient conditions for PG&E.

PG&E

Figure 3-22: Prices and temperatures for PG&E for 8 days in July 1997.

A first observation that can be made is that on workdays, the peak prices lag the peak temperatures by about one to three hours. The same time shift can be observed for the cooling load on a building. The thermal mass of the walls lags the load to the structure that is caused by an increase in ambient temperature. RTP prices therefore seem to be influenced by the thermal building load, which again suggests that air conditioning loads are an important factor in determining the prices. On the other hand, the peak price seems not to be strongly correlated to the peak temperature of each day. For example Tuesday, July 8th, has a dry bulb peak temperature of about 72 °F and a peak price of 0.1 $/kWh. The day after, Wednesday, July 9th, has a dry bulb peak temperature of only 70 °F but a peak price higher than 0.1 $/kWh. The higher wet bulb temperature of that day might explain partly the higher price. Comparing Monday, July 7th, and Tuesday, July 8th, makes it also difficult to correlate price and temperature. Monday is only slightly warmer than Tuesday, but the peak price of 1.40 $/kWh is much higher than the 0.10 $/kWh on Tuesday. Friday, July 11th, has similar peak temperatures than Monday, July 7th, but prices are much lower.

The daily maximum dry bulb temperature was correlated with the daily peak prices for the whole month of July 1997 in Figure 3-23 and Figure 3-24. The prices are shifted to a time 3 hours earlier than they actually occur to consider the difference in time between the two peaks. The second plot is an enlargement of the first plot; the scale is changed to keep out the influence of the very expensive days.

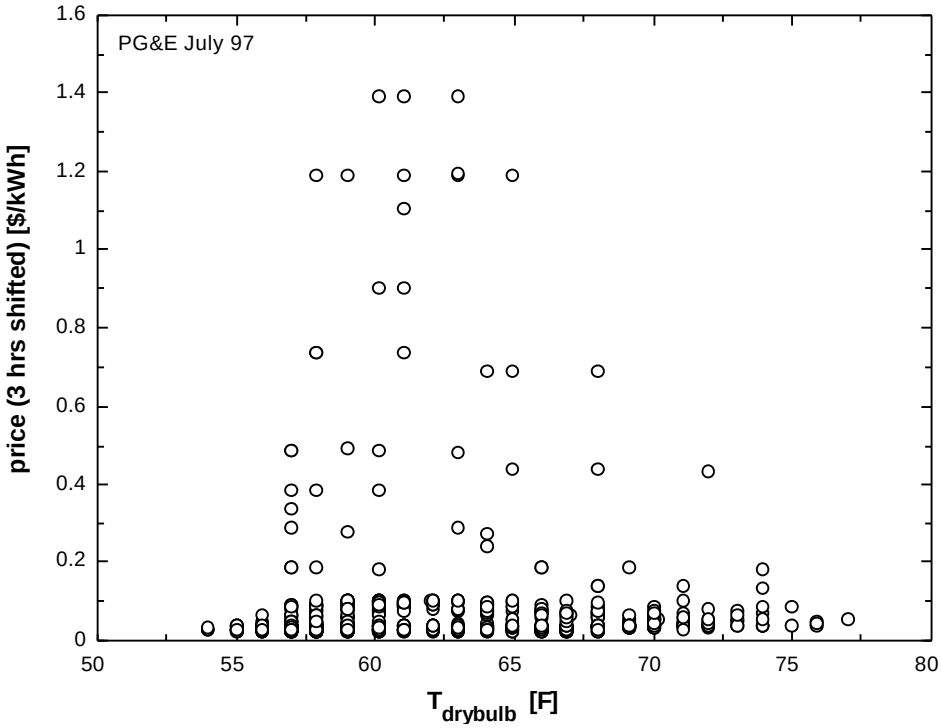

Figure 3-23: Daily PG&E RTP peak prices and maximum outdoor air dry bulb temperature

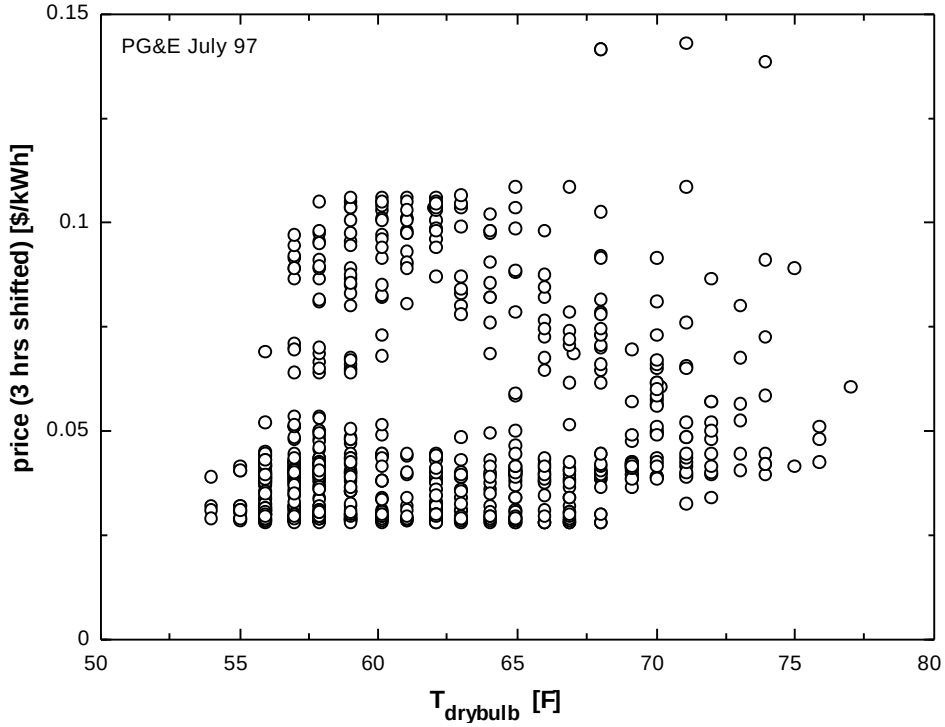

Figure 3-24: Daily PG&E RTP peak prices and maximum outdoor air dry bulb temperature.

As it can be seen, even if the higher prices are not shown on the plot, it is difficult to correlate RTP prices with dry bulb temperature. Also eliminating the weekends, which have somewhat different price profiles than the weekdays, did not change the plots significantly.

The next two plots show the relation between prices and wet bulb temperature. Again, it can be observed that prices are somewhat related to the temperature, but still scattered very much.

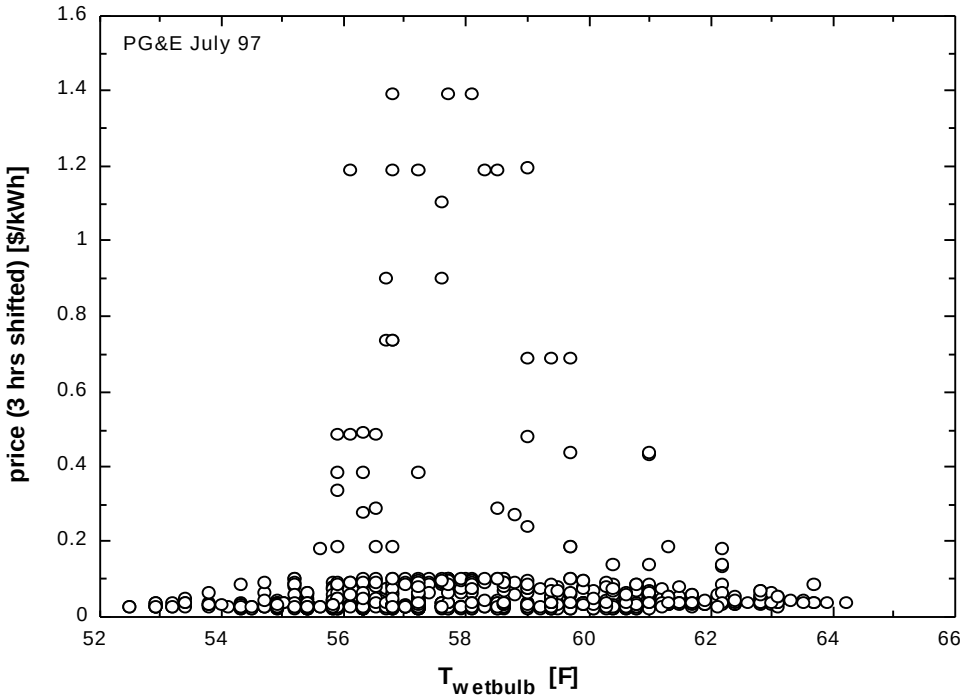

Figure 3-25: Daily PG&E RTP peak prices and maximum outdoor air wet bulb temperature.

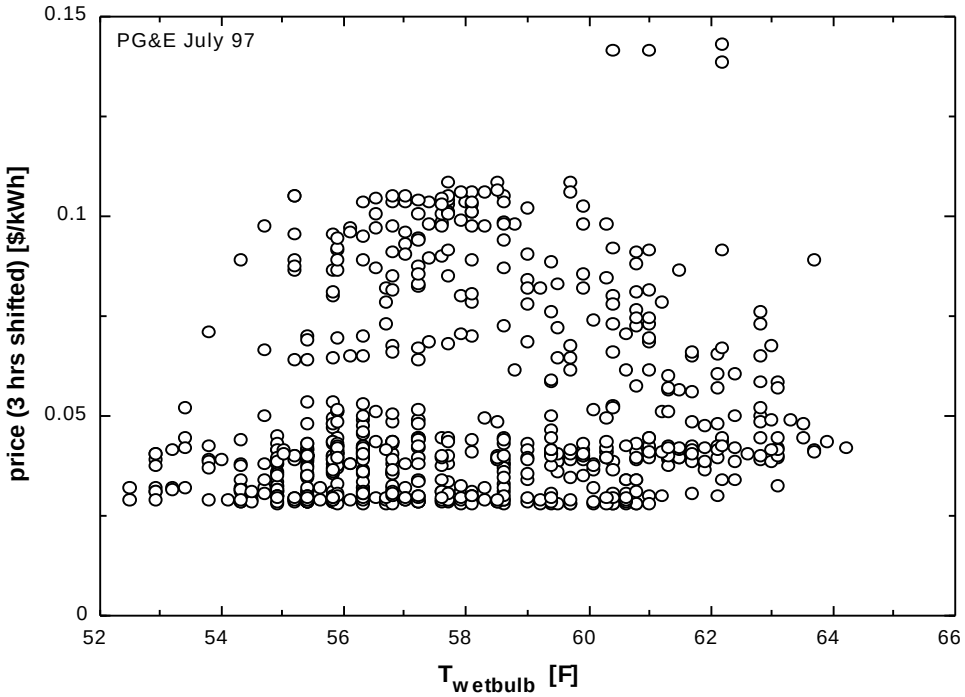

Figure 3-26: Daily PG&E RTP peak prices and maximum outdoor air wet bulb temperature.

A similar analysis was done for the Southern prices in July 1997. The Southern prices are less fluctuating and therefore the correlation is a little better.

The first series of plots shows the same week in July 1997 than for PG&E.

Southern

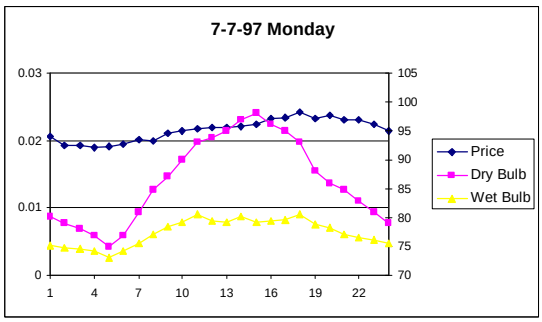

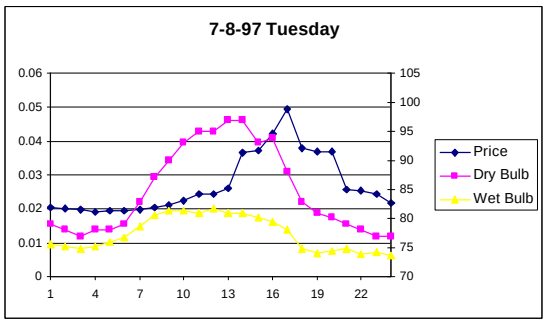

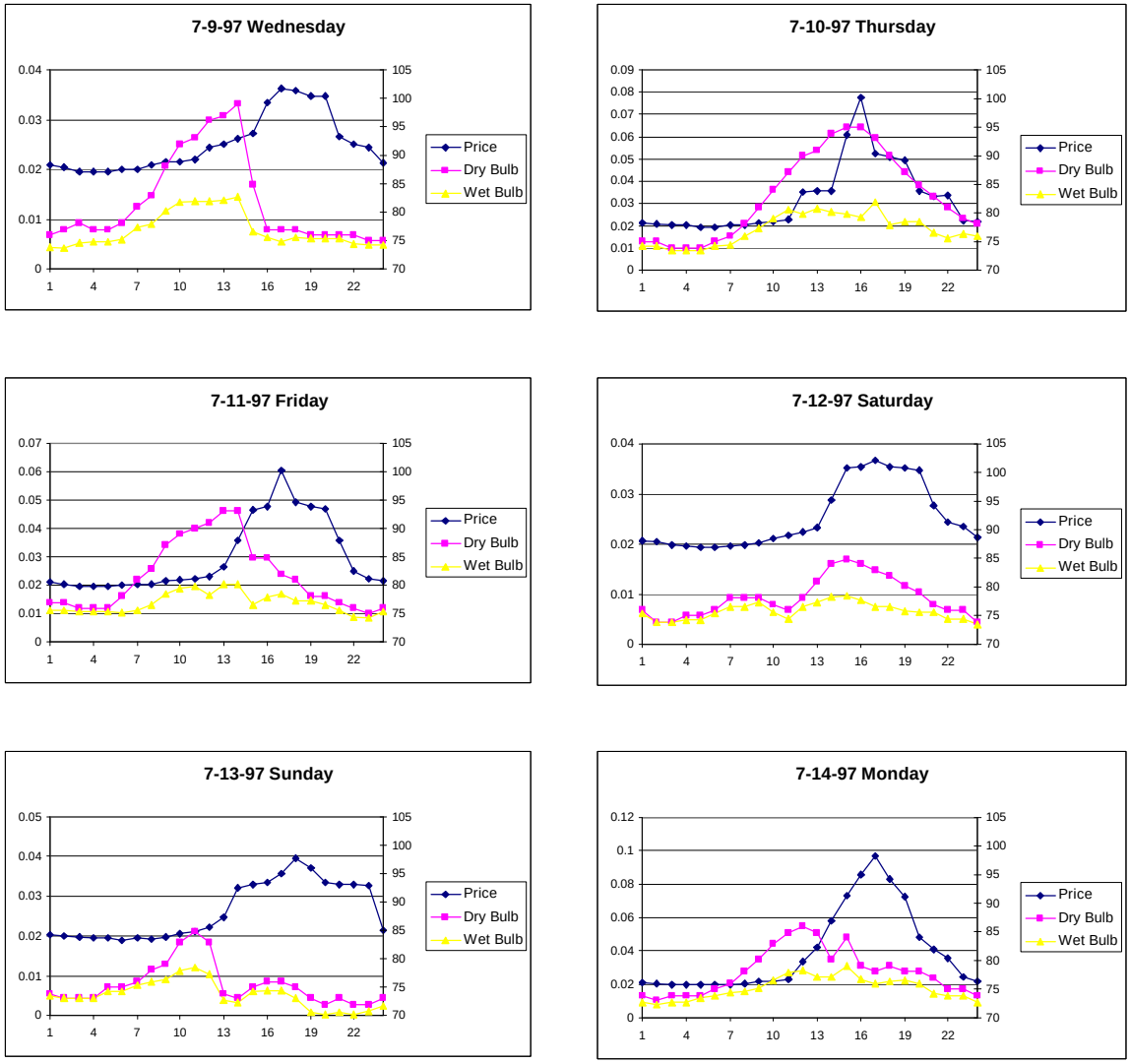

Figure 3-27: Prices and temperatures for Southern for 8 days in July 1997.

Again, the time shift between peak prices and peak temperatures can be observed. Also under the Southern pricing scheme, days with higher temperatures might have lower prices. Wednesday, 9th has higher temperatures than Thursday, 10th, but prices on Thursday are higher than prices on Wednesday.

The next series of plots shows daily July 1997 peak prices versus maximum dry bulb and wet bulb temperatures.

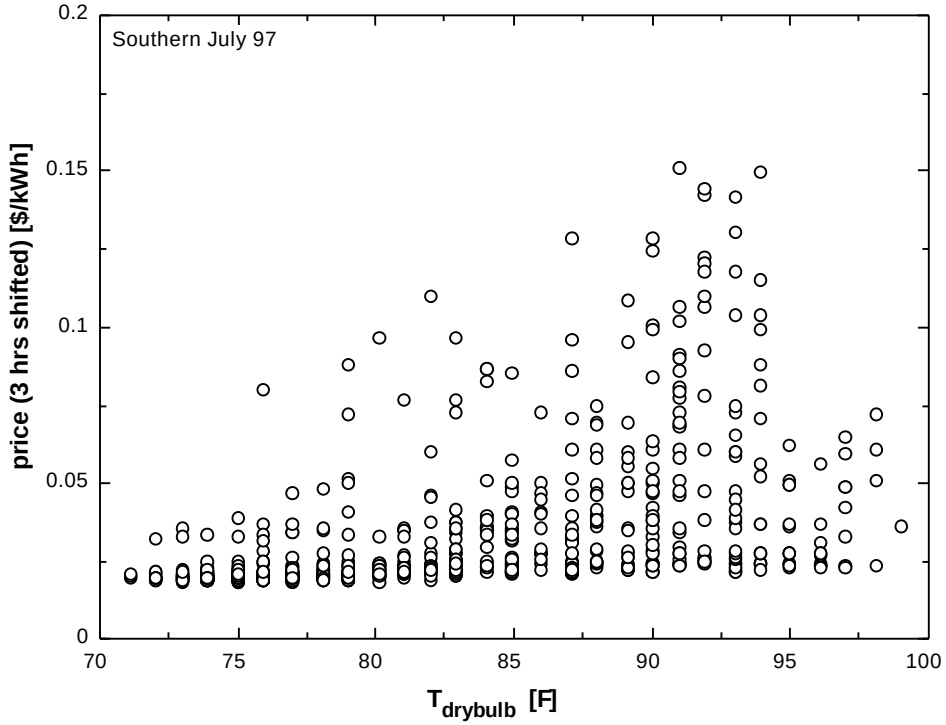

Figure 3-28: Daily Southern RTP peak prices and maximum outdoor air dry bulb temperature.

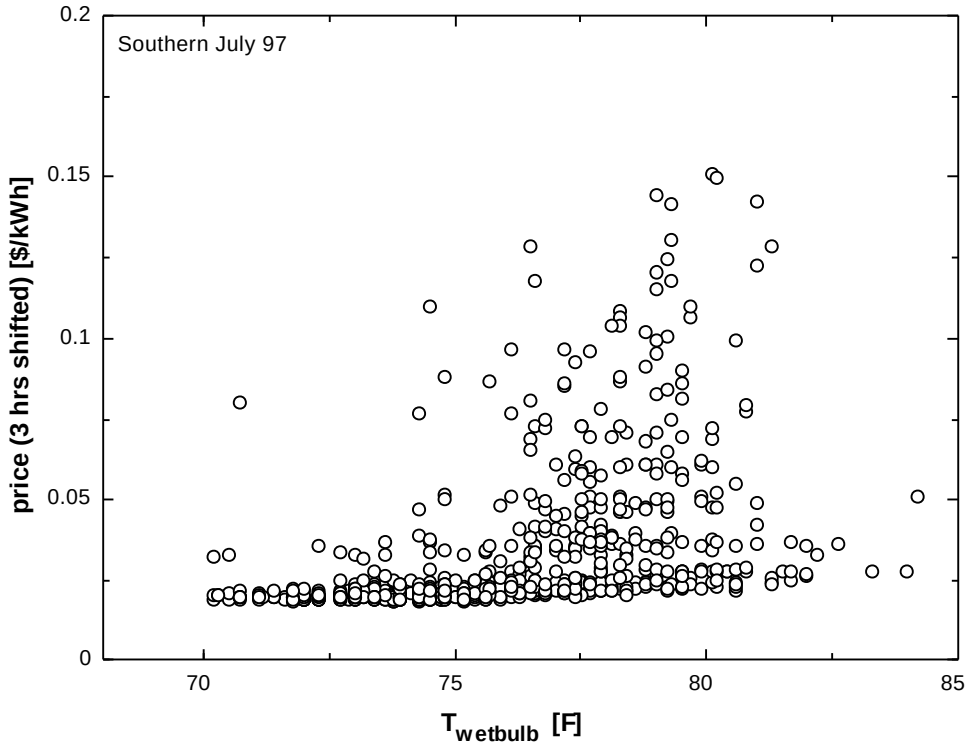

Figure 3-29: Daily Southern RTP peak prices and maximum outdoor air wet bulb temperature.

For July 1997, the wet bulb temperatures in Alabama are extremely high; they never fall below 70 °F. The plots show that the higher prices only occur for higher temperatures. But also at very high temperatures, prices can be relatively low.

Forecasting future real-time prices based on the expected temperatures would allow taking measures in advance to adapt to the forecasted prices. The relation between RTP prices and local ambient dry bulb and wet bulb temperatures was explored in this section. A simple relationship between prices and temperatures was not found to exist. Prices are relatively independent of the temperature data for the months investigated. The weather data are only local data, while the real-time prices are valid for a larger region that a utility serves. It may be that the regional weather patterns influence the prices. Prices are also determined from the market price, which is not influenced by local weather data. From this section, it can be concluded that the real-time prices for the next day cannot be predicted by the use of local weather data alone.

3.4 Chapter Summary

Electricity demand is not constant over a day and there are great differences in demand over the year. Unlike many sources of energy, electricity is a form of energy that is not easily (or cost-effectively) stored in large amounts. Therefore, the electricity supply has to continuously vary to meet the demand for electricity directly. This results in an electricity production cost that also varies greatly depending on the time. Traditional electricity pricing approaches are based on average production cost. Real-time pricing is an emerging rate structure developed in response to the trend toward open markets and competition in the US electricity markets. The next day hourly electricity price is determined based on the projected electricity market or production cost. The costumer is notified of the coming prices on a short-term basis. Real-time pricing structures can be classified into one-part and two-part pricing structures. Under a one-part structure, the real-time electricity price includes all costs. Under a two-part structure the real-time price is set close to the marginal cost, which results in a lower real-time price. An access fee covers the additional costs under the two-part structure.

Real-time pricing offers advantages and disadvantages for both, the utility and the customer. Setting price close to cost is an economically efficient way to balance supply and demand. Real-time pricing also offers potential savings: the customer can reduce the electricity cost by shifting demand to hours of cheaper prices, the utility benefits from a flattened aggregate demand profile. On the other hand, real-time pricing shifts the pricing risk to the customer and the customer is also confronted with the problems on how to react to the real-time prices.

Real-time pricing data sets from three different utilities in the US were investigated. The data sets show a great variety in prices compared to each other. The one-part PG&E pricing structure has the highest peak prices of up to 1.60 $/kWh and also the biggest difference between peak and average daily prices. It therefore offers the biggest incentive for demand shifting. Compared to that, the two-part Southern and Niagara Mohawk pricing structures have lower peak prices and offer reduced incentives to shift demand.

Price fluctuations within a day, from day to day and over the year can be significant in all cases. The day-to-day price fluctuations within the PG&E data are bigger than in the two other data sets. The Niagara prices have the least fluctuations from day to day. Seasonal differences in the price profiles can be observed. During the summer month, the profiles have one significant peak in the afternoon. During colder months, the profiles are much flatter, and two peaks can be observed: one peak around noon and another peak in the later evening. In general, the summer peak prices are higher than the winter peak prices; the magnitude of the difference depends on the utility. Under the PG&E structure, weekends can be clearly distinguished from weekdays. For the other two structures, the difference is not as significant.

The dependence of real-time prices from local weather data has been investigated. The results suggest that there is no correlation between daily maximum air temperatures and the daily maximum real-time prices.

Chapter 4 Results

4.1 Baseline Operation

Before developing and evaluating any load shifting strategies, a base case for comparison and evaluation has to be established. In this investigation the base case had the warehouse refrigeration equipment operating continuously, i.e. the set point temperatures were kept constant and the equipment was operated to meet the loads as they occur. Yearly simulations of the base case were run using Madison weather data. Simulations were also run for the design "day", which is the day with the highest load based on the Madison weather data. To compensate for thermal capacitance effects of the warehouse and stored products, design day calculations were repeated multiple times. The results presented are for the 7^{th} day out of a series of design day runs.

Depending on what is of interest, the results presented in the following sections are either for the freezer, the dock or the whole warehouse, which is the freezer and the dock combined. The dock was kept at a constant 1 °C (34 °F). The freezer set point temperature was set to –18 °C (0 °F).

4.1.1 Design day operation

4.1.1.1 Massive wall warehouse

For the massive wall warehouse construction, the highest freezer load that occurred on the 7^{th} day is 690 KW_t (196 tons), which represents the design load. Table 4-1 shows the distribution of the average freezer loads for the design day. The loads are compared to the values for a typical 100,000 ft^2 freezer as presented in the ASHRAE refrigeration handbook (ASHRAE 1990).

Table 4-1: Distribution of average design day freezer load and comparison with ASHRAE typical warehouse

Distribution of Load/ KW_t		%	ASHRAE typical freezer/ KW_t		%
$Q_{transmission}$	320	50	$Q_{transmission}$	345	49
$Q_{inf,sens}$	121	19	$Q_{infiltration}$	35	5
$Q_{inf,lat}$	35	5			
$Q_{defrost}$	18	3	$Q_{internal}$	175	25
Q_{fans}	32	5			
Q_{forks}	64	10			
Q_{lights}	45	7	$Q_{product}$	25	3
Q_{people}	8	1	Others	123	18
Q_{total}	**638**	**100**	**Q_{total}**	**703**	**100**
$Q_{sensible}$	603	94			
Q_{latent}	35	6			

Transmission loads are nearly the same for both freezers, while the simulated freezer has higher infiltration loads. On the other hand, 18% of the loads for the ASHRAE freezer are listed as others, which can explain the difference. The sum of the loads for the simulated freezer is not exactly equal to the cooling load for the design day. This little difference of less than 1% can be explained by round-off errors in the calculations. Figure 4-1 graphically illustrates the distribution of the loads.

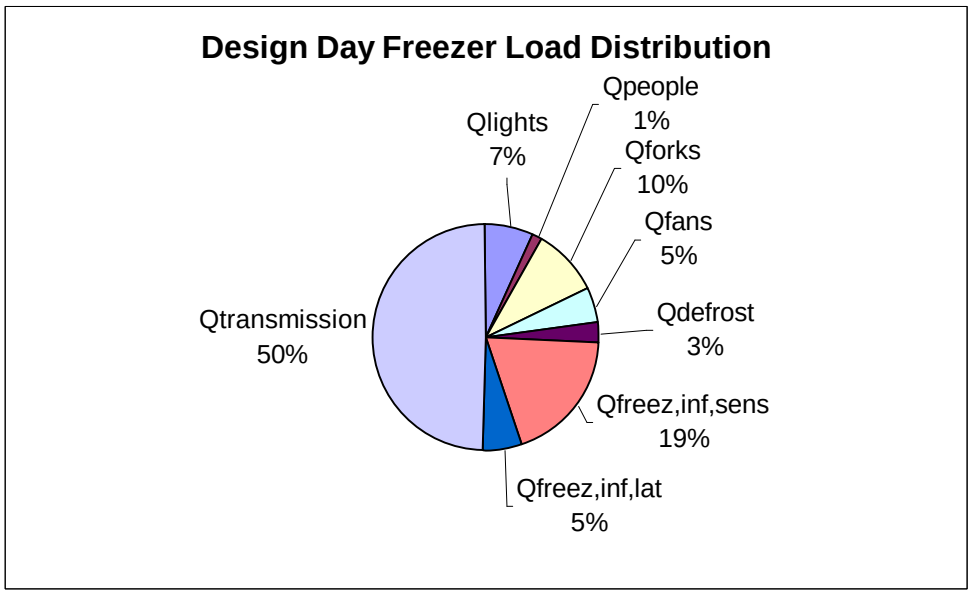

Figure 4-1: Distribution of design day freezer loads for massive wall.

A similar distribution of refrigeration loads can be created for the dock. Figure 4-2 considers the dock infiltration balance. Infiltration from ambient to the dock is a load on the dock while infiltration from the freezer to the dock is a credit.

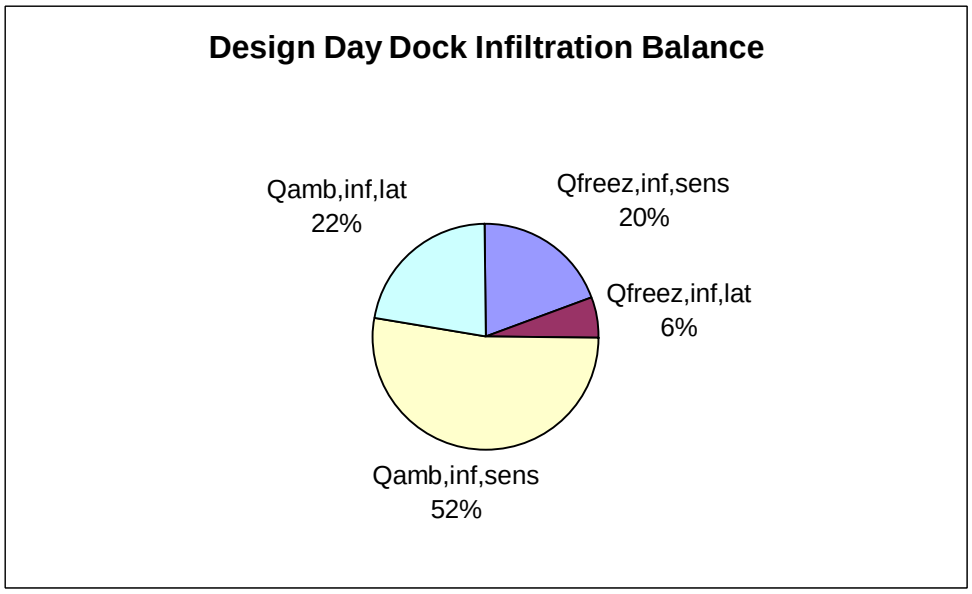

Figure 4-2: Design day dock infiltration balance.

On the design day, 26% of the infiltration to the dock is from the freezer and therefore partly compensates for infiltration of outdoor air.

4.1.1.2 Lightweight wall warehouse

For the warehouse with the lightweight wall construction, the peak design load is higher than for the massive wall case. The design load for the lightweight wall construction is 915 KW_t (260 tons). The distribution of loads for the lightweight wall is similar to the massive wall, as shown in Figure 4-3.

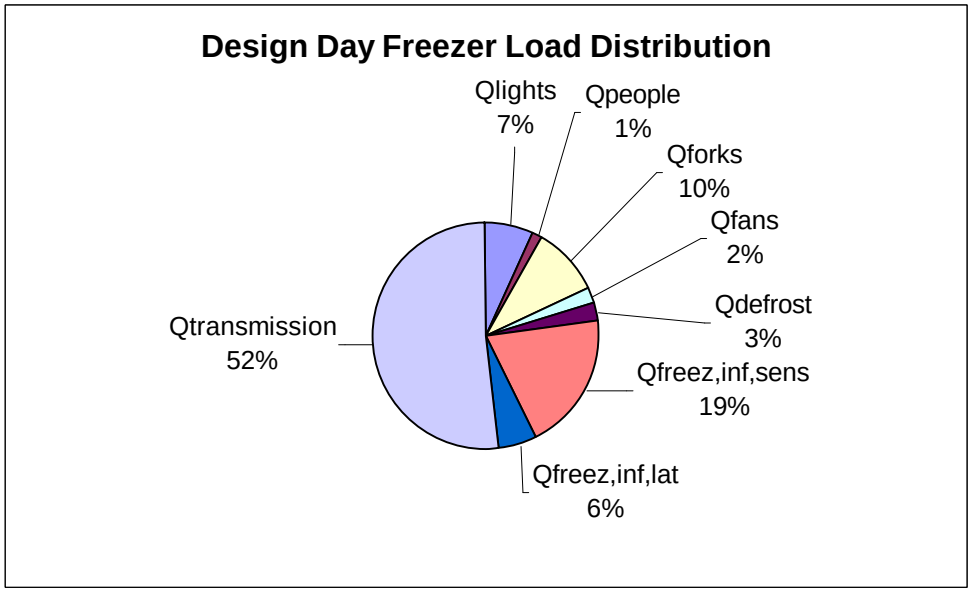

Figure 4-3: Distribution of design day freezer loads for lightweight wall.

The distribution of loads is nearly the same than for the massive wall. The share of the transmission and latent infiltration loads is slightly higher while the share of the evaporator fans loads decreased. The reduced load from the fan power can be explained by reviewing the evaporator fans model used. For the lightweight wall construction, the installed refrigeration capacity is higher. At times when the warehouse loads are highest, the equipment is operated at full power, as are the evaporator fans. It is assumed that always enough evaporating capacity is installed. In both cases, the evaporators have the same maximum mass flow capacity. However, at off-peak times, the lightweight warehouse is operated at a lower part load ratio when compared to the massive warehouse. As shown in the evaporator model section in equation (2-26) the required fan power is dependent on the part load ratio. This ratio decreases more for the lightweight wall case than for the massive wall case, therefore the fan power decreases.

4.1.2 Yearly operation

With the design day load known and the resulting refrigeration capacity required for each wall construction known, yearly simulations were run. The results from annual simulations are presented in the next two sections.

4.1.2.1 Massive wall warehouse

The total annual cooling load and the resulting annual electricity demand for the freezer and for the dock are shown in Table 4-2.

Table 4-2: Yearly Cooling Load and Power demand for massive wall

	Sensible Cooling Load/ kWh_t	Latent Cooling Load/ kWh_t	Total Cooling Load/ kWh_t	Total electricity demand/ kWh_{el}
Freezer	4,060,160	155,121	4,215,281	1,647,379
Dock	550,649	213,893	764,542	575,260
Total	4,610,809	369,014	4,979,823	2,222,640

Figure 4-4 and Figure 4-5 further illustrate the yearly warehouse performance.

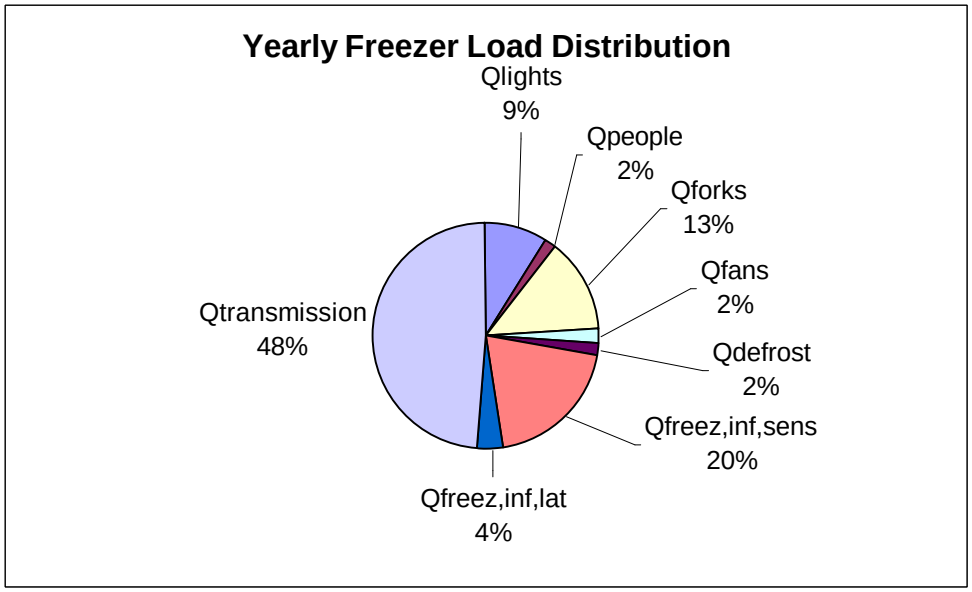

Figure 4-4: Yearly freezer loads for massive wall

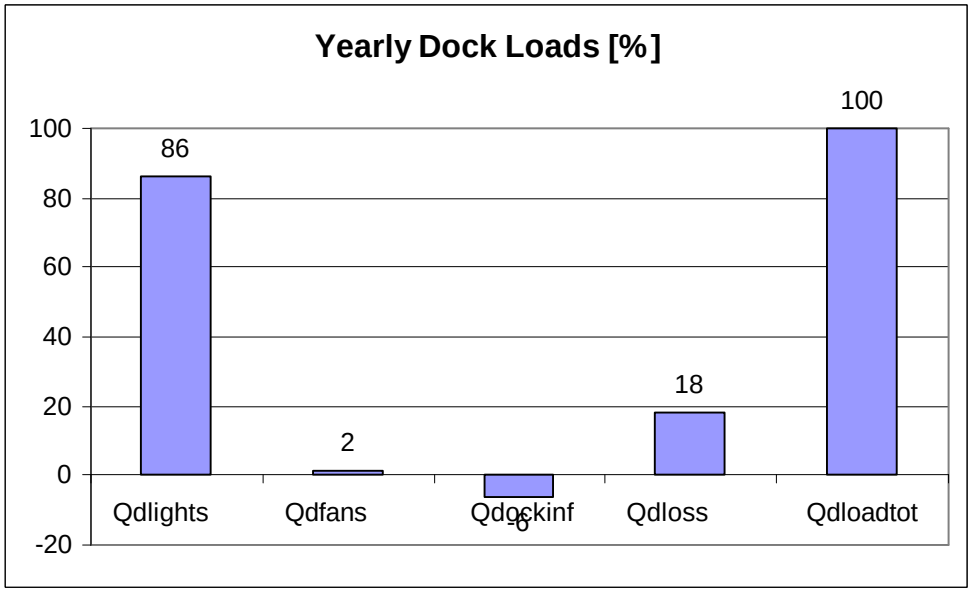

Figure 4-5: Yearly dock loads for massive wall

The distribution of the yearly freezer loads is similar to the design day results with nearly half of the loads from transmission and one quarter from infiltration. For the dock, the biggest source of gains is the dock lights. These are operated constantly throughout the year with a relatively high power input. Over the year, the dock infiltration balance is negative. The infiltration credits from the freezer are bigger than the infiltration loads from ambient, which results in a net infiltration cooling credit for the dock over the year.

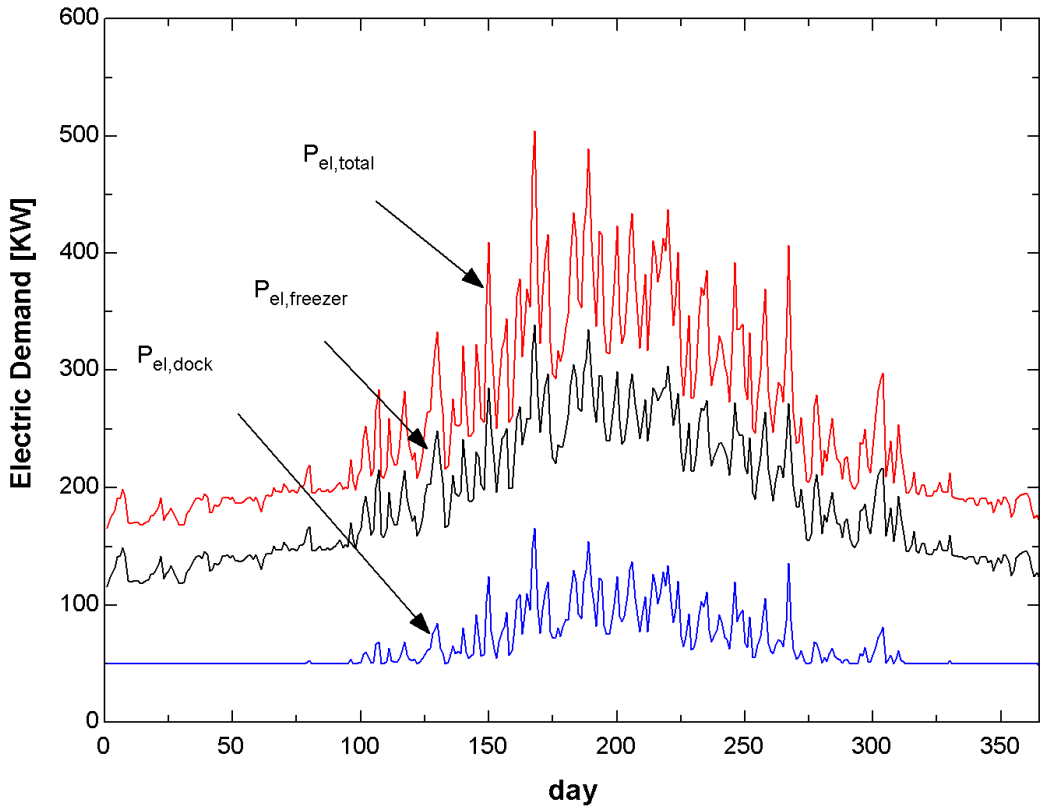

Figure 4-6: Average daily power demand over year

Figure 4-6 shows the average daily electric power demand of the warehouse. During days with high loads in summer, the power demand exceeded the daily demand during the winter by more than 2.5 times. The plot also shows that the dock power demand during colder months is practically constant. Only the dock lights consume power at that time of the year. The dock gets sufficient cooling credit from the freezer or even from ambient that the dock set point temperature can be maintained without additional cooling. The dock refrigeration equipment is only operated in summer and the dock power demand correspondingly increases. The ratio of dock and freezer electric power demand over the year is shown in Figure 4-7.

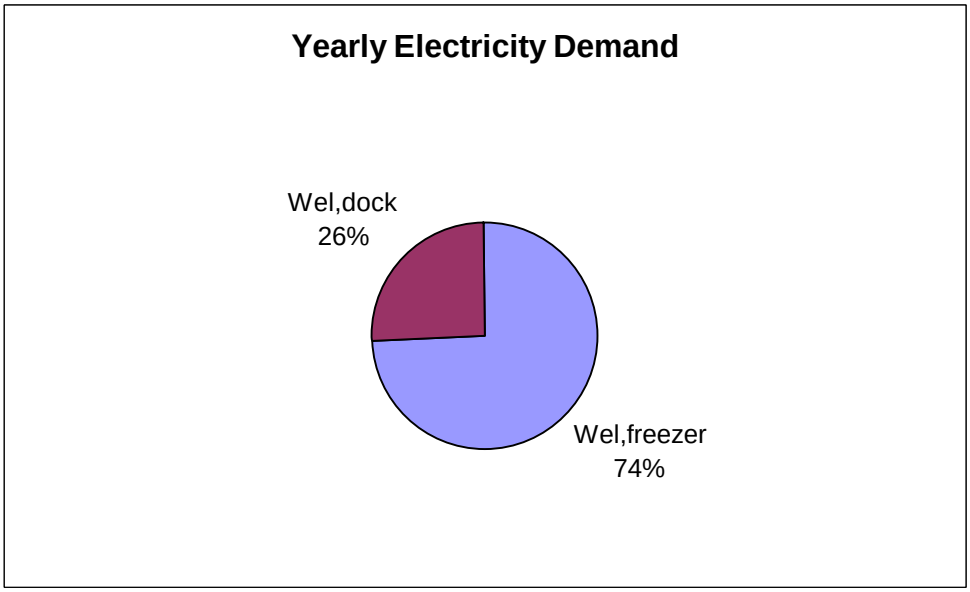

Figure 4-7: Ratio of yearly power demand.

Even though the dock refrigeration equipment is not operated in winter, the dock contributes to one-fourth of the total power demand for the entire warehouse. This fact also has to be kept in mind when floating the freezer in summer months. As can be seen from Figure 4-6, it is mainly in summer months when the dock electric power demand increases. The dock operation is therefore an important contributor to the overall operating cost of the warehouse.

Transmission loads are the biggest share of the loads for the freezer. Transmission loads through the freezer walls were calculated by the transfer-function approach used in TRNSYS. Knowing the ambient and freezer conditions, the heat gains through walls and roof were computed with a relatively high level of confidence. The floor heat gain however is less well known. Figure 4-8 shows the distribution of yearly transmission loads between floor and walls.

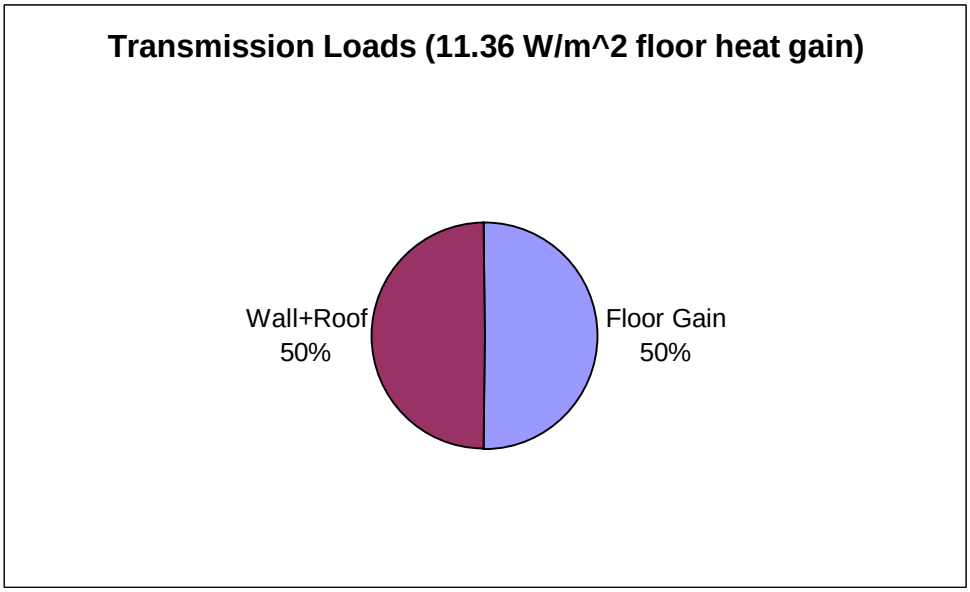

Figure 4-8: Yearly transmission loads for freezer.

As the plot shows, 50% of all transmission loads over the year are through the floor. The ratio of floor loads to wall and roof loads seems relatively high. On the other hand, the floor loads are constant over the year, while mainly in colder months and during night, when no solar radiation reaches the walls and roof, the transmission loads through the walls are greatly reduced. Furthermore, the walls and roof are well insulated, while the floor is not that well insulated.

4.1.2.2 Lightweight wall warehouse

The annual results for the lightweight wall warehouse are very similar to the results for the massive wall warehouse. Table 4-3 summarizes the results.

Table 4-3: Yearly Cooling Load and Power demand for lightweight wall

	Sensible Cooling Load/ kWh_t	Latent Cooling Load/ kWh_t	Total Cooling Load/ kWh_t	Total electricity demand/ kWh_{el}
Freezer	4,061,038	156,438	4,217,476	1,609,134
Dock	540,927	212,045	752,972	573,138
Total	4,601,965	368,483	4,970,448	2,182,273

Compared to Table 4-3, the annual results for the lightweight wall warehouse are nearly identical. Similar plots as shown for the massive wall can also be created for the lightweight wall; the results are basically the same.

4.2 Demand Shifting Strategy

When looking at the real-time pricing curves, it becomes obvious that a possibility for cost savings might be realized if the demand during high price periods could be lowered. The lowering of demand at a certain time usually has to be compensated for by a higher demand at another time. Under RTP, the natural question that arises is: what represents the "best" strategy of demand shifting that delivers the highest savings compared to continuous operation. A complicating factor is that the best strategy on a certain day might not be the best strategy on another day with different conditions. Altwies (1998) explored three strategies for operation under time-of-use pricing. The first option explored was full demand shifting, which means that the refrigeration equipment was completely shut down during the on-peak window and operated at full power during the off-peak time. Load leveling is a second strategy in which the equipment was operated at a constant level 24 hours a day. The operating level had to be chosen such that the average warehouse load was met and that the product temperature stayed below the critical temperature. As a third option, a combination of the two strategies would be operating at a lower level during the day and a higher level during night. Altwies (1998) concluded that full demand shifting offers the biggest savings but also requires the most refrigeration capacity installed.

Besides these three strategies, many more are possible under RTP rate structures. For example the warehouse could be precooled only for a few hours before shutting down the equipment completely during high price periods. The equipment is operated later at a level that keeps the warehouse temperature constant without precooling. At a certain hour, precooling resumes again.

Not only the equipment operation during precooling has to be considered, but also the time at which the equipment is shut down must be chosen carefully. The loads on the

warehouse depend on the time of the day. Therefore shutting down the equipment at a time when loads are lower might allow the refrigeration equipment to remain off longer, even if the hourly savings might be lower at that time of the day. Overall, this could result in greater operation cost savings.

In this study, demand shifting was only performed for the freezer. The dock refrigeration equipment was operated to keep the dock temperature constant throughout the day.

4.2.1 Load shifting parameters

Before exploring different demand shifting strategies, parameters had to be identified that signify changes in operation strategy. From the many variables describing the refrigerated warehouse model in TRNSYS, the following were chosen:

- Wall type: The use of a massive and a lightweight wall construction for the freezer was investigated. Both walls have the same overall U-value of 0.2612 W/m^2-C (0.046 BTU/hr-ft^2-F), but differ in their thermal capacitance of the wall construction.
- Installed refrigeration capacity: The installed refrigeration capacity is represented by the number of compressors installed. Under design conditions, one Vilter VSS-451 high stage compressor delivers 302 KW_t (86 tons) of cooling. For the base case without any additional capacity for precooling installed, the freezer is operated with three compressors for the massive wall construction, which corresponds to 906 KW_t (258 tons) of refrigeration capacity. The lightweight wall construction requires four compressors in the base case, which corresponds to 1208 KW_t (344 tons) of installed refrigeration capacity. The installation of additional refrigeration capacity to a total of up to six compressors, which deliver 1,812 KW_t (688 tons), was investigated. At the same time it was assumed that the installed evaporator and condenser capacity is always sufficient.
- $Time_{off}$/ $Time_{on}$: These are the times of the day when the refrigeration equipment is turned off and the time when it is turned on again. These two variables establish the duration of the floating window and the location of this window at the same time.

- T_{high}, T_{low}: T_{high} is the temperature to which the freezer is set during high cost period ("on-peak"). Usually this variable was set to 0°C (32°F), which means that the freezer temperature was allowed to increase above –18 °C (0 °F) which leads to the potential for damage of the stored products when the floating duration was chosen too long. At the same time, this high set point assured that the equipment remained turned off during the on-peak period.

  T_{low} was usually set to –30°C (-22°F), a temperature the freezer usually did not reach even if the equipment was operated at its maximum capacity. This low set point assured full load operation during off-peak times.

As a further option, a strategy with a fixed precooling time before floating was explored. The two additional parameters associated with this strategy are the precooling time before floating, $t_{preccol}$, and the temperature at which the freezer is kept after cooling has resumed but before precooling restarts, $T_{intermediate}$.

4.2.2 Possible floating duration

When initial runs of the warehouse simulation were performed that implemented the option of precooling the freezer and shutting down the equipment during times of the highest prices, it became obvious that the duration over which the equipment could be shut down strongly influenced the resulting operating cost and product tempratures. The longer the equipment was idled, the higher the possible cost savings were because operation during more hours at higher energy prices was avoided. On the other hand, the floating duration was limited to avoid an increase in freezer and product temperature beyond a critical value. From these considerations it was concluded that a means to predict the maximum possible floating duration for the next day had to be devised to facilitate decision making on the warehouse operation during the next day. The maximum possible floating duration means that the freezer is precooled as much as possible, and the equipment serving the freezer is then completely shut down during the floating period. During the freezer floating period the dock refrigeration equipment is always operated to maintain the dock temperature at 1 °C (34 °F).

For a given warehouse type and installed refrigeration capacity, the possible floating duration of the warehouse is a function of ambient conditions, which mainly determine the load on the warehouse. Transmission loads through the walls and the roof depend on ambient dry bulb temperature and solar incident radiation; infiltration loads depend on ambient dry bulb and wet bulb temperatures. Furthermore, equipment performance is affected by the wet bulb temperature, which influences the condensing temperature of the refrigerant. High ambient temperatures and incident radiation limit the ability to precool the warehouse. When the equipment is then shut off, higher loads shorten the duration until the zone or the product temperature reach the critical temperature limit and the equipment has to be operated again.

For this study, a subset of the Madison weather data comprised of 35 different days was chosen and parametric simulation runs were performed for each of these 35 days. The days chosen had daily maximum temperatures that ranged from 10 °C (50 °F) to 35 °C (95 °F) and daily average temperature ranging from 2.5 °C (37 °F) to 28 °C (82 °F). For each day, 4 or 5 runs were performed with the floating duration set to different values. The floating window was consistently centered at 4 p.m. because the RTP data investigated suggested that the highest prices usually occur in the afternoon hours near 4 p.m. Bias as a result of initial conditions in the simulation were eliminated by running the weather data for each day over 7 consecutive days to allow convergence to a quasi-steady periodic solution. Only the results for the 7^{th} day were then considered.

In order to reduce calculation effort, days with maximum temperatures colder than 10 °C (50 °F) were not considered in the parametric runs. In winter months with colder average temperatures, the RTP profiles are much flatter than on summer days with higher ambient temperatures. The greater difference between peak price and average price for the warmer days makes load shifting more likely to be cost-effective on the warmer days. Therefore only the warmer days with maximum temperatures of 10 °C (50 °F) or higher were considered possible days for load shifting and the allowable floating duration was investigated for these day types.

The product corner temperature was chosen to be the critical value that constrained the maximum possible floating duration. A strict criterion would be that the corner temperature does not exceed –18 °C (0 °F). Imposing this strict criterion results in shorter maximum floating durations than if the corner temperature is allowed to float to a higher temperature. Allowing the corner temperature to increase to –17 °C (1.5 °F) or even –16 °C (3 °F) results in a considerable extension of the possible floating duration.

Installation of additional refrigeration capacity is also likely to influence the floating duration. The more refrigeration capacity installed, the more the freezer can be precooled, which would result in longer possible floating durations.

As a result of the parametric runs, the possible floating duration was modeled as a function of daily average or maximum temperature for a given refrigeration capacity installed (usually expressed by the number of compressors) and the corresponding maximum allowable corner temperature.

4.2.2.1 Massive wall warehouse

The following plots show the results from the parametric runs. Each plots shows the data points for the possible floating duration for the 35 days of Madison weather data. Each data point gives the possible floating duration as a function of the average or the maximum temperature of the day. Results for different numbers of compressors, which represents the installed refrigeration capacity, are overlaid on the plots. Three compressors is the base case, up to six compressors installed are considered. The plots are for allowable corner temperatures of –18 °C and –16 °C.

The tables show the corresponding curve fits derived from the possible floating duration data. The curve fits were calculated by performing linear regression analysis on the data generated by the simulations. More plots and correlations for different parameters can be found in the appendix A.

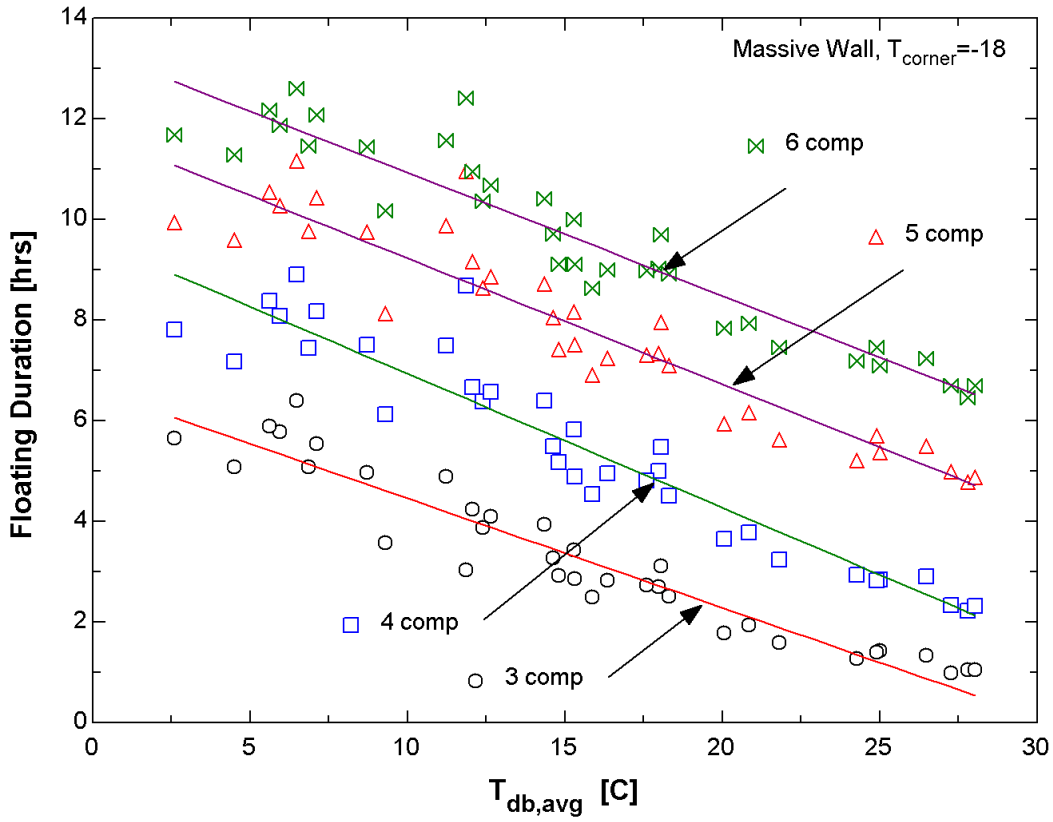

Figure 4-9: Floating duration as function of average daily dry bulb temperature for massive wall and maximum corner temperature of –18 ℃.

Table 4-4: Correlations for maximum floating duration as a function of average daily temperature for massive wall and maximum corner temperature of –18 ℃

# Comp	Refrig. Capacity/ KW_t (tons)	Correlation	R^2
3	302 (86)	FloatDur=6.6263 - 0.21716·T_db_avg	91%
4	604 (172)	FloatDur =9.5961 - 0.26631·T_db_avg	90%
5	906 (258)	FloatDur =11.727 - 0.25019·T_db_avg	88%
6	1208 (344)	FloatDur =13.375 - 0.24472·T_db_avg	90%

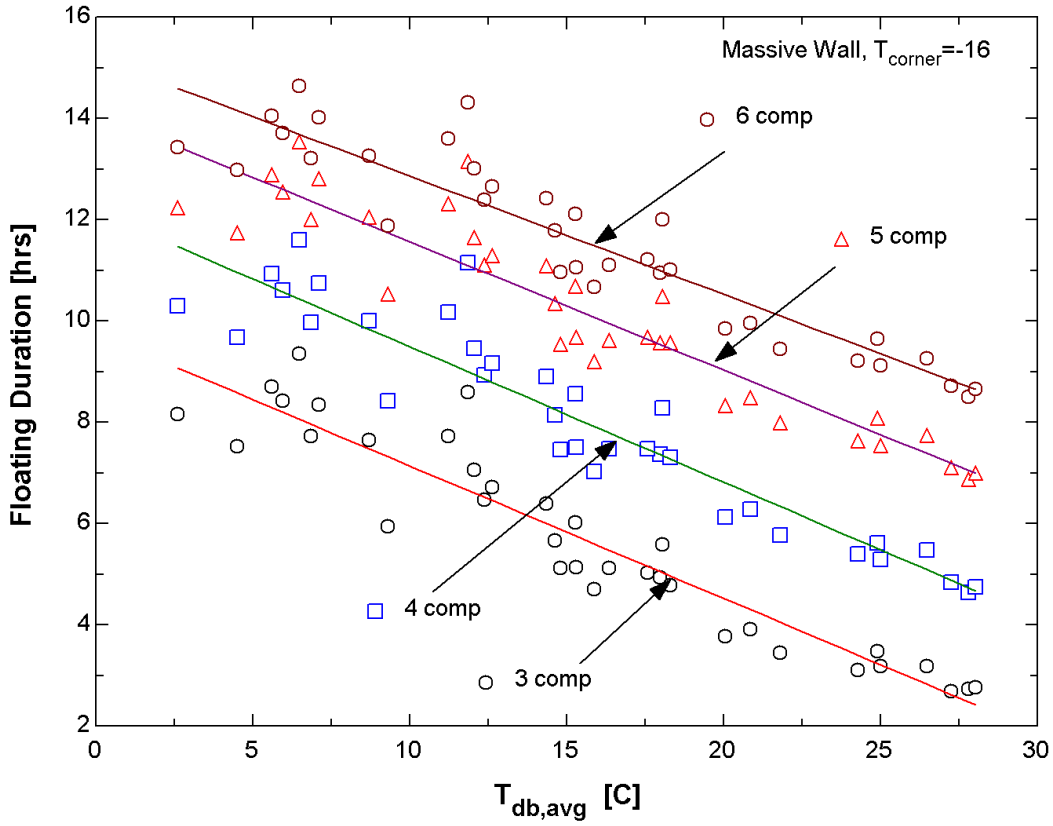

Figure 4-10: Floating duration as function of average daily dry bulb temperature for massive wall and maximum corner temperature of –16 ℃.

Table 4-5: Correlations for maximum floating duration as a function of average daily temperature for massive wall and maximum corner temperature of –16 ℃

# Comp	Refrig. Capacity/ KW_t (tons)	Correlation	R^2
3	302 (86)	FloatDur =9.7531 - 0.26165·T_db_avg	89%
4	604 (172)	FloatDur =12.162 - 0.26732·T_db_avg	88%
5	906 (258)	FloatDur =14.102 - 0.25388·T_db_avg	87%
6	1208 (344)	FloatDur =15.203 - 0.23404·T_db_avg	87%

From Figure 4-9 and Figure 4-10, several observations can be made. With the ambient temperature increasing, the possible floating duration decreases. An increase of 5 °C in dry bulb temperature results in a possible floating duration reduction by about 1.5 hours.

Increasing the installed refrigeration capacity by 86 tons form 3 to 4 compressors increases the possible floating duration of about 2 hours. Adding more capacity increases

the possible floating duration even more. Theoretically, if more and more capacity is added, the possible floating duration should reach a limit because further precooling would be rate-limited by the stored product. In Figure 4-10 this affect can be observed: Adding a sixth compressor does not increase the possible floating duration as much as did adding the fourth compressor.

Allowing a higher corner temperature extends the floating duration considerably: For example, for an average dry bulb temperature of 15 °C and 3 compressors installed, a maximum allowable corner temperature of –18 °C allows only about 3.5 hours of floating. If the product corner temperature is allowed to increase to up to –16 °C, the possible floating duration jumps to nearly 6 hours, an improvement of 2.5 hours. This observation makes clear that the choice of an appropriate allowable corner temperature can have a similar effect as the installation of additional refrigeration capacity.

When applying the above correlations, one has to keep in mind that these are only curve fits that provide recommendations for the allowable floating duration based on the average of the daily weather pattern. For days where the weather pattern is very different from the average, the correlations can give floating duration that are too long or too short. From Figure 4-9 and Figure 4-10 it can be seen that some days exist for which the allowable floating duration is far from the result the correlation would give. In order to ensure that the corner temperature remains all the time below the critical value, an alternative least squares curve fit should be used based on data that is below all the data points for the desired combination of walls, compressors and corner temperatures. On the other hand, this conservative approach will lead to a relatively short allowable floating duration, which will reduce the possible savings under a real-time pricing structure.

Correlations similar to those for the daily average temperature have also been found for the daily maximum temperature. Figure 4-11 shows a plot of the possible floating duration as a function of the next day maximum temperature.

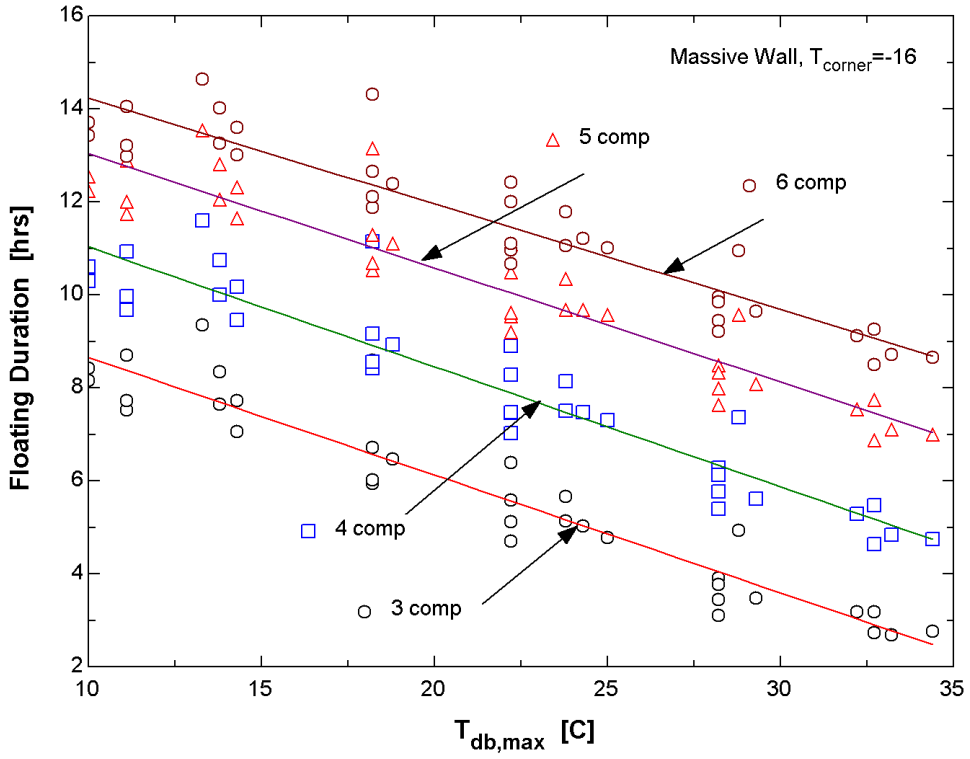

Figure 4-11: Floating duration as function of maximum daily dry bulb temperature for massive wall and maximum corner temperature of –16 ℃.

Table 4-6: Correlations for maximum floating duration as a function of maximum daily temperature for massive wall and maximum corner temperature of –16 ℃

# Comp	Refrig. Capacity/ KW_t (tons)	Correlation	R^2
3	302 (86)	FloatDur =11.185 - 0.25311·T_db_max	90%
4	604 (172)	FloatDur =13.611 - 0.25794·T_db_max	88%
5	906 (258)	FloatDur =15.488 - 0.24542·T_db_max	88%
6	1208 (344)	FloatDur =16.494 - 0.22691·T_db_max	88%

Basically, no difference in prediction of duration can be observed if the daily maximum temperature is used instead of the daily average temperature. The R^2 values are in the same range for both temperatures used.

Overall, for the massive wall warehouse configuration investigated, the observed floating duration seems to be highly predictable only as a function of the next day average or

maximum dry bulb temperature. The R^2 values confirm a strong correlation between the floating duration and the outside air temperature.

4.2.2.2 Lightweight wall warehouse

Similar parametric runs as for the massive wall construction were performed for the lightweight wall construction. From design day calculations performed earlier during this study, it was already known that the lightweight wall construction requires 4 compressors in the base case, which is one compressor more than the massive wall construction because of the higher peak load. For the lightweight wall warehouse, the effect of 1 and 2 additional compressors was investigated. Also in this case, higher allowable corner temperatures of –17 °C (1.5 °F) and –16 °C (3 °F) were studied. Figure 4-12 and Figure 4-13 show results for the lightweight wall that can be compared to the results for the massive wall presented in Figure 4-9 and Figure 4-10.

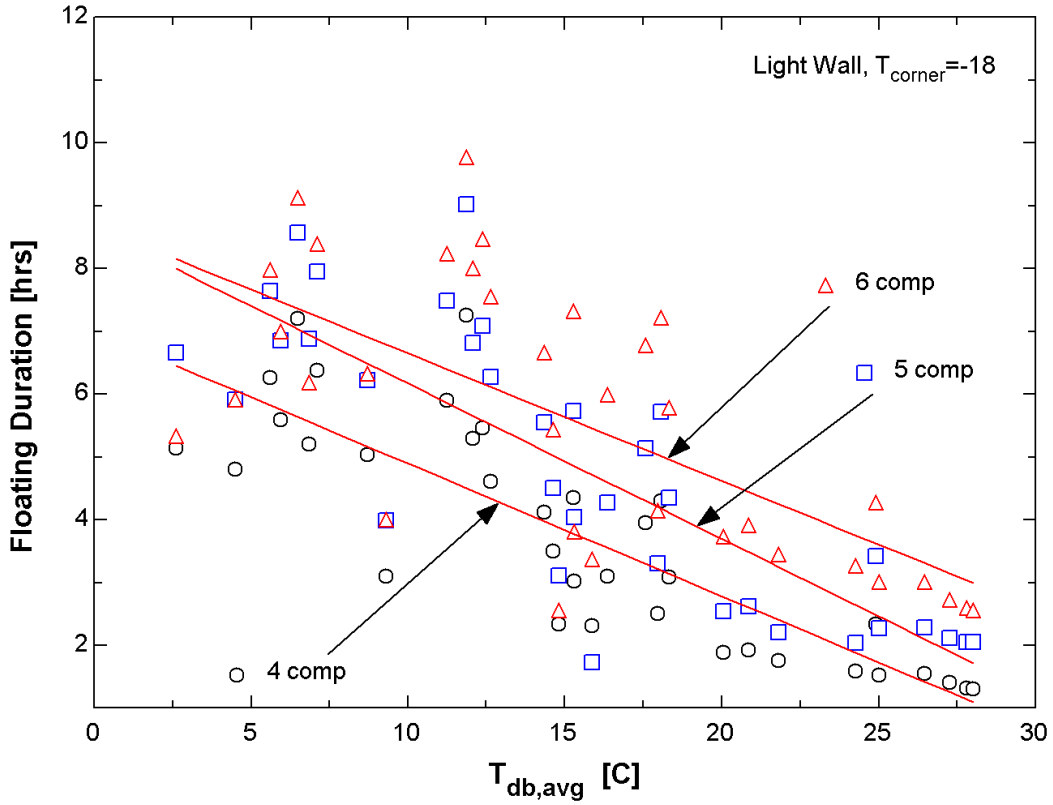

Figure 4-12: Floating duration as function of average daily dry bulb temperature for lightweight wall and average corner temperature of –18 ℃.

Table 4-7: Correlations for maximum floating duration as a function of average daily temperature for lightweight wall and average corner temperature of –18 ℃

# Comp	Refrig. Capacity/ KW_t (tons)	Correlation	R^2
4	604 (172)	FloatDur=7.0003 - 0.21106·T_db_avg	72%
5	906 (258)	FloatDur=8.6339 - 0.24717·T_db_avg	67%
6	1208 (344)	FloatDur=8.6784 - 0.20315·T_db_avg	46%

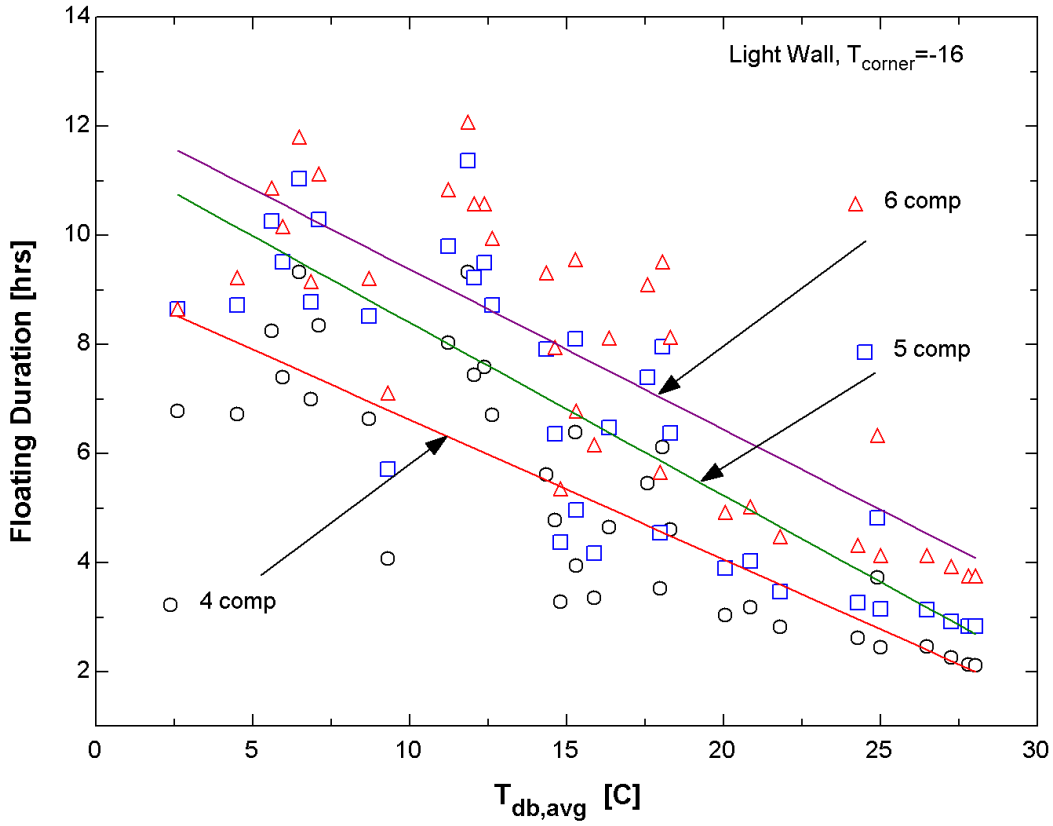

Figure 4-13: Floating duration as function of average daily dry bulb temperature for lightweight wall and average corner temperature of –16 ℃.

Table 4-8: Correlations for maximum floating duration as a function of average daily temperature for lightweight wall and average corner temperature of –16 ℃

# Comp	Refrig. Capacity/ KW_t (tons)	Correlation	R^2
4	604 (172)	FloatDur=9.1828 - 0.25639·T_db_avg	69%
5	906 (258)	FloatDur =11.556 - 0.31702·T_db_avg	71%
6	1208 (344)	FloatDur =12.310 - 0.29374·T_db_avg	65%

Compared to the massive wall, the lightweight wall construction makes the possible floating duration much less predictable. The data points in the plots are much more scattered and the R^2 value is lower. Days with similar average temperatures can have very different possible floating durations. For example, in Figure 4-13 for a day with an average temperature of about 15 °C and 4 compressors installed, the floating duration can range between 3 and more than 6 hours. For the massive wall, the same average

temperature and 3 compressors, Figure 4-11 shows that the floating duration can be between 4.5 and 6.5 hours, which is a smaller range.

Results for the lightweight wall warehouse were also obtained for the daily maximum temperature and different allowable corner temperatures. These results can also be found in the appendix A.

All together, the scattered results for the lightweight wall construction make estimating the possible floating duration much more difficult. In order to prevent product from exceeding the critical value, a very conservative estimation has to be used for the floating duration. This again leads to only very short possible floating durations, which limits the possible savings under a real-time pricing structure. Furthermore, the lightweight wall construction also results in shorter floating durations for the same number of compressors installed compared to the massive wall.

Both, the increased uncertainty in predicting the floating duration and the shorter floating duration compared to the massive wall can be explained by the decreased thermal capacity of the lightweight construction. First, the increased capacity of the massive wall flattens out the change in load on the warehouse during the day and therefore limits the peak loads. Also hourly fluctuations in the daily weather pattern are flattened out, which make the daily average temperature a good indicator for the day. For the lightweight wall warehouse, the hourly changes are not flattened out to the same extent and short-term events in the daily weather data affect the inside of the warehouse much faster, which results in more unpredictability. Secondly, the additional storage capacity of the massive wall also allows for a longer floating duration in general.

4.2.2.3 Influence of additional temperature information

In the preceding section, the possible floating duration was correlated as function of daily average or of daily maximum dry bulb temperatures for the 35 days of weather data investigated. For the massive wall, the results obtained were. R^2 values were always around 90%. For the lightweight wall, R^2 values were lower, only around 70%. In this

section the use of different predictors and combinations of these is examined. Not only the dry bulb temperature is considered but also the wet bulb temperature. Table 4-9 and Table 4-10 show combinations of different predictors and the resulting R^2 values. The results shown in all the tables are all for an allowable corner temperature of –16 °C (1.5 °F).

Table 4-9: Influence of different predictors on accuracy of floating duration prediction for massive wall, 3 compressors installed, T_{corner}=-16 °C

Predictors used				
T_db_avg	T_db_max	T_wb_avg	T_wb_max	R^2
X				89.1%
	X			89.6%
		X		79.3%
			X	75.0%
X		X		90.1%
	X		X	89.6%
X	X	X	X	92.2%

Table 4-10: Influence of different predictors on accuracy of floating duration prediction for massive wall, 6 compressors installed, T_{corner}=-16 °C

Predictors used				
T_db_avg	T_db_max	T_wb_avg	T_wb_max	R^2
X				86.6%
	X			87.5%
		X		75.4%
			X	71.0%
X		X		88.5%
	X		X	87.6%
X	X	X	X	90.2%

Using the daily average or the daily maximum temperature as a predictor leads approximately to the same R^2 values. Using only the wet bulb temperature as a predictor leads to worse results, the R^2 value decreases considerably. Infiltration through the loading dock can explain the reduced influence of the wet bulb temperature. All the infiltration loads to the freezer are through the dock. The air is dehumidified in the dock before it enters the freezer. This eliminates any direct influence of the wet bulb temperature on the freezer load. The air entering the freezer from the dock is of a relatively constant humidity ratio as the dock is kept at relatively constant conditions.

Also, using combinations of the predictors or even all of the four does not lead to much higher R^2 values than if using only one dry bulb predictor.

The results obtained for the lightweight wall are a little different. Table 4-11 and Table 4-12 show the R^2 values for the use of 4 compressors and 6 compressors and an allowable corner temperature of -16 °C (3 °F).

Table 4-11: Influence of different predictors on accuracy of floating duration prediction for lightweight wall, 4 compressors installed, T_{corner}=-16 °C

Predictors used				
T_db_avg	T_db_max	T_wb_avg	T_wb_max	R^2
X				68.7%
	X			76.3%
		X		54.3%
			X	53.6%
X		X		76.0%
	X		X	79.1%
X	X	X	X	79.3%

Table 4-12: Influence of different predictors on accuracy of floating duration prediction for lightweight wall, 6 compressors installed, T_{corner}=-16 °C

Predictors used				
T_db_avg	T_db_max	T_wb_avg	T_wb_max	R^2
X				65.1%
	X			71.7%
		X		49.8%
			X	48.8%
X		X		74.7%
	X		X	75.3%
X	X	X	X	76.0%

Again, the wet bulb temperatures alone are the poorest predictors. Combinations of predictors seem to improve the correlation over a single predictor for the two cases shown. All four predictors give the best results for the lightweight wall. But overall, the R^2 values are still much lower than for the massive wall. Even with several predictors it is difficult to predict the possible floating duration for the lightweight wall.

As a conclusion, it is found that the floating performance of the warehouse with the massive walls seems predictable with either the next day average or maximum dry bulb temperature known. A single predictor variable is sufficient; the use of multiple predictors does not significantly improve the prediction.

For the lightweight wall warehouse, floating performance prediction is much more difficult, the uncertainty associated with the prediction is much higher. Multiple predictors seem to improve the results compared to a single predictor, but the uncertainty is still larger than for the massive wall. Therefore, from a standpoint of predicting possible floating durations for a refrigerated warehouse, the use of a more massive wall construction seems highly recommended. Furthermore, the massive wall construction results also in lower peak load.

4.2.2.4 Implementation of correlation into simulation

A TYPE was created to implement a floating duration correlation into TRNSYS. Two regression coefficients, which depend on the wall construction used, the number of compressors installed and the allowable maximum corner temperature, are required inputs to the type. Also the next day average or maximum temperature, depending on the correlation used, has to be specified. Given these inputs, type 113 estimates the allowable duration of floating for the next day.

4.2.3 Next day weather data

For the floating duration calculation either the next day average or maximum dry bulb temperature has to be known. In most cases the next day maximum and next day average temperatures are readily available from weather forecasts.

For the purpose of the simulation, next day weather data was easily available in the weather data file. The dry bulb temperatures for the next day are read from the weather data file and a separate unit calculates the average and the maximum for the next day. This result is then used for the floating duration calculation. Compared to reality, this approach is a little more accurate as the data that will drive the simulation on the next day

is actually read in advance. In reality, only a forecast associated with uncertainty is available.

A second option that could be explored if there is no next day weather data available is to assume that the next day weather will be the same as the current day. This assumption leads to more uncertainty, but for many days of the year, this assumption might still lead to relatively good results compared to the simplicity of implementation.

4.2.4 Best floating window

From the analysis performed before, the maximum possible floating duration can be estimated. Now, the next day real-time price profile has to be analyzed and a decision has to be taken during which time window the refrigeration equipment is shut down. If only the price profile is considered, the window with the highest potential cost savings is the window with the highest integrated cost over the estimated floating period. Figure 4-14 shows four different possible six-hour duration floating windows centered around the peak price period.

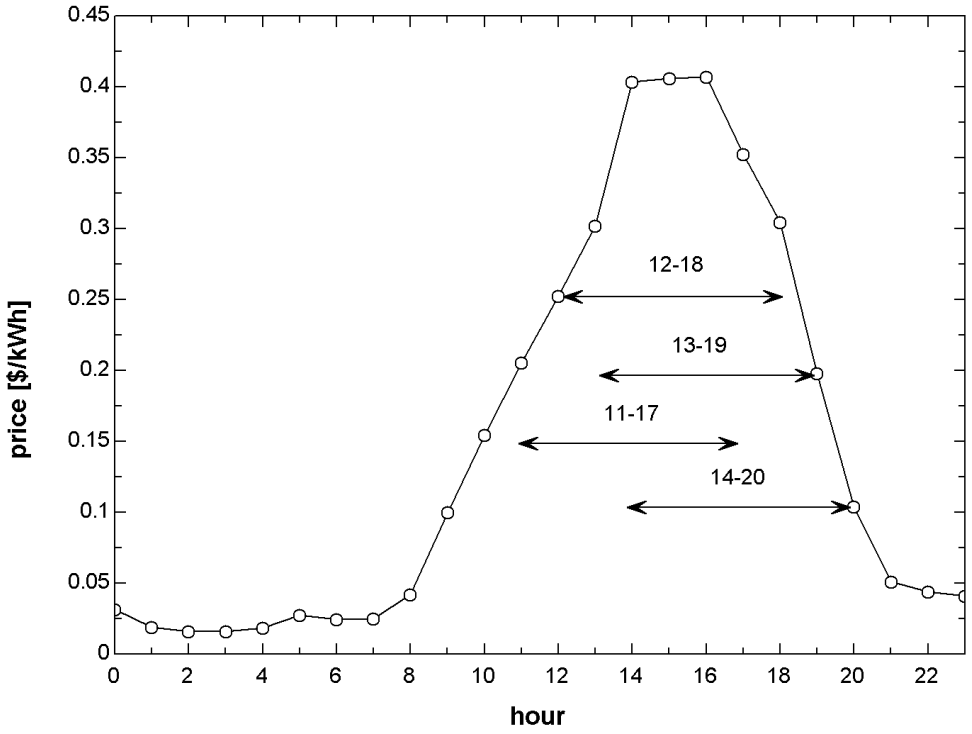

Figure 4-14: Different windows for a maximum possible floating duration of 6 hours.

For the day pricing curve shown, the window from hour 12 to hour 18 would offer the highest savings since the integrated cost during this period is highest. The cost is also higher than for the window from hour 13 to hour 19 because the price in hour 12 is higher than the price in hour 19 and the windows have the same prices for the hours in between.

This approach considers only the savings potential that could be realized during the shutdown period, it does not consider the cost associated with the precooling during the hours the rest of the day. The cost for precooling has to be considered. The best floating window would be the window with the lowest overall daily operating cost and not the window with the highest savings. Unfortunately, in order to calculate the operation cost associated with each shutdown window, the electric power demand for each of the next day operation alternatives would have to be known in advance. The electric power demand of the warehouse for the next day could be calculated with the help of a simulation, but next day's hourly weather data would be required, including hourly

values of solar incident radiation. The implementation of such a calculation would be difficult. Furthermore, in most cases the window with the lowest operation cost will supposedly be the window with the highest savings calculated with the simpler integrated savings approach presented above. For some days, the lowest operation cost might occur for windows slightly different than the highest savings window. Given the difficulty of predicting the cost for each possible floating window for the next day, the floating period was chosen to be the period with the highest integrated savings. In section 4.3.1.4, a sensitivity analysis is described in which the effect on the daily operating cost of shifting the floating window one hour earlier or later compared to the recommendation from the integrated savings calculation is investigated. Only a few days in the year, higher savings result if the shifting is done one hour earlier or later. In the TRNSYS simulation, a type was created that calculated the best floating window for the next simulation day given the possible floating duration.

4.2.5 Corner temperature during year

Once the types that calculate the possible floating duration and the best floating window were implemented in TRNSYS, yearly simulations with every day demand shifting were run and the daily maximum corner temperatures were monitored. In this scenario the load shifting was done every day, no matter if cost savings could be achieved or not. Figure 4-15 and Figure 4-16 show the daily average ambient dry bulb and daily maximum product corner temperature over the year for the massive wall and the –18 °C and the –16 °C corner temperature correlations.

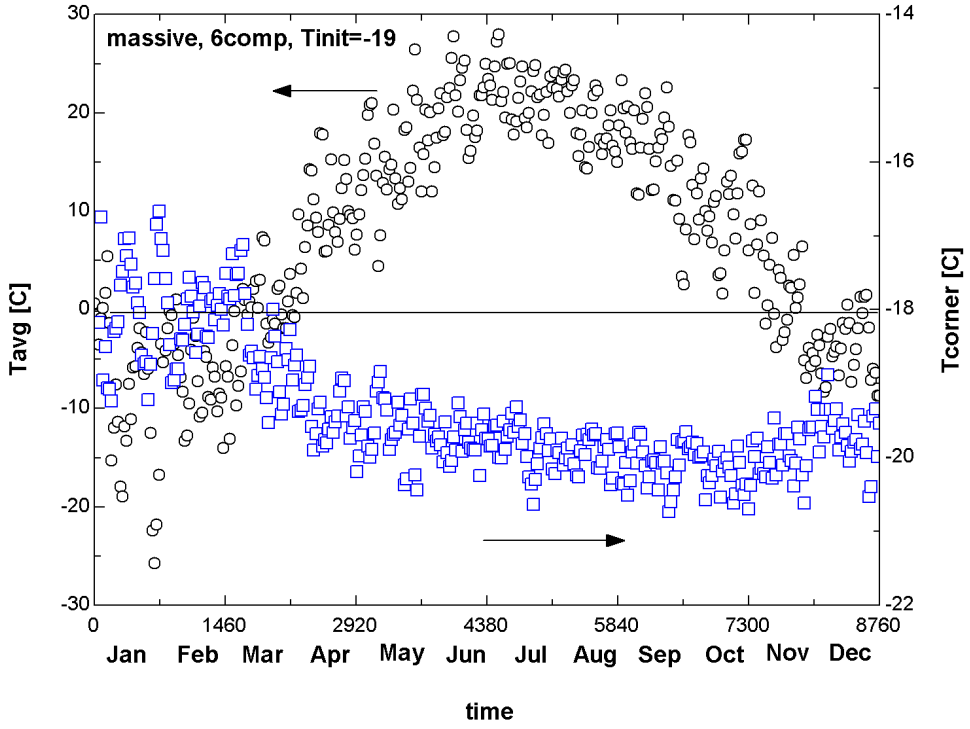

Figure 4-15: Maximum daily corner temperature over year for –18 ℃ correlation, massive wall, 6 compressors

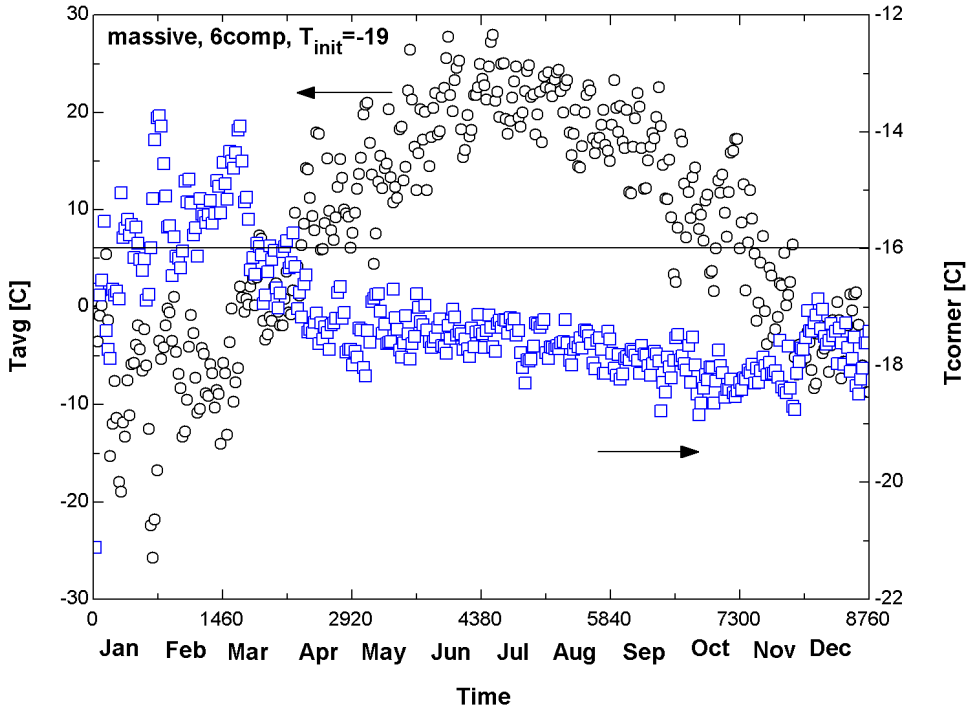

Figure 4-16: Maximum daily corner temperature over year for –16 ℃ correlation, massive wall, 6 compressors

Both plots show that the correlations over predict the possible floating duration at the beginning of the year in the months of January and February. As a result, the product corner temperature gets too warm. The rest of the year, the correlations predict the floating duration well. The corner temperature remains under the critical value for the rest of the year, the product is even slightly overcooled. The trend to increased product temperature at the beginning of the year can be explained by review of the regression analysis and understanding the basis upon which the correlations were derived. The coldest of the 35 days of weather data used for the parametric runs had a maximum temperature of 10 °C (50 °F). The correlations are therefore not valid for days considerably colder than 10 °C. The correlations predict a floating duration that is too long for very cold days as they occur in January and February for Madison weather data.

For the lightweight wall construction considered, Figure 4-17 and Figure 4-18 show the daily maximum corner temperature over the year.

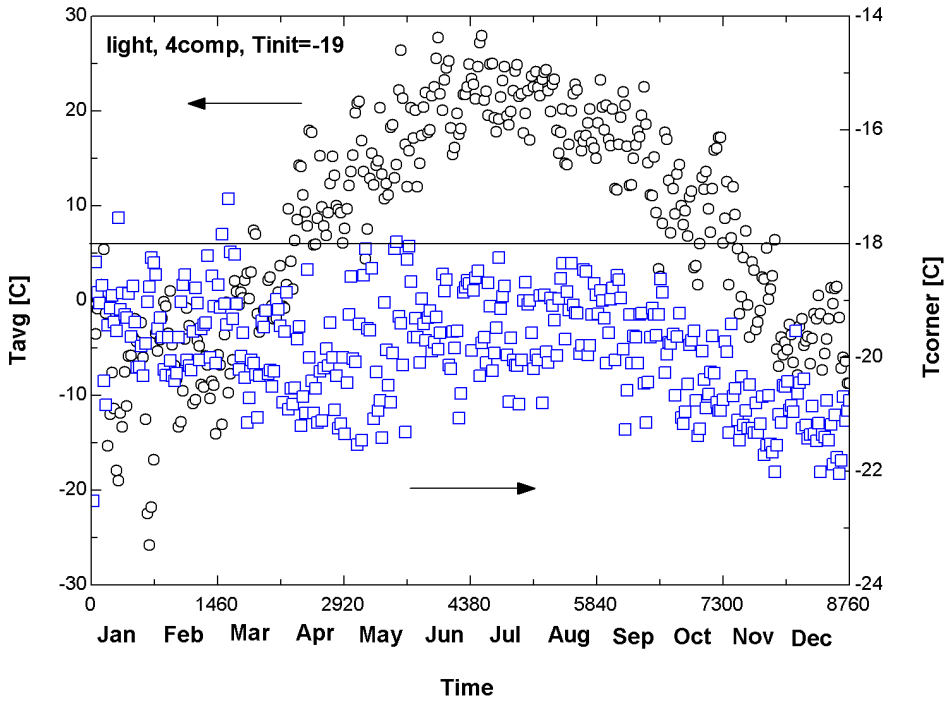

Figure 4-17: Maximum daily corner temperature over year for –18 °C correlation, lightweight wall, 4 compressors

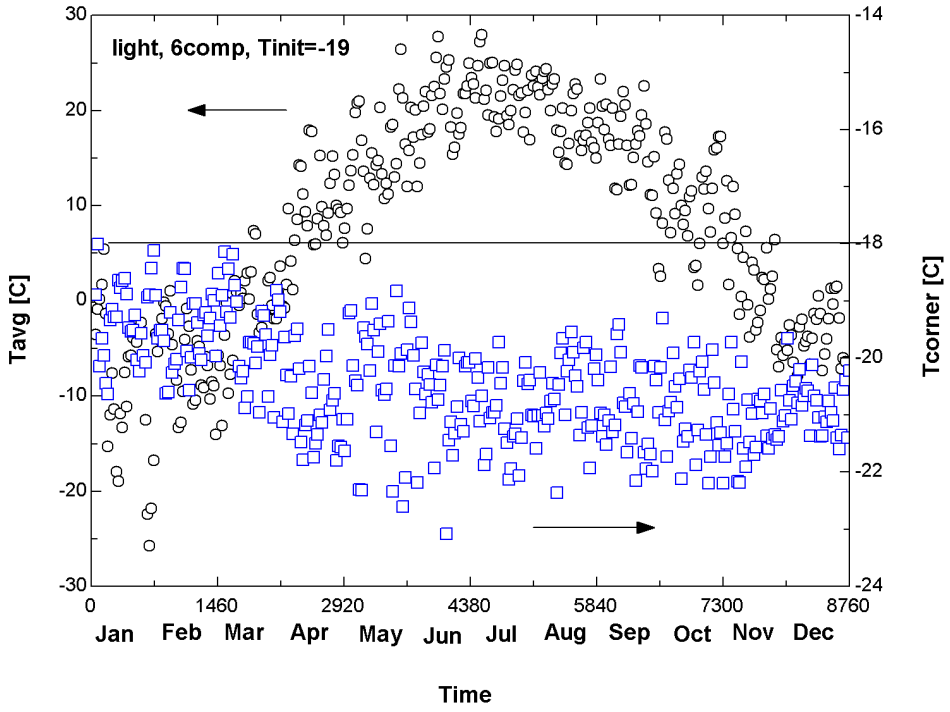

Figure 4-18: Maximum daily corner temperature over year for –18 °C correlation, lightweight wall, 6 compressors

Again, it can be observed that the lightweight wall construction results in more scattered corner temperatures. The range of daily maximum corner temperatures is much larger for the lightweight wall. Interestingly, the –18 °C corner temperature correlation really keeps the corner temperature below –18 °C, even at the very cold days in January and February, when the daily temperatures are in a range were the correlation was not intended to work properly. The correlation seems to be sufficiently conservative, but it has to be considered that the predicted possible floating durations are shorter than for the massive wall.

4.3 Demand Shifting Results

With the possible floating duration and the best floating window known, TRNSYS simulations with different load shifting strategies were run. As one output, the warehouse power demand for every hour of the year was recorded. If the power demand for every hour and the real-time price for every hour are known, the resulting operation

cost can be calculated. Unfortunately, the real-time prices obtained were for different utilities in different parts of the US. Besides, the real-time pricing data given is from a specific period of time in the past. In order to match the simulation with the real-time prices, the weather data used in the simulation would have to be for the same geographic region and the same period of time from which the real-time pricing data is derived.

However, in Chapter 3, the relationship between weather data and real-time prices was investigated. It was shown that the real-time prices are not strongly correlated to daily fluctuations in weather data. On the other hand, real-time price patterns change depending on the time of the year. Therefore it was assumed that real-time prices from different utilities in the US could be combined with Madison weather data and the results should still be representative. To estimate the influence of the change in real-time prices from day to day, the order of the occurrence of the daily real-time prices in each month was changed. The simulation was run again with the changed order of real-time prices. Section 4.3.1.2 discusses the effect.

The results for load shifting are generally compared to the base case where the equipment is operated to maintain the freezer temperature at a constant –18 °C. For the massive wall construction, 3 compressors are installed in the base case, while 4 compressors are installed for the lightweight wall construction.

4.3.1 PG&E pricing structure

The PG&E pricing structure has by far the biggest difference between peak prices and off-peak prices. Therefore this pricing structure offers the biggest possible savings for demand shifting compared to baseline operation. Different warehouse operational scenarios are explored in this section with the end goal of minimizing daily operation costs. The full demand shifting operation strategy means that the compressors are operated at full capacity during off-peak and the warehouse is precooled as much as possible. During the floating period, the compressors are off. Next, the influence of a changed order of real-time prices on the yearly savings is examined. Besides that, reduced precooling duration is explored, which means that the equipment is operated at

full power only for a certain period before the equipment is shut down for floating. Last, the influence of shifting the floating window to an earlier or later time is investigated.

4.3.1.1 Full demand shifting

Simulations were performed with different combinations of installed refrigeration capacity and possible floating duration correlations used and the results are presented in this section. More simulation runs were performed for the massive wall construction because the massive wall allows for a longer floating duration for the same number of compressors, which results in higher savings. Two options are compared: The first option is the base case with 3 compressors for the massive wall and 4 compressors for the lightweight wall installed and no load shifting done at all. In the second option, the same number of compressors or more is installed and the shifting is done daily. The daily electricity cost is compared in both cases. If load shifting offered savings over continuous operation, the day was marked as a day with possible savings. At the end of the year, all possible savings were summed up. This sum is an indicator for the maximum potential savings that would be achieved if all days where savings were possible were recognized as such days in advance and the equipment would then be operated in load shifting mode. For days where no savings were realized, no floating would be done in reality. The results should be seen as indicators under which conditions savings are possible. From these results, recommendations for the development of a real-time pricing controller can be made.

Table 4-13 compares the yearly electricity cost for the standard configuration with the massive wall for demand shifting and continuous operation: 3 compressors are installed, and the correlation for a maximum corner temperature of –18 °C (0 °F) is used.

Table 4-13: Yearly electricity cost for massive wall, 3 compressors, T_{corner}=-18 °C

Cost for continuous operation/ $	Cost for daily floating operation / $	Days with potential savings	Max potential savings /$
169,440	295,515	0	0

For the base case, no potential savings with full demand shifting were realized. Even for days when real-time prices peak at 1.60 $/kWh, demand shifting offered no savings. This

can be explained be the very short possible floating duration for this configuration. Having only 3 compressors installed does not offer enough precooling capacity and the –18 °C-correlation for the possible floating duration allows only a short floating duration on the warmer days. The resulting floating window and the cost savings during this window are insufficient to compensate for the additional cost penalty incurred for precooling. In section 4.3.3, explanations are given for the high precooling cost.

Installing additional compressors offers more precooling capacity and a longer floating duration to achieve savings. A similar effect results from a higher allowable product temperature. Table 4-14 shows the results for the massive wall, different numbers of compressors installed and different allowable corner temperatures.

Table 4-14: Potential savings for different combinations of installed capacity and allowable corner temperature for massive wall

#	#comp	T_{corner}-corr.	Days with potential savings	**Max potential savings /$**
1	3	-18	0	**0**
2	3	-16	87	**7,105**
3	6	-18	22	**8,658**
4	6	-16	56	**14,547**

Installation of 3 additional compressors or allowing the corner temperature to increase offers additional potential savings of several thousand dollars per year. Case #2 offers savings on more days, but the savings per day are smaller in the average. Case #3 and #4 offer more savings at fewer days, the savings are more concentrated on certain days.

A day-to-day analysis is shown in Table 4-15. The table shows all days when saving occurred for 6 compressors in combination with the –18 °C correlation and the –16 °C correlation.

Table 4-15: Days with possible savings for massive wall, 6 compressors, T_{corner}=-16 °C and –18 °C.

day	Baseline cost/ day	Max. RTP Price/ $/kWh	**Savings for –16 corr/ day**	**Savings for –18 corr/ day**
29	238.46	0.069	19.87	
64	273.24	0.105	0.027	
133	245.50	0.097	28.59	10.45

day	Baseline cost/ day	Max. RTP Price/ $/kWh	**Savings for –16 corr/ day**	**Savings for –18 corr/ day**
141	267.63	0.088	8.47	
142	230.07	0.088	21.98	
147	403.75	0.126	7.56	
153	278.06	0.103	48.63	29.26
154	328.80	0.098	26.18	
156	311.02	0.084	16.27	
159	330.66	0.113	11.06	
160	393.50	0.107	24.68	
161	401.07	0.097	23.70	
162	360.89	0.088	27.22	
163	284.82	0.088	46.73	
166	2595.32	1.385	1161.51	936.29
167	429.49	0.083	11.97	
168	1543.23	0.369	375.34	75.04
169	1109.96	0.377	453.48	243.08
170	284.95	0.090	13.18	
173	491.89	0.110	21.36	
175	407.65	0.128	23.12	
180	403.07	0.114	40.08	
181	422.29	0.110	24.51	
183	483.70	0.102	8.96	
184	469.83	0.109	14.25	
187	508.15	0.110	25.45	
188	3448.45	1.427	1245.75	789.10
189	1913.99	0.407	337.90	
191	335.54	0.089	26.22	
194	1507.42	0.406	337.48	48.47
196	2590.95	1.447	1072.40	903.52
197	2506.32	1.434	1003.41	773.43
198	2835.10	1.434	1131.17	893.20
201	2862.20	1.469	1114.80	880.69
202	1280.99	0.444	248.78	
208	1708.27	0.507	291.69	
209	1424.79	0.487	284.81	106.57
215	2547.59	1.218	782.79	615.14
216	3505.98	1.591	1242.42	927.94
217	1763.96	0.502	360.45	109.81
222	1147.63	0.309	89.78	
223	1651.49	0.543	261.83	
224	2043.97	0.582	384.08	50.52
230	830.81	0.315	48.07	26.05
231	812.62	0.309	15.38	
232	1112.63	0.316	49.03	
233	1202.71	0.318	23.57	
240	1296.20	0.413	158.86	
243	1844.44	1.159	606.09	569.71
245	1908.18	1.134	531.52	525.41
252	1439.15	0.356	161.53	
253	1025.70	0.378	140.04	108.03
254	786.28	0.331	19.91	
338	325.73	0.142	76.40	19.33
341	638.54	0.326	10.51	

day	Baseline cost/ day	Max. RTP Price/ $/kWh	**Savings for –16 corr/ day**	**Savings for –18 corr/ day**
344	618.71	0.294	5.79	17.05
Sum			**14,546.64**	**8,658.09**

The higher allowable corner temperature of –16 °C nearly doubles the potential savings compared to the –18 °C correlation. Comparing the days when the savings occur for both correlations shows that savings for the –18 °C correlation are only on days when also savings for the –16 °C correlation occur. The –16 °C correlation offers bigger savings on these days and additional savings on other days. Nevertheless it has to be considered that the savings on many days are small compared to the total daily cost. In reality, demand shifting probably would not be done if the calculations indicate that the possible savings are very small compared to total daily cost. The uncertainly if these small savings can be realized or if demand shifting is actually more expensive than baseline operation might lead an operator to decide not to perform any load shifting on these days.

Figure 4-19 plots the daily savings compared to baseline operation versus the daily peak price. The results are for 6 compressors installed and the –18 °C and the –16 °C correlation.

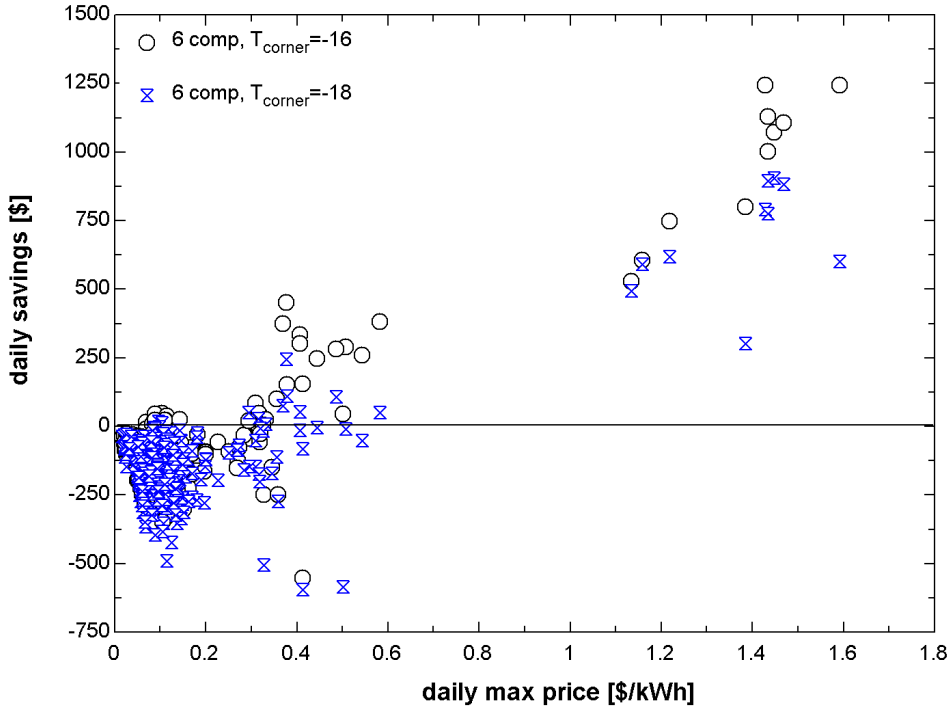

Figure 4-19: Daily savings vs. daily peak price for 6 compressors, massive wall and allowable corner temperature of –18 °C and –16 °C.

From the plot it can be seen that the highest savings occur in both cases on days with the highest prices. If the peak price is higher than 0.6 $/kWh, a day always offers potential savings in both cases. The –16 °C correlation offers higher savings and savings on additional days. For days with a peak price lower than 0.2 $/kWh, no savings can be realized in most cases. The days with lower peak prices occur much more often during the year than the high price days.

Several simulation runs were also performed for the lightweight wall construction. But from the above results with only little savings compared to the total electricity cost for the massive wall, it could already be estimated that the lightweight wall with a shorter possible floating duration would offer only reduced savings compared to the massive wall. Table 4-16 shows possible savings for the lightweight wall. The baseline operation cost for the lightweight wall is $ 172,664.

Table 4-16: Potential savings for different combinations of installed capacity and allowable corner temperature for lightweight wall

#	#comp	T_{corner}-corr.	Days with potential savings	**Max potential savings /$**
1	6	-18	4	**770**
2	6	-16	15	**4,693**

The smaller potential savings for the lightweight wall make demand shifting even less likely to be successful. The lower potential savings compared to the massive wall confirm again that the massive wall construction is highly recommended.

4.3.1.2 Changed order of real-time prices

As mentioned before, the real-time pricing data obtained is neither for the same location nor for the same period in time than the weather data used in the simulation. In order to estimate the effect of a change in the order in which the prices occur, the PG&E real-time pricing data file was modified: the order of the daily prices within each month was randomly changed and simulations were run again. Table 4-17 shows the effect.

Table 4-17: Effect of changed order of real-time prices

		Given order of RTP		**Changed order of RTP**	
#comp	T_{corner}-corr.	Days with potential savings	**Max potential savings /$**	Days with potential savings	**Max potential savings /$**
6	-18	22	**8,658**	25	**6,633**
6	-16	56	**14,547**	54	**14,783**

Comparing the simulation runs performed with the changed order of real-time prices to the standard price order shows that the potential savings are influenced by the order in which the prices occur. But overall, the total yearly potential savings are still in the same order of magnitude. Also the number of days at which savings occur remains in the same range. A day-to-day comparison was done, comparing the days at which savings occur in both cases. It was found that the days very high peak prices around 1.20 $/kWh and more offer savings in both cases. For the days with very high prices it is the mainly the pricing factor that determines the savings potential, no matter what the exact weather pattern is. Days where the peak price is lower might offer savings in the one case, but not in the other. In this case, it is the daily weather pattern and the possible floating duration

resulting from this pattern that determine if savings are possible on a given day. A colder weather day results in a longer possible floating duration and savings on a certain pricing day, while a warmer weather with a shorter floating duration does not offer savings on this day. On a yearly average, the number of days with possible savings is approximately constant and the sum of possible savings remains in the same range, even if the order of real-time prices is changed.

4.3.1.3 Reduced precooling duration

From the simulation results presented in the previous sections, it was found that the possible savings resulting from full demand shifting are relatively small compared to the yearly electricity cost. The savings realized from shutting down the equipment during expensive hours are countered by increased electricity demand at times of equipment operation. Two effects that will be discussed in section 4.3.3 are responsible for these results. First, precooling the warehouse to a lower temperature leads to a higher overall load for the warehouse. Second, if the warehouse is kept at a lower temperature, the refrigeration equipment operates at lower COP for delivering colder air to the freezer to precool stored product. On most days, these two effects combined lead to an increase in cost that is not compensated for by the savings achieved during floating. A reduced precooling duration takes on the idea of limiting the hours of precooling and therefore operating the equipment at a higher efficiency due to a higher freezer temperature at certain times of the day. At the same time, the precooling duration should still be chosen long enough for sufficient thermal storage to keep the product cold during floating.

In one simulation, the precooling duration was chosen to be 6 hours every day, 6 compressors were installed and the massive wall construction used. For the floating duration correlation, in preliminary runs it was found that the –18 °C correlation for 6 compressors originally used would lead to a much too high product temperature. The possible floating duration calculated from this correlation was too long for only 6 hours of precooling. Table 4-18 shows the results with the 4-compressor –18 °C correlation with 6 compressors actually installed. With this correlation, the product temperature could still not be kept below the desired –18 °C, but at least below –16 °C.

Table 4-18: Potential savings for reduced precooling duration for massive wall

#	#comp	T_{corner}-corr.	Days with potential savings	**Max potential savings /$**
1	6	-18/ 4 comp	5	**322**

The result indicates that the precooling duration of only 6 hours is too short to allow for a long enough floating duration for considerable savings. A longer precooling duration would probably allow for longer floating, but at the same time the desired effect of limiting the duration of low equipment performance due to the lower warehouse temperature would be reduced. Therefore this result was seen as indicator that full demand shifting offers the greatest potential savings.

4.3.1.4 Earlier/ later shifting time

In section 4.2.4 the idea of the best floating window was introduced. It was concluded that in most cases the window with the biggest integrated savings should usually also be the window that offers the smallest cost over the whole day. In this section, the effect of shifting the floating window to one hour earlier or later is explored.

Table 4-19: Effect of shifting floating window for massive wall

#comp	T_{corner}-corr.	**Max savings window (standard)**		Shift 1 hour later		Shift 1 hour earlier	
		Days with pot. savings	**Max potential savings /$**	Days with pot. savings	**Max potential savings /$**	Days with pot. savings	**Max potential savings /$**
6	-18	22	**8,658**	21	**6,962**	17	**6,600**
6	-16	56	**14,547**	52	**13,286**	47	**12,381**

The results show that the integrated savings approach works well. The floating window that offers the highest savings also results in the lowest cost over the year if demand shifting would only be done on days with potential cost savings. Shifting one hour earlier or one hour later results in less potential savings over the year. Also the number of days with potential savings is reduced. A day-to-day comparison showed that the days with savings are basically still the same, but the savings per day decrease. Only a few days offer more savings if the shifting is done 1 hour earlier or 1 hour later.

4.3.2 Southern pricing structure

In the previous section, demand shifting under the PG&E real-time pricing structure was investigated. The PG&E structure has the biggest difference between peak prices and off-peak prices and offers the biggest possibility for savings through demand shifting compared to the other two pricing structures investigated in this study. However, in all cases investigated, the maximum possible savings depending on the operating strategy are lower than 10% of the yearly electricity cost if no demand shifting is done. From these results it becomes clear that the Southern and Niagara Mohawk pricing structure with their lower ratio of average peak to average off peak price offer even less potential savings than the PG&E structure. Therefore, the focus of the simulation runs was more on the PG&E prices and less on the other two structures. Nevertheless, a few runs were performed with the Southern pricing structure. Table 4-20 shows the results.

The baseline electricity cost under the Southern structure for the massive wall and 3 compressors installed is 80,443 $/year. This cost is much lower than the 169,440 $/year that electricity would cost under the PG&E pricing structure. However, it has to be considered that the PG&E structure is one-part pricing, where all cost is included in the energy charge. Southern offers a two-part structure where the energy cost is lower, but a considerable access fee might have to be added. Unfortunately, no information about this access fee was obtained and no estimation of the total cost under the Southern structure could be made.

Table 4-20: Potential savings under Southern pricing structure for massive wall

#	#comp	T_{corner}-corr.	Days with potential savings	**Max potential savings /$**
1	6	-18	12	**1,083**
2	6	-16	38	**4,838**

The Southern pricing structure offers much less potential savings than the PG&E structure. For the –16 °C-correlation, the potential savings are about 6 % of the baseline electricity cost. Still, potential savings of less than 5,000 $/year are small. Therfore, further investigation of potential savings under this pricing structure seemed not favorable.

4.3.3 Reasons for high precooling energy demand

The results presented earlier in this chapter indicate that demand shifting for refrigerated warehouses operating under real-time pricing leads to small potential operating cost savings. With only the needed refrigeration capacity installed to maintain the warehouse at –18 °C (0 °F) on the design day, no savings where possible unless the product temperature was allowed to increase above –18 °C. With additional installed capacity, savings are possible on days with high peak prices compared to the daily average price. On days with lower peak prices no savings can be realized.

In the process of analyzing the simulation results, it was found that precooling the warehouse requires much more energy than constant operation. The additional energy needed for precooling leads to much higher operating costs during the hours of precooling. Only if the electricity prices during the floating hours exceed a certain level relative to the precooling price will the savings achieved during floating compensate for the much higher energy cost during precooling.

The magnitude of the penalty paid for the precooling is surprisingly high, but two effects combine to exacerbate the energy penalty during precooling. First, operating the warehouse at a lower temperature during precooling increases the net cooling load on the warehouse. Second, the refrigeration equipment operates much less efficiently at the lower evaporator temperatures required during precooling. Figure 4-20 shows the average freezer air temperature during a typical precooling and floating cycle over 48 hours.

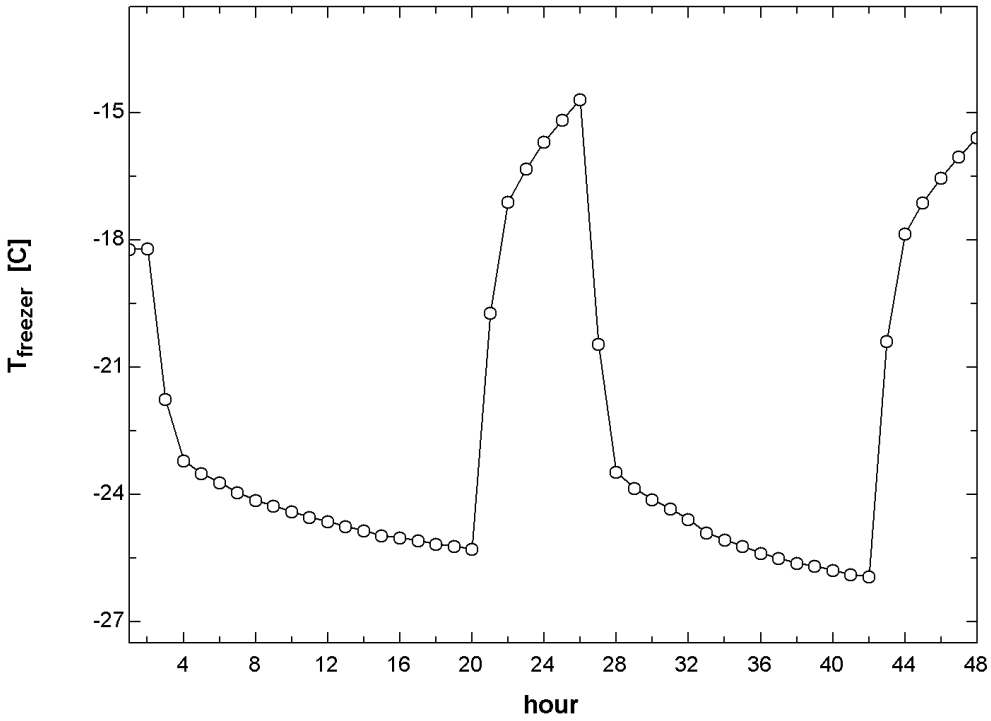

Figure 4-20: Freezer temperature during typical precooling and floating cycle.

Once precooling starts, the freezer temperature decreases rapidly by 5 to 6 °C and then continues decreasing at a lower rate. The rapid initial decrease in the freezer air temperature is attributable to the low heat capacity of air in the warehouse. Once the air itself is precooled, the product and warehouse envelope begin to cool down. The added thermal capacity of precooling stored products and the warehouse envelope results in a lower rate of temperature change. The equipment is turned off before the freezer temperature reaches steady state at the lower precooling temperature. The temperature increases rapidly again by 8 to 9 °C as it warms the air and continues increasing at a slower rate before cooling resumes again. The fact that the freezer reaches a lower temperature so quickly causes higher net refrigeration loads on the freezer, which is shown in Figure 4-22 and will be discussed there.

The lower freezer temperature also requires a lower refrigerant temperature in the evaporators. That decreases the available cooling capacity per compressor and increases the power demand per compressor. Figure 4-21 shows the compressor COP as a function of freezer temperature and ambient wet bulb temperature under full load. The equipment model is described in detail in section 2.3.

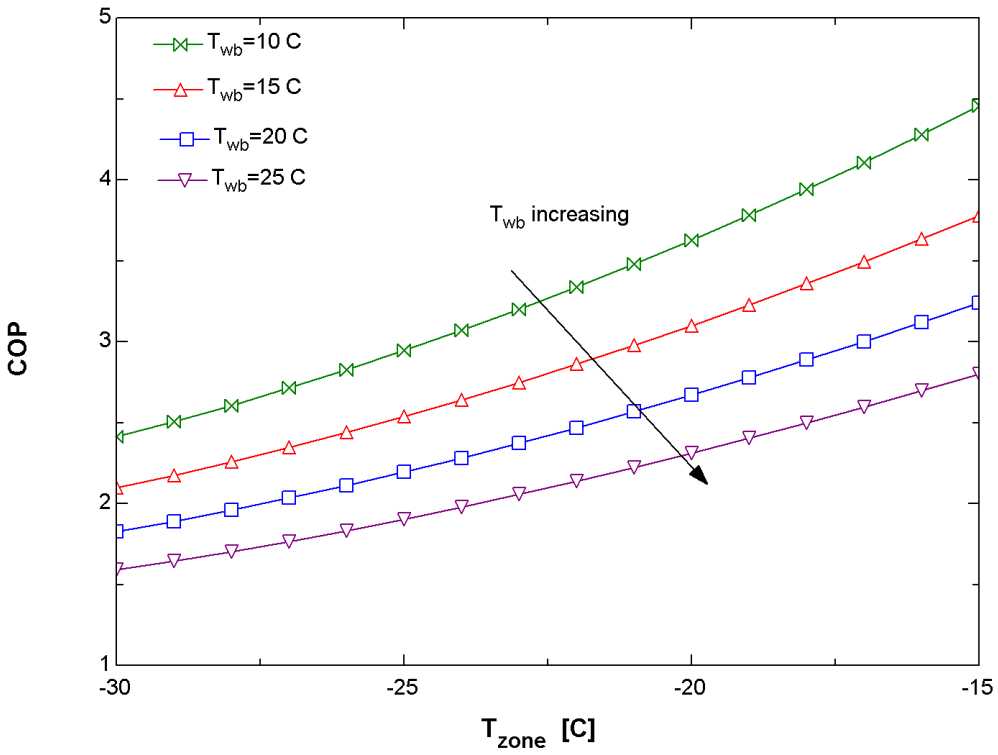

Figure 4-21: Compressor COP as a function of freezer and ambient wet bulb temperature

For example, for a wet bulb temperature of 20 °C (68 °F), the equipment COP decreases from about 2.9 to about 2 if the zone temperature drops from –18 °C (0 °F) to –26 °C (-15 °F).

Both effects, the increased warehouse load and the lower equipment COP combined, result in a higher electricity demand for precooling. Figure 4-22 shows the combined effects of the increased load at a lower temperature and the great increase in daily

electricity demand. The plot was calculated for a warm summer day with a maximum temperature of 28 °C (82 °F) and for keeping the freezer set point temperature constant. Decreasing the set point temperature from –15 °C to –30 °C results in more than doubling the cooling load. The electricity consumption increases by a factor of nearly 4.

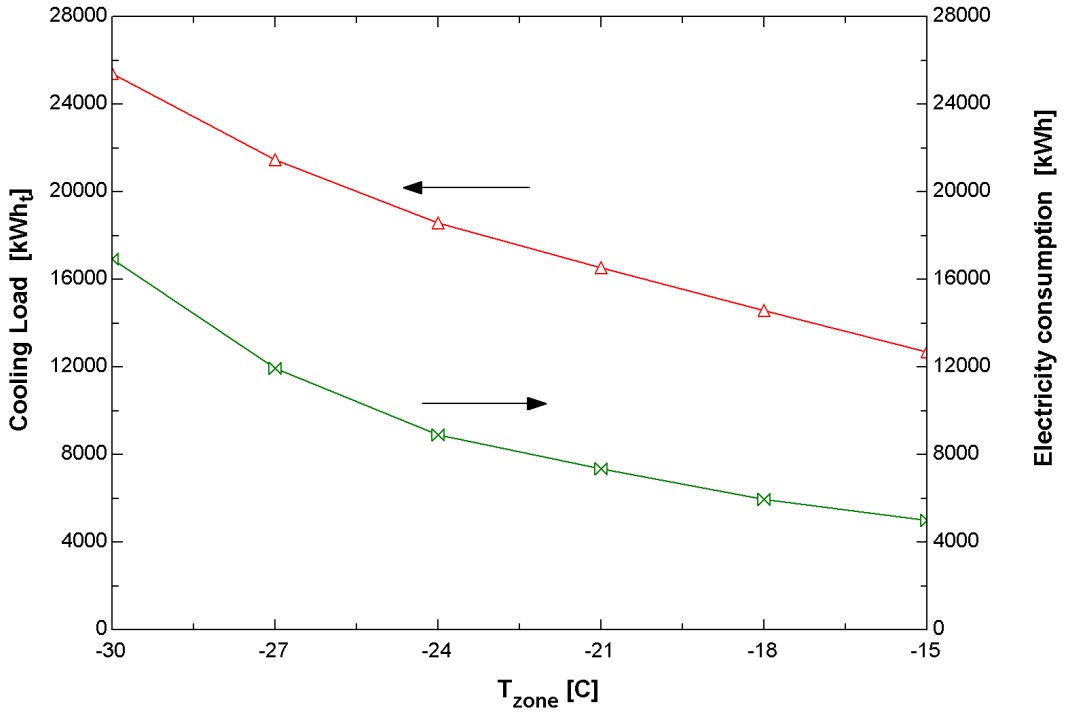

Figure 4-22: Daily freezer cooling load and electricity demand as function of set point temperature

The above considerations show that precooling certainly results in much higher energy consumption. The increased energy consumption during a precool period can only be compensated for by proportionally higher real-time prices during floating vs. precool periods.

4.4 RTP- Controller

As only a few days during the year offer likely benefits by demand shifting, a decision has to be made every day to determine if demand shifting should be performed on the next day or if continuous operation is more desirable. In the sections before, two options

were compared. Warehouse continuous operation over the year (base case) was compared to everyday demand shifting. From the two yearly results, days with potential savings under demand shifting could be identified. Based on these results, criteria have to be identified, which characterize days with potential savings in advance.

4.4.1 Critical price ratio

From the day-to-day comparisons previously presented, it was observed that the days at which demand shifting yielded cost-benefits were mainly price-determined. When the order of occurrence of the daily real-time prices was changed, a day was more likely to be a day with potential savings if it had the same price pattern than if it had the same weather pattern compared to the simulations without changed order of prices. Therefore, the next day real-time price profile is seen as the principle indicator to determine if demand shifting on the next day will provide operating cost savings.

Different indicators and combinations of indicators were formulated. First an indicator that also involved the equipment performance was created. Ratio1 in equation (4-1) is defined as the daily average COP for the freezer equipment times the integrated daily real-time price under continuous operation divided by average COP for the freezer equipment times the integrated real-time price during hours when the equipment is operated when demand shifting is performed.

$$ratio1 = \frac{COP_{avg,day} \cdot price_{\text{int},day}}{COP_{avg,shifting} \cdot price_{\text{int},shifting}} \tag{4-1}$$

$COP_{avg,day}$	Average daily COP under continuous operation
$Price_{int,day}$	Integrated daily real-time price
$COP_{avg,precooling}$	Average COP during hours of equipment operation when demand shifting is performed
$Price_{int,precooling}$	Real-time price integrated over hours of equipment operation when demand shifting is performed

Figure 4-23 shows the potential savings compared to baseline operation for 6 compressors, the –18 °C correlation for the corner temperature and the massive wall. The ratio was calculated for the simulation runs presented in the previous sections.

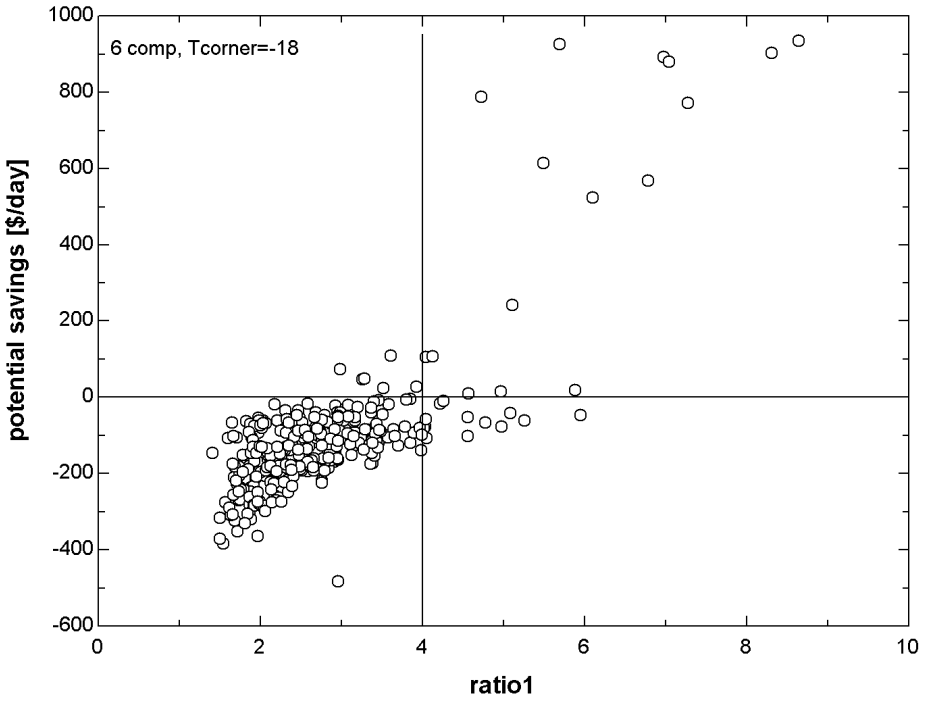

Figure 4-23: Potential savings vs. ratio 1 for 6 compressors, -18 ℃ correlation, massive wall.

The plot shows that ratio1 is not a clear indicator for savings. Once the ratio is greater than 4, savings are possible, but even for a ratio of 6, losses are still possible.

A ratio that only considers the real-time prices without taking into account the equipment performance is defined by equation (4-2)

$$ratio = \frac{price_{avg,day}}{price_{avg,shifting}} \tag{4-2}$$

$price_{avg,day}$ Average real-time price over day (continuous operation)

$price_{avg,precooling}$ Average real-time price during hours of equipment operation when demand shifting is performed

The ratio is the average real-time price of the next day divided by the average price during the hours when the equipment is operated if the freezer would be precooled. The following figures show the potential savings when demand-shifting is performed (compared to baseline operation) for each day of the year versus the price ratio for each day.

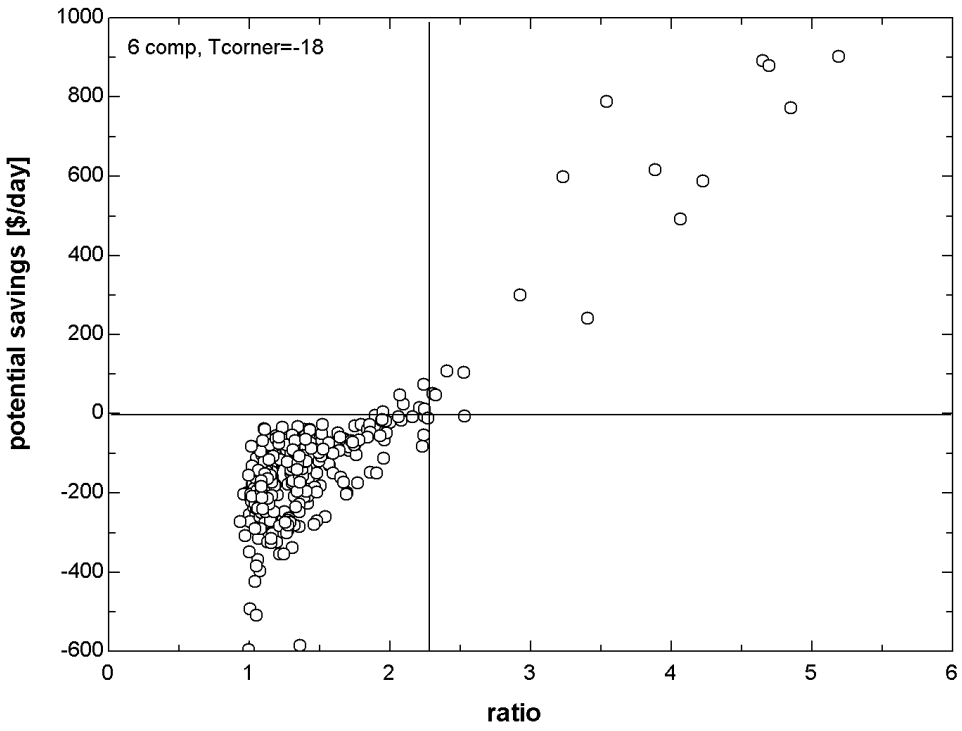

Figure 4-24: Potential savings vs. ratio for 6 compressors, allowable corner temperature of –18 ℃, massive wall.

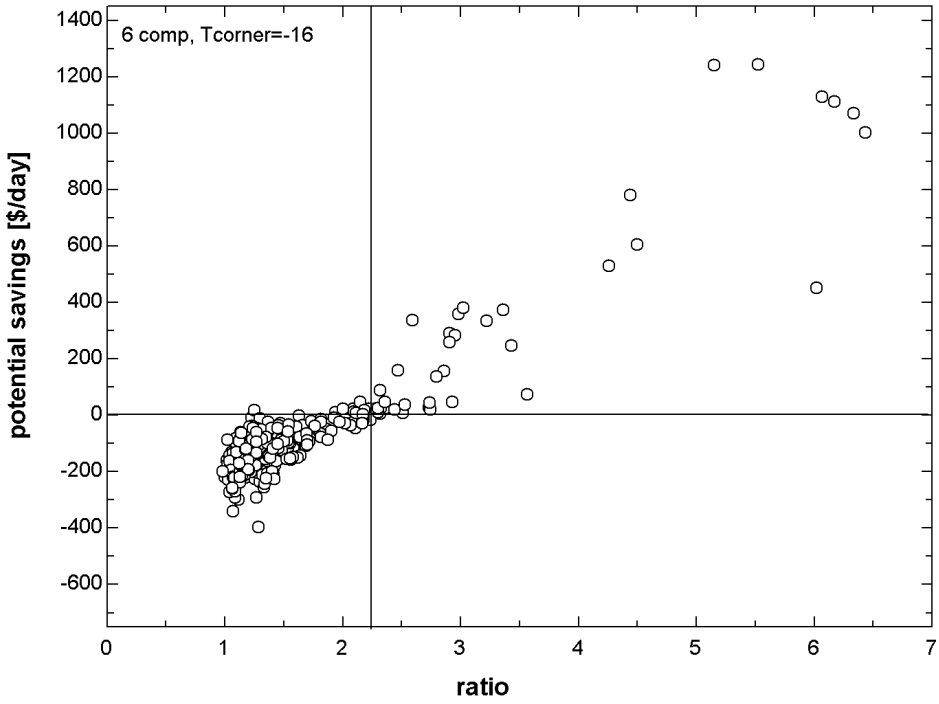

Figure 4-25: Potential savings vs. ratio for 6 compressors, allowable corner temperature of –16 ℃, massive wall.

The plots show the ratio of prices is a criterion that clearly distinguishes days with savings from days when money is lost when floating. For the massive wall and 6 compressors installed, potential savings can be realized if the price ratio is around 2.2 or higher, no matter which corner temperature relation is used. Similar plots were also generated for the changed order of real-time prices, for the Southern pricing structure and for the lightweight wall construction under the PG&E structure. In all cases, the critical price ratio remained at about 2.2. Figure 4-26 shows a plot for the lightweight wall, 6 compressors and the –16 °C corner temperature correlation.

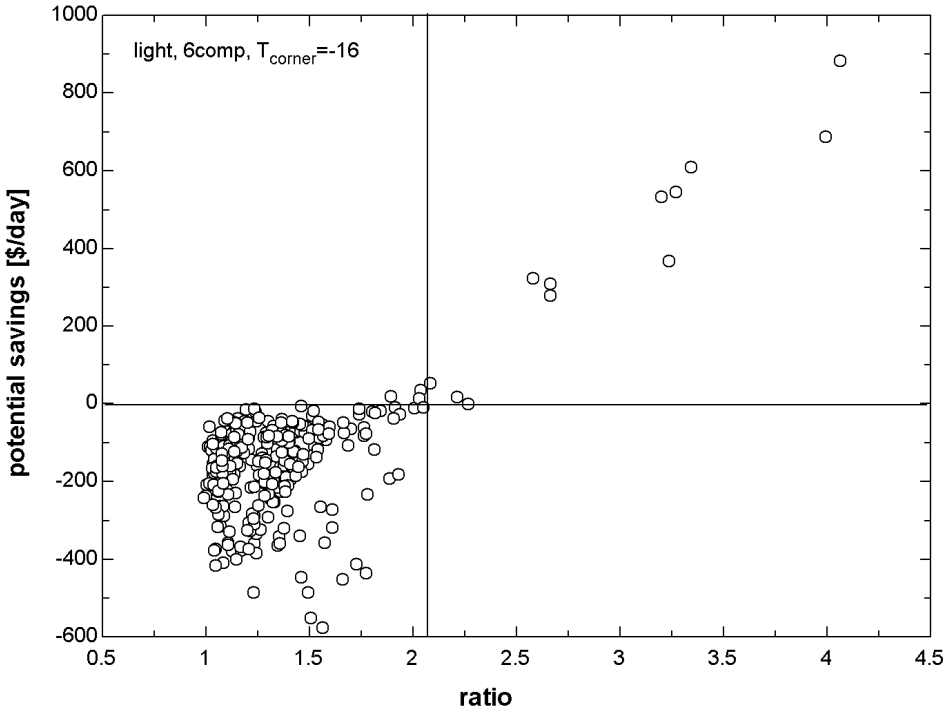

Figure 4-26: Potential savings vs. ratio for 6 compressors, allowable corner temperature of –16 ℃, lightweight wall.

4.4.2 RTP-controller type

The previously presented plots show that the real-time price profiles alone without characteristics of the equipment can be used to estimate if the next day is likely to offer savings under demand shifting warehouse operation. The plots are based on the data obtained from comparing baseline operation and daily demand shifting. In reality, demand shifting will only be performed if savings are likely to be obtained. A controller in TRNSYS was developed to discriminate days for demand shifting.

The possible floating duration for the next day, based on the next day temperature, has to be supplied to the controller. At 4 p.m., the controller reads the next day real-time prices and first calculates the floating window with the highest integrated real-time prices. Once the floating window is determined, the hours of cooling for the next day are known: the hours before and after the floating window. This information given, the next day average real-time price and the next day average price during cooling can be calculated, which gives the next day pricing ratio. Comparing this value to the critical pricing ratio,

which is needed as parameter for the TYPE, the controller decides if demand shifting is performed on the next day or if the warehouse is operated continuously.

The starting time for precooling is another variable that has to be determined. A fixed starting time could be used, for example midnight or 4 p.m., i.e. immediate precooling. Immediate precooling would offer the longest possible precooling duration, but also precooling may start at the hours with higher energy prices. Real-time prices usually peak around 4 p.m.; therefore immediate precooling would cause a relatively high precooling cost. On the other hand, a precooling start at midnight would offer lower prices, but also a reduced precooling duration. Given these two possibilities, a compromise was chosen for the controller TYPE: precooling starts at the hour when it also would resume after floating, even if the floating was not performed on that day. This makes the starting time somehow flexible, but it also automatically adjusts the precooling duration to the weather data. A series of warmer days gives shorter possible floating durations, which gives longer precooling durations. At colder times of the year, the floating and precooling durations are then adjusted correspondingly.

4.4.3 Realized savings

The savings achieved with the new RTP controller type integrated into the TRNSYS are presented in Table 4-21. Floating is not performed every day, but only on days when the price ratio exceeds the critical value.

Table 4-21: Potential savings and savings achieved with RTP controller

#comp	T_{corner}-corr.	**Savings with RTP controller (critical ratio = 2.2)**	
		Days with floating	**Savings compared to baseline operation /$**
6	-18	26	**12,581**
6	-16	44	**17,976**

Surprisingly, the savings achieved with the RTP controller are higher than the projected potential savings presented in Table 4-14 from daily demand shifting. These projected potential savings were the sum of all days on which savings occurred compared to baseline operation. The main reason for the difference is that for daily demand shifting the average freezer temperature over the year is lower, which results in a higher freezer

load and reduced savings compared to the base case. With the RTP controller, the average freezer temperature over the year is higher, which results in a reduced load compared to daily demand shifting. Section 4.4.4 shows the freezer and product corner temperatures over the year.

Figure 4-27 shows the PG&E real-time pricing profiles for the days when the critical price ratio exceeded 2.2 and demand shifting was performed.

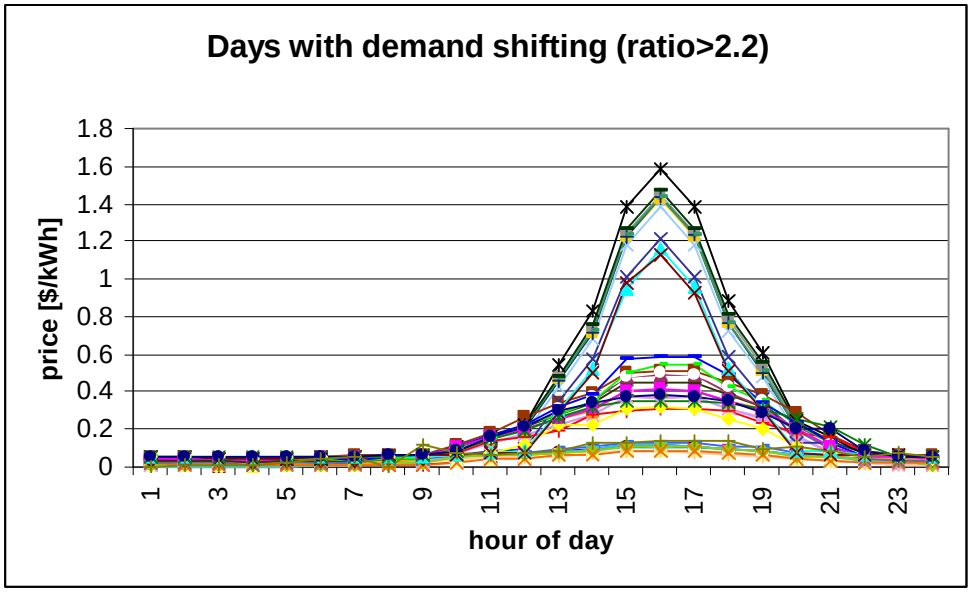

Figure 4-27: PG&E pricing profiles for the 44 days when demand shifting is performed for 6 compressors, massive wall and –16 ℃ correlation

The days with very high peak prices can be clearly distinguished. Also many days with peak prices greater than 0.30 $/kWh are among the demand shifting days, while only few days with lower peak prices had a high enough price ratio. The price profiles all show the typical summer pattern with a price peak around 4 p.m.

4.4.4 Product temperature

Figure 4-28 and Figure 4-29 show the average daily freezer temperature over the year for the every day floating case (case 1) and the RTP controller case (case 2) for two different floating duration correlations.

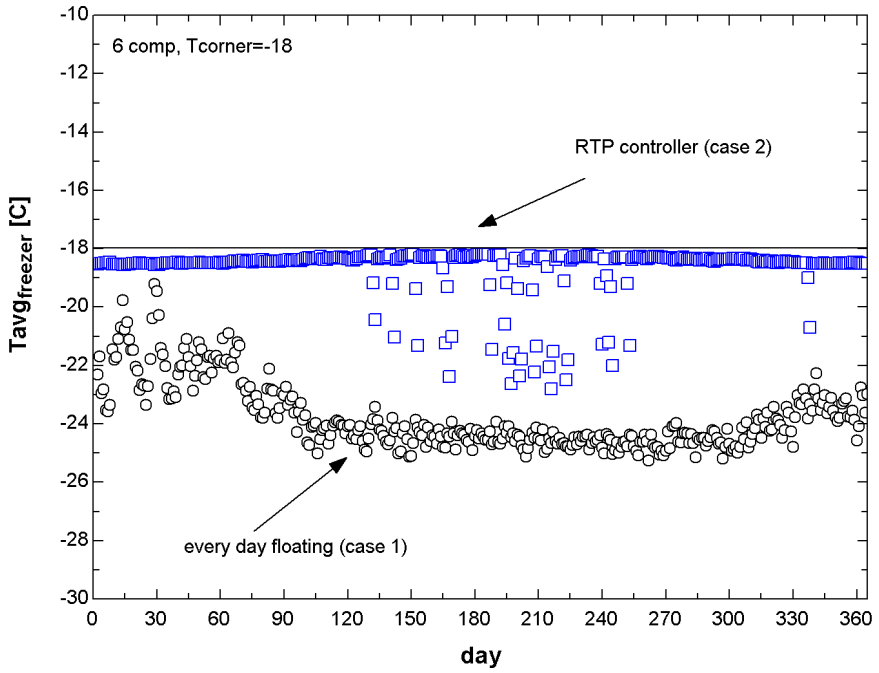

Figure 4-28: Average freezer temperature during year for 6 compressors, massive wall, -18 ℃ correlation

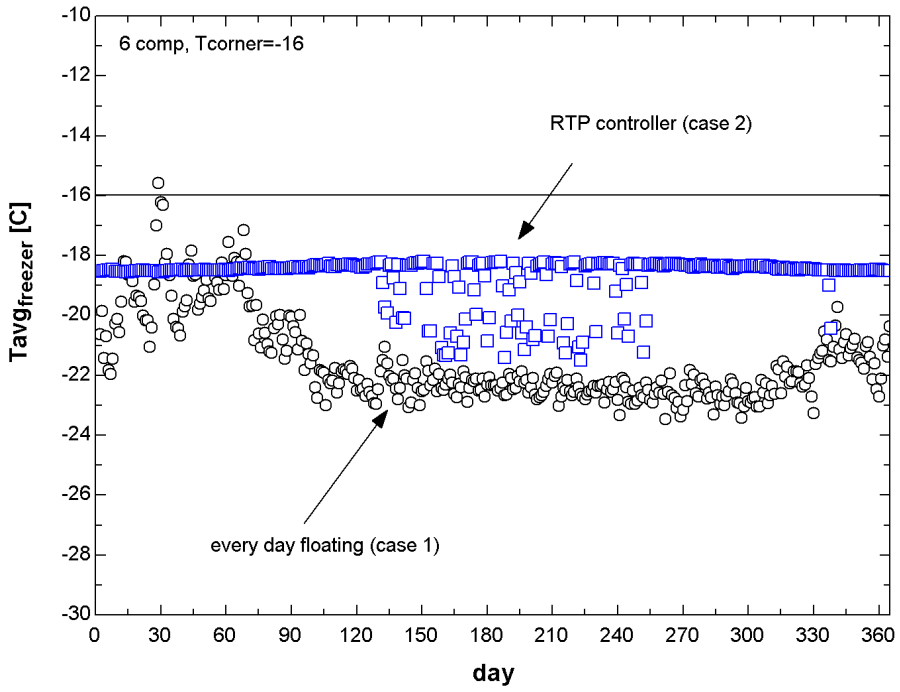

Figure 4-29: Average freezer temperature during year for 6 compressors, massive wall, -16 ℃ correlation

For case 1, the average freezer temperature is lower in both cases, for the –18 °C and the –16 °C correlation. This results in a higher freezer load for the case 1 compared to case 2. Therefore, the savings that can be achieved compared to the base case are smaller in case 1.

The plots also indicate why the savings for the –16 °C correlation do not differ as much between case 1 and case 2 as for –18 °C correlation. For the –16 °C correlation, the average temperature curves shown in the plots are closer together than for the –18 °C correlation. Therefore the difference in freezer load between the two cases is less, which also brings the potential savings (case 1) and the achieved savings (case 2) closer together.

The product corner temperature over the year for the simulation runs with the RTP controller implemented is shown in the following plots. Also the daily average temperature over the year is shown.

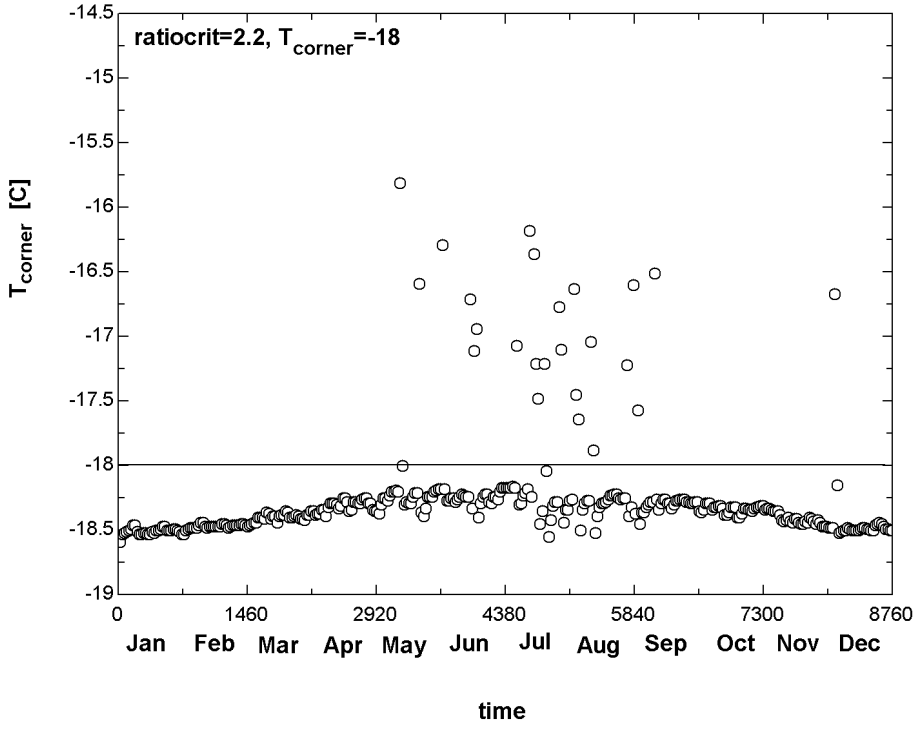

Figure 4-30: Maximum daily corner temperature over year for –18 °C correlation, massive wall, 6 compressors, RTP controller critical ratio=2.2

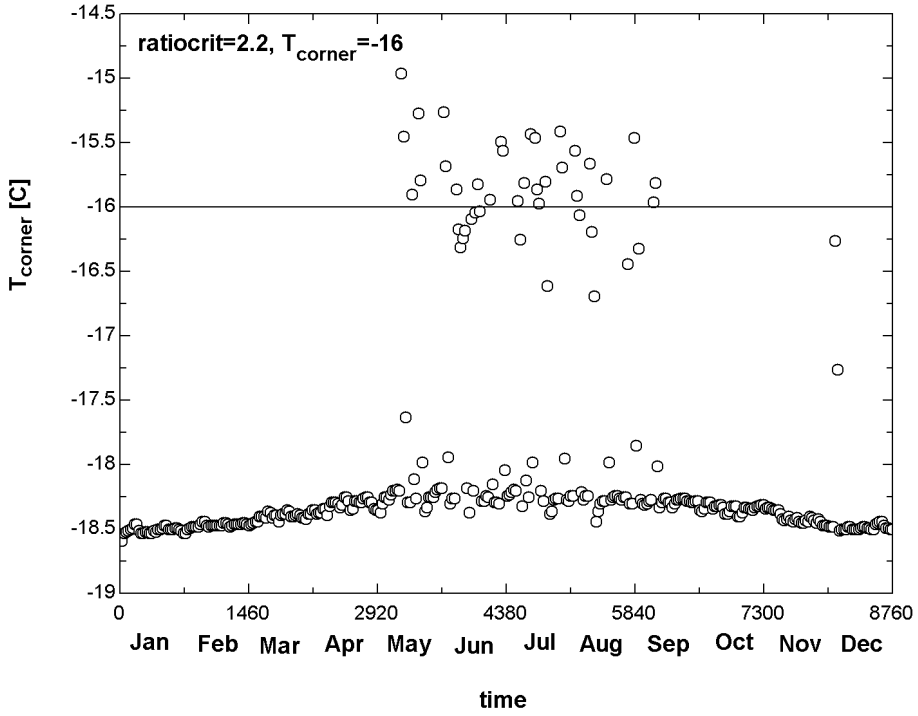

Figure 4-31: Maximum daily corner temperature over year for –16 °C correlation, massive wall, 6 compressors, RTP controller critical ratio=2.2

With the RTP controller installed, the corner temperatures exceed relatively often the critical values of –18 °C or –16 °C for the two correlations if demand shifting is performed. For the –18 °C correlation, the critical value is exceed more often than for the –16 °C correlation. This can be explained by the fact that the corner temperature is closer to the critical value for the –18 °C correlation with the freezer set point also at –18 °C. The temperature buffer is smaller in that case.

Comparing these two plots to Figure 4-15 and Figure 4-16 which show the corner temperature for every day floating, it can be observed that the average corner temperature over the year is higher for the case with the RTP controller implemented. Figure 4-28 and Figure 4-29 explain why the critical corner temperature is exceeded with the RTP controller: the product is at higher temperature before floating starts and therefore, the corner temperature reaches a higher value for the same floating duration. This indicates that the floating duration equations derived from every demand shifting give different results if demand shifting is only performed on selected days.

The risk associated with product temperature cycling also depends on the type of warehouse the demand shifting is performed on. Demand shifting occurs only on a few days with high real-time prices. This already reduces the risk of damage to the product because the days with cycling are limited. The type of refrigerated warehouse also influences the product damage risk: for a distribution warehouse where the product is stored only for short time periods, temperature cycling to a temperature higher than the critical value should not result in damage because it is not likely to happen very often while the product is stored in the warehouse. The situation is different for a long-term storage warehouse. Product temperature cycling can occur more often because the product is more likely to be stored during more days of high prices and demand shifting. For long-term storage, a more conservative floating duration correlation should be used.

4.5 Chapter Summary

Under baseline operation, the set point temperature is –18 °C (0 °F) for the freezer and 1 °C (34 °F) for the dock. The design day load is 690 KW_t (196 tons) for the massive wall construction, which requires 3 compressors installed, and 915 KW_t (260 tons) for the lightweight wall construction, which requires 4 compressors installed. For the design day as well as over the whole year, the load distribution is similar for both wall constructions. For the freezer, the biggest share is transmission loads with about 50 % and infiltration loads with about 25 % of the total load. Over the year, the freezer contributes to about 75% of the electricity demand, 25 % of the total demand is from the dock.

The baseline electricity cost per year is $169,440 for the massive wall construction and $172,664 for the lightweight wall construction under the PG&E structure. Under the Southern pricing structure, the yearly electricity cost is $80,443 for the massive wall construction.

The possible floating duration is an important variable in developing strategies for demand shifting. The possible floating durations for different combinations of installed

refrigeration capacity and wall constructions can be forecasted as a function of the next day average or maximum dry bulb temperature. Inclusion of additional variables does not improve the predictions. The massive wall construction results in longer possible floating durations than the lightweight wall construction. Furthermore, the massive wall construction makes the possible floating duration more predictable than the lightweight wall construction. Installation of additional refrigeration capacity or allowing a higher product corner temperature increases the possible floating duration considerably. With the possible floating duration known, the best floating window can be determined. The best floating window is usually the window with the highest integrated real-time prices.

The PG&E pricing structure offers the biggest incentives for demand shifting. Nevertheless, with only the base capacity of 3 compressors installed, only minimal savings through demand shifting seem possible. Installation of additional refrigeration capacity increases the savings potential through demand shifting, but the savings are relatively small compared to the yearly electricity cost. For 6 compressors installed and the massive wall construction, the potential savings are in the range of $7,000 to $15,000, which is 4 % to 10 % of the yearly electricity cost. The light wall construction offers only reduced savings compared to the massive wall construction. The days with potential savings are mainly determined by the real-time price. A simulation with a changed order of real-time prices combined with the same order of weather data indicated savings in the same order of magnitude. The simulations confirmed that the best floating window is usually the window with the highest integrated real-time price.

The small potential savings are mainly due to high electrical operating costs associated with precooling. On most days, the savings during floating hours are too small to compensate for the higher operating cost for precooling. The high precooling operating cost is due to two factors. First, the lower precooling freezer temperature results in higher cooling loads. Second, the lower freezer temperature decreases the refrigeration equipment efficiency considerably.

A criterion is needed to decide if demand shifting on the next day would offer savings. The ratio defined by the next day average real-time price divided by the next day average real-time price during the hours of equipment operation under demand shifting was found to be a very good indicator if demand shifting would offer savings. For the warehouse modeled, the price ratio has to exceed 2 to 2.2 that savings can be realized. An RTP controller was created that decides if demand shifting is performed on the next day. The results show savings higher than the projected potential savings. This is due to the higher yearly average freezer temperature, which also results in higher product corner temperatures.

Chapter 5 Conclusions

5.1 Transfer-Function Modeling

Different modeling options for the walls and the refrigerated product were compared: finite-difference modeling and transfer-function modeling. Transfer-functions reduced the calculation time during the simulation and were in good agreement with the finite-difference results for the walls.

The transfer function approach was extended to allow simulating the refrigerated products in storage. However, the approach requires that the product core temperature be equal to the average freezer temperature. The constantly changing average freezer temperature under demand shifting operation leads to long-term inaccuracies in the transfer-function approach and a finite-difference approach was used.

5.2 Real-time Pricing Rates

Real-time pricing profiles showed significant hourly and day-to-day price fluctuations and differed considerably among the utilities. A one-part pricing structure is likely to make demand shifting more economically viable due to the larger difference between average peak and off-peak prices than a two-part pricing structure.

Seasonal differences in the price profiles can be observed. During the summer month, a significant peak in the afternoon is common. During colder months, the profiles are flatter, and two peaks can be observed, around noon and in the later evening. Summer peak prices are higher than the winter peak prices; the magnitude of the difference depends on the utility.

Investigation of the relationship between real-time prices and local weather data showed no significant correlation between the two. The very high peak prices on certain days cannot be explained by local weather data. Therefore, projecting real-time prices on the basis of projected temperatures is difficult.

5.3 Method Developed

A method was developed to determine cold storage warehouse operational strategies aimed at minimizing the electricity cost under a real-time pricing structure. The method developed relies on first determining the maximum possible duration of refrigeration system floating (shutdown). A simple method of forecasting the allowable floating duration was developed based on the forecasted outside air temperatures for the next day.

With the maximum possible floating duration known, the floating window with the lowest operating cost is then determined. It was found that the best floating window is the window with the highest integrated real-time prices. Once the best floating window is known, the operating cost under demand shifting could be compared to the continuous operation cost. In many situations, there is not an appreciable difference between peak electricity prices and the off-peak electricity prices – making load shifting uneconomical.

From the simulation runs, a criterion was found to recognize days that likely offer savings under demand shifting. The ratio defined by the daily average real-time price divided by the average real-time price during the hours when the equipment is operated in demand shifting mode is a very good indicator if savings are possible. For the warehouse modeled, savings are likely to be realized for a ratio greater than 2 to 2.2.

5.4 Refrigerated Warehouse Operation under Real-time Pricing

From the many options explored and simulations run, several conclusions for obtaining savings for refrigerated warehouse operation under real-time pricing can be given. Based on the warehouse that was simulated recommendations are:

- Massive wall construction results in a lower design day peak refrigeration load, which requires less installed refrigeration capacity than light wall construction. In the case of demand shifting, the massive wall offers a longer maximum possible floating duration, which makes demand shifting more flexible and likely to yield operating cost savings. Furthermore, the maximum possible floating duration can

be predicted with a much higher certainty for the massive wall construction.

- For the warehouse configurations modeled, only minimal savings are projected by the use of demand shifting under a real-time structure without installation of additional refrigeration capacity, additional capacity has to be installed to enable savings.

- Installation of additional refrigeration capacity offers the possibility of savings in electricity cost through demand shifting. The largest savings that also represent the biggest share of the yearly savings occur only on a few days with very high real-time peak prices. This fact minimizes any risk (perceived or real) associated with temperature cycling of stored products.

- Days yielding operating cost savings under real-time pricing are mainly price determined. If the peak price exceeds 0.6 $/kWh, savings are possible and are not strongly dependent on the ambient conditions.

- If demand shifting is performed, the best floating window is the window centered within the highest integrated real-time price period.

- The ratio defined by the average daily real-time price divided by the average price during hours when the equipment is operated in demand shifting mode is a very good indicator if savings are possible.

- Overall, the savings realized through demand shifting are relatively small compared to the yearly electricity cost under baseline operation. The potential savings are too small to justify investment into additional refrigeration capacity to make demand shifting possible. Only with the necessary capacity for demand shifting already installed, demand-shifting implementation into warehouse operation can be recommend.

- In general, potential benefits from switching from a standard electricity rate to a real-time pricing rate have to be questioned. The potential savings for demand shifting in refrigerated warehouse operation under real-time pricing are small, but the pricing risk associated with the fluctuating electricity prices is high. Only if the real-time pricing rate is likely to yield a lower yearly operation cost even without demand shifting, switching can be recommended.

- The relatively small savings under demand shifting are due to two factors. Precooling results in a lower warehouse temperature, which increases the warehouse load. Second, the refrigeration equipment operates far less efficient at a lower temperature. Both factors increase the energy demand and the cost for precooling considerably. This makes precooling profitable only under high real-time prices.

The following summarize the steps in establishing the daily operating strategy for a warehouse under a real-time price rate structure.

1. Obtain daily real-time prices (usually this occurs at approximately 4:00 pm for most utilities).
2. Obtain either the next-day's forecast high temperature or daily average temperature.
3. Based on the forecasted ambient temperature, determine the maximum allowable shift period (a characteristic of the individual warehouse and stored product).
4. Center the maximum allowable shift window within the highest integrated price period for the next day.
5. Calculate the ratio of the average daily electricity price to the average electricity price during hours when the equipment is operated in demand shifting mode. If this ratio is less than 2 run the warehouse continuously (no set-back). If the ratio is greater than 2.2, begin precooling as soon as the real-time prices become reasonably cheap and plan on shifting during the next day's window.
6. Repeat steps 1-5 each day

5.5 Future Work Recommendations

The simulation results indicate that the potential savings for demand shifting under real-time pricing are relatively small. The savings are mainly determined by the possible floating duration, which limits the number of hours with high real-time prices during which the equipment can be idled. A second factor contributing to poor economics under RTP is the low freezer temperature during precooling, which results in a high cost associated with precooling as mentioned before. During this study, no model verification could be done on an existing warehouse structure. Comparing the freezer temperature predicted by the model to the freezer temperature in a refrigerated warehouse during a precooling and floating cycle would help evaluating the model and implement possible corrections in the model to match the model results with experimental results if necessary.

Other demand shifting options for refrigerated warehouses should be explored. Besides using the stored product as thermal energy storage, the condenser cooling water could be used as storage (if the condensers are water cooled). Decreasing the condensing temperature of the refrigerant results in an increased compressor COP. As a possibility, condenser cooling water could be precooled during off-peak hours, stored in a tank and then be used during on-peak hours, when higher real-time prices and higher ambient temperatures usually occur. The precooled condenser cooling water would lower the equipment power demand due to improved equipment performance.

Improving the convergence of the model would allow the calculation to proceed faster, which would allow to run more simulations in a given period of time. Adding more and more components to the simulation slowed down the calculation speed and convergence problems in the model required use of a relatively small time step of $1/16^{th}$ of an hour, which further slowed down the calculations.

As part of improving the TRNSYS model, certain components could also be improved. The constant node spacing in the product finite difference model results in far more nodes than would be necessary. Close to the surface, fine node spacing is necessary because of

the larger change in product temperature during precooling and floating in order to calculate the product heat flow correctly. In the center of the product however, coarser grid spacing could be used because the product temperature remains nearly constant in the middle. The adjusted node spacing would reduce calculation effort.

In the simulation, the assumption is made that only the installed refrigeration capacity is the limiting factor for demand shifting. It is assumed that sufficient evaporator and condenser capacity is installed. For the evaporator model, this resulted in the assumption that even for less refrigeration capacity installed, the evaporator air mass flow rate is the same than for the double refrigeration capacity installed. This assumption leads to a lower part load ratio for the evaporator air mass flow rate, which reduces the fan power required if less refrigeration capacity installed as can be seen from the evaporator model presented in section 2.3.2. The overall effect of this assumption on the simulation results is small, but improving the evaporator model would result in a more exact calculation of fan power heat input.

The condenser model used is a relatively simple model, which is accurate enough to give good estimations of the refrigerant condensing temperature. However, no fan power demand for the condenser fans has been considered in the simulation. Adding a more detailed condenser model would allow estimation of condenser fan power demand and the associated cost. As for the evaporators, a more detailed model would also allow to consider the installed condenser capacity as a limiting factor for demand shifting.

A rather high level of uncertainty is associated with the heat transmitted through the heated floor of the warehouse. Further investigation of the expected floor load would allow making a more accurate estimation of this load.

Changes in warehouse and product parameters and use of different weather data for different locations would allow estimating the sensitivity of the model and the results to changes in boundary conditions.

Appendix A: Possible floating duration correlations

Massive Wall, allowable corner temperature of –18 ℃, next day maximum temperature

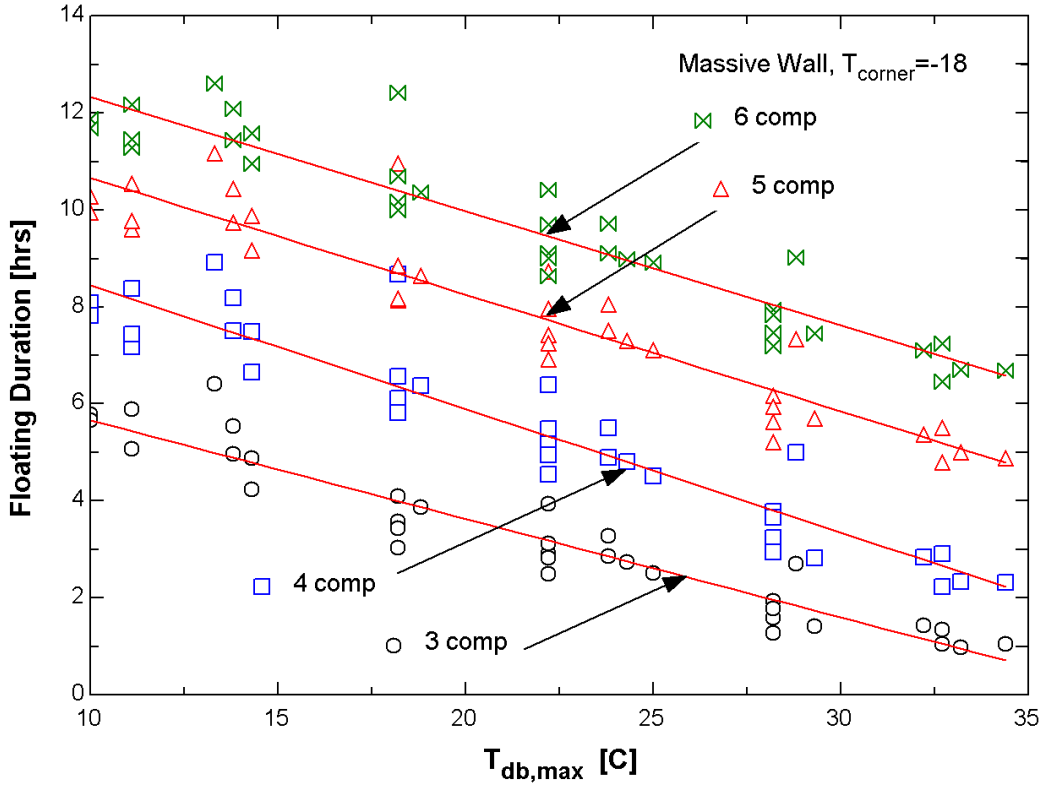

# Comp	Refrig. Capacity/ KW_t (tons)	Correlation	R^2
3	302 (86)	FloatDur =7.6903 - 0.20302*T_db_max	91%
4	604 (172)	FloatDur =10.995 - 0.25491*T_db_max	88%
5	906 (258)	FloatDur =13.066 - 0.2406*T_db_max	87%
6	1208 (344)	FloatDur =14.692 - 0.23574*T_db_max	89%

Light Wall, allowable corner temperature of –18 ℃, next day maximum temperature

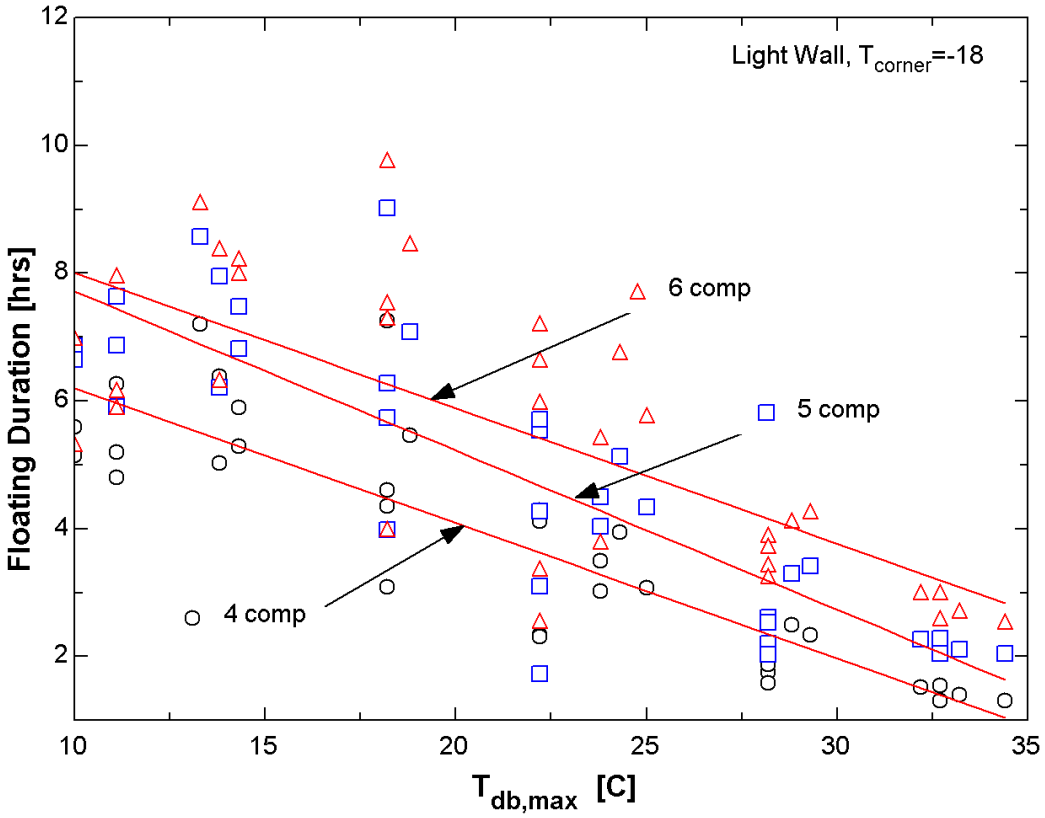

# Comp	Refrig. Capacity/ KW_t (tons)	Correlation	R^2
4	604 (172)	FloatDur =8.3102 - 0.21132*T_db_max	77%
5	906 (258)	FloatDur =10.202 - 0.24906*T_db_max	73%
6	1208 (344)	FloatDur =10.123 - 0.21191*T_db_max	54%

Light Wall, allowable corner temperature of –16 ℃, next day maximum temperature

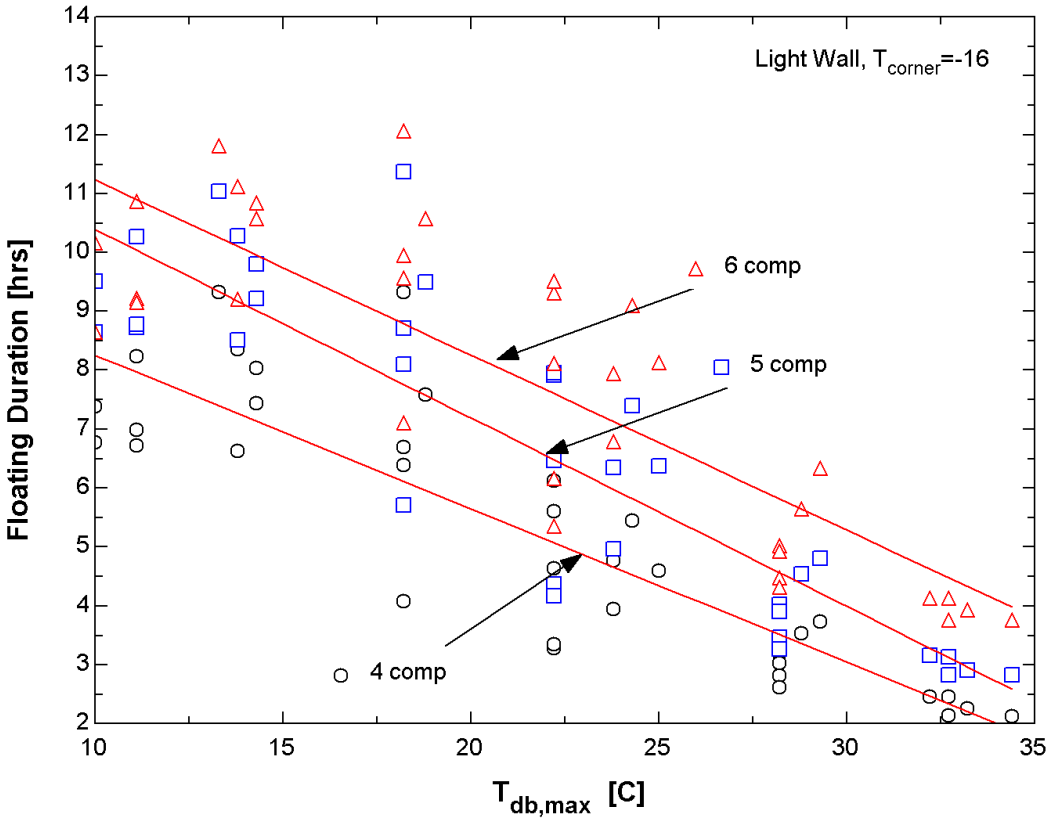

# Comp	Refrig. Capacity/ KW_t (tons)	Correlation	R^2
4	604 (172)	FloatDur =10.858 - 0.26057*T_db_max	76%
5	906 (258)	FloatDur =13.593 - 0.32016*T_db_max	78%
6	1208 (344)	FloatDur =14.203 - 0.29734*T_db_max	72%

Appendix B: TRNSYS non-standard type descriptions

TYPE 101 Infiltration Load

This type calculates the infiltration load through an opening into a refrigerated space corresponding to Downing and Meffert (1993). The formula used is:

$$Q_{\inf} = \left[2491.47 Area\, r_{in} \sqrt{1 - \frac{r_{out}}{r_{in}}} \sqrt{height} F_m (1 - E) \right] (h_{out} - h_{in}) = \dot{m}_{\inf} \Delta h$$

$$F_m = \left[\frac{2}{(1 + \frac{r_{in}}{r_{out}})^{\frac{1}{3}}} \right]^{\frac{3}{2}}$$

In case that the inside air has a lower density than the outside air, the densities in the formula are changed (the enthalpies are kept the same). Therefore the infiltration load is calculated as a negative gain to the space.

Parameter		
1	Area	Area of the opening to the refrigerated space in m^2
2	Height	Height of the opening in m
3	E	Effectiveness of a door protection device or opening fraction of door
Input		
1	h_{out}	Enthalpy of outside air in KJ/Kg
2	h_{in}	Enthalpy of inside air in Kj/KH
3	ρ_{out}	Density of outside air in Kg/m^3
4	ρ_{in}	Density of inside air in Kg/m^3
Output		
1	Q_{inf}	Infiltration Load through opening in Kj/hr
2	m_{inf}	Infiltration mass flow rate in Kg/hr
3	Δh	Difference in enthalpy between outside and inside air in Kj/Kg

Type 102 Set temperature profile

This type gives as output a forcing set temperature profile with a low and a high set point. The low and the high temperature have to be specified. The component inputs are the time of day when the high set point is desired and the time of day when the low temperature is desired. The type calculates the set temperature corresponding to the time of the day.

Input		
1	houroff	Hour of day when higher set point is desired
2	hourcool	Hour of day when lower set point is desired
3	T_{high}	High set point temperature
4	T_{low}	Low set point temperature
Output		
1	T_{out}	Set point temperature depending on time of day
2	daytime	Time of day based on simulation time

Type 105 Finite-difference model of frozen product

This type models a block of frozen product stored in the refrigerated warehouse. It calculates the heat flow from the product into the zone as a function of the zone temperature. An explicit Euler finite-difference scheme is used. The product model is 2-dimensional and assumed symmetric about the midline. The heat transfer to the top and front side is represented through a heat transfer coefficient; the heat transfer through the bottom is represented through a resistance. The overall heat flux is calculated by multiplying the 2-D heat flux by the width of the corresponding Areas of the sides of the block. At the beginning of the calculation the product temperature is set to an initial value.

Parameter		
1	Height	Height of the pile in m
2	Halfwidth	Width of the pile from corner to the symmetry line in m
3	Depth	Depth of the pile in 3-D in m
4	xmax	Number of finite-difference nodes over the half width of the product
5	ymax	Number of finite-difference nodes over the height of the product
6	T_{init}	Initial temperature of the frozen product in C
7	Step	Time Step used for the calculations in hr
Input		
1	T_{zone}	Zone temperature in C
2	c_p	Specific heat of product in Kj/Kg-C
3	k	Conductivity of product in W/m-C
4	ρ	Density of product in Kg/m^3
5	h_{top}	Heat transfer coefficient on the top side of the product in W/m^2-C
6	h_{front}	Heat transfer coefficient on the front side of the product in W/m^2-C
7	T_{floor}	Temperature of the floor of the warehouse in C

8	R_{floor}	Resistance between floor and frozen product in m^2-W/C
Output		
1	$Q_{product\text{-}zone}$	Heat flow from product into the zone in KJ/hr
2	$T_{topcorner}$	Temperature of the top corner of the product in C
3	$T_{bottomcorner}$	Temperature of the bottom corner of the product in C
4	$T_{frontmidlle}$	Temperature in middle of product front in C

TYPE 108 Refrigeration Equipment with compressor staging
TYPE 107 Refrigeration Equipment without compressor staging

This type models the refrigeration equipment used to condition a space. The type uses a curve fit model to represent the power consumption, the available cooling capacity and the part load behavior of a compressor and simplified models for a condenser and an evaporator.
Compressor: A compressor can be modeled using curve fit data obtained from the actual testing of a compressor. An output variable is calculated as a function of the suction and the discharge temperature of the compressor. The coefficients for the curve fits have to be supplied to the model.
Evaporator: The suction temperature for the compressor depends on the evaporator. The model assumes that the suction temperature is the temperature at the air side of the evaporator minus a constant approach temperature: $T_{suction}=T_{vent}-dT_{evap,ref.}$
Condenser: For wet bulb temperatures above 5 C, the condensing temperature is the wet bulb temperature plus a constant approach temperature for the condenser. If the wet bulb temperature drops below 5 C, the condensing temperature is kept constant at the value 5C plus the approach.
Besides, the type also calculates the number of compressors necessary to supply the design load. From the curve fit data, the cooling capacity per compressor is calculated as a function of design wet bulb and ventilation flow stream temperature. Knowing the design load, the design number of compressors is then determined. This design calculation is only performed at the first call of the component.
TYPE 107: Always the design number of compressors is in use.
TYPE 108: Only the necessary number of compressors to supply the cooling load is in use, the additional compressors are shut down.

Parameter		
1	LoadDes	Design Load for the cooling equipment in tons
2	$T_{wb,des}$	Design wet bulb temperature in C
3	$T_{vent,des}$	Design ventilation flow stream temperature in C
4	$\Delta T_{evap,ref}$	Approach temperature for evaporator on refrigerant side in C
5	ΔT_{cond}	Approach temperature for condenser in C
6-11	Power coefficients	The six coefficients used to determine the maximum power consumption of one compressor as a function of suction and discharge temperature
12-17	Capacity coefficients	The six coefficients used to determine the maximum available cooling capacity of one compressor as a function of suction and discharge temperature

18-23	Part Load Behavior coefficients	The six coefficients used to determine the fraction of the full load power consumption at part load as a function of the fraction of available full load capacity used
Input		
1	T_{vent}	Temperature of ventilation flow stream in C
2	T_{wb}	Wet bulb temperature in C
3	Qtotal	Actual cooling load the equipment has to supply in KJ/hr
Output		
1	PeakCap	Maximum cooling capacity of one compressor for the design load in tons
2	numbercomp	Number of compressors necessary to supply the design load
3	Pelecmax	Maximum Power consumption of one compressor under full load in KW
4	Pelec	Electrical Power consumption of the equipment under the actual load in KW
5	MaxCap	Maximum available cooling capacity per compressor under the current conditions in KJ/hr
6	Cap	Maximum available cooling capacity of the equipment under the current conditions in Kj/hr
7	FractFLC	Fraction of the maximum available cooling capacity needed to supply Qtotal in %
8	FractFLP	Fraction of the maximum power consumption needed to supply the actual load in %
9	T_{cond}	Condensing temperature in C
10	T_{sst}	Saturated suction temperature of the compressor in C
11 (only type 108)	Compuse	Number of compressors actually in use

Type 109 Fan Power

This type calculates the heat input associated with the operation of the evaporator fans. Two equations describe the heat input. The maximum heat input is calculated based on the rated evaporator mass flow rate:

$$Q_{rated} = \frac{\dot{V}_{max} \cdot \Delta P}{\eta_{motor}\eta_{fan}} = \frac{\dot{m}_{max} \cdot \Delta P}{\rho \eta_{motor}\eta_{fan}}$$

The heat input at part load depends on the part load ratio (PLR) represented by the control function for the evaporator mass flow rate, CF:

$$Q_{actual} = Q_{rated} \cdot PLR^{\frac{3}{0.65}}$$

Parameters		
1	dP	Rated pressure drop over evaporator fans in kPa
2	$\dot{m}_{max}$	Rated evaporator mass flow rate in Kg/hr
3	η_{motor}	motor efficiency
4	η_{fan}	Fan efficiency
5	ρ_{air}	Density of air in Kg/m^3
Input		
1	CF	Control function (controller output)
Output		
1	Q_{fans}	Heat input from evaporator fans in KJ/hr
2	P_{fans}	Evaporator fan power demand in KW
3	$Q_{evap,max}$	Rated evaporator fan heat input in Kj/hr

Type 112/ Type 119 Next day average and maximum temperature

The two types read data from a weather data file and calculate the next day average and maximum temperature. Type 112 reads the data after midnight for the coming day; type 119 reads the data on the day before after 4 p.m. The weather data has to be supplied in a separate data file with a name different from the one used for the TYPE 89 data reader. The file has to be in the TMY format used in TRNSYS. The data for the first hour of the year has to start in the first line.

Parameter		
1	WeatherLU	Logical Unit of the weather data file
Output		
1	T_{avg}	Next day average temperature
2	T_{max}	Next day maximum temperature

Type 113 Possible floating duration

This type calculates the possible floating duration based on the regression coefficients from the floating duration regression analysis.

$FloatDur=C1+C2*T_{depending}$

In a second step, the possible floating duration is centered around a center time and the time of the equipment shut down and when it is operated again is calculated. This floating window calculation is later taken over by type 114/118, which bases the best floating window on the prices.

Parameters		
1	C1	First regression coefficient
2	C2	Second regression coefficient
Input		
1	$T_{depending}$	Temperature the possible floating duration depends on, usually T_{max} of T_{avg} of the next day
2	centertime	Time the floating window should be centered around
Output		
1	houroff	Hour of day the equipment is shut down
2	houron	Hour of day the equipment is operated again
3	timefloat	Possible floating duration

Type 114 Best floating window

This type calculates the best floating window for equipment shutdown based on the possible floating duration and the real-time prices. The possible floating duration is needed as an input and the real-time prices of the coming 24 hours are read from a real-time pricing data file. This data file needs to be in space-delimited format and must have a different name than the real-time pricing data file used for other pricing calculations. The window with the highest integrated real-time price is seen as the best floating window.

Parameter		
1	RTPLU	Logical unit number of real-time pricing data file
Input		
1	timefloat	Possible floating duration
Output		
1	houroff	Time equipment is shut down before floating
2	houron	Time equipment is turned on after floating
3	timefloatint	Integer value of possible duration

TYPE 116 Proportional Controller

The proportional controller compares the set temperature with the actual temperature. If the actual temperature is above the set temperature plus a dead band temperature, the control function γ is set to 1. If the actual temperature is below the set point, the control function is set to 0. For an actual temperature between the set point and set point plus dead band, the control function is calculated: $g = \frac{T_{actual} - T_{set}}{T_{dead}}$

The variable NSTK promotes controller convergence. If during a simulation time step the controller is called more than NSTK times, the controller output is set to the last iteration value.

Parameter		
1	T_{dead}	Dead band temperature width above base set temperature
2	NSTK	Number of iteration calls of the component in one time step before the output is set to the last iteration value
Input		
1	T_{actual}	Tempearture to be compared to the set point
2	T_{set}	Base set point temperature
Output		
1	γ	Control function

Type 118 RTP controller

This RTP controller type is based on the best floating window type 114. The next day pricing data is read after 4 p.m. on the day before. From the RTP data and the possible floating duration, the best floating window is determined. Based on that, the price ratio for the next day is calculated. If the price ratio is less than the critical price ratio, the set point temperature for the next day is kept constant; the outputs T_{high} and T_{low} are both set to T_{cont}.
If the price ratio exceeds the critical price ratio, demand shifting will be performed on the next day. The output T_{high} is set to T_{upper} and T_{low} is set to T_{lower}.

Parameters		
1	RTPLU	Logical unit number of real-time pricing data file
2	ratiocrit	Critical price ratio
3	T_{upper}	Upper set point temperature during floating
4	T_{lower}	Lower set point temperature during precooling
5	T_{cont}	Set point temperature for continuous operation
Input		
1	timefloat	Possible floating duration
Output		
1	houroff	Time equipment is shut down before floating
2	houron	Time equipment is turned on after floating
3	timefloatint	Integer value of possible duration
4	T_{high}	High set point temperature output
5	T_{low}	Low set point temperature output

Type 120 Set temperature profile with reduced precooling duration

This type gives as output a forcing set temperature profile. Three temperatures are needed as input: a low, an intermediate and a high temperature. Furthermore, the starting time for the high set point, the starting time for the intermediate set point and the precooling duration at the low set point have to be specified. The type calculates the set temperature corresponding to the time of the day. The output is the low set point during the precooling duration before the high set point is the output at houroff. At hourcool, the intermediate set point is set.

Input		
1	houroff	Hour of day when equipment is turned of and higher set point is desired
2	hourcool	Hour of day when lower set point is desired
3	T_{high}	High set point temperature
4	T_{low}	Low set point temperature
5	$T_{intermediate}$	Intermediate set point temperature
6	tprecool	Precooling duration in hrs
Output		
1	T_{out}	Set point temperature depending on time of day
2	daytime	Time of day based on simulation time

Appendix C: TRNSYS input file

```
ASSIGN \TRNSYS15\Project\warehousemodel.LST     6
ASSIGN \TRNSYS15\ASHRAE.COF          8
ASSIGN \TRNSYS15\WEATHER\RTP\RTPPGE.txt  19  ! RTP file for TYPE 9 data reader
ASSIGN \TRNSYS15\WEATHER\RTP\RTPPGE.prn    201   ! RTP controller for best window calculation TYPE 118
ASSIGN \TRNSYS15\WEATHER\madisn.wi  20 ! weather data for TYPE 89
ASSIGN \TRNSYS15\WEATHER\Mad2.wi  200  ! weather data for avg temp and max temp calculation TYPE 119
ASSIGN \TRNSYS15\Project\warehousemodel.OUT    27
ASSIGN \TRNSYS15\Project\warehousemodel.ou1    28
ASSIGN \TRNSYS15\Project\warehousemodel.ou3    29
ASSIGN \TRNSYS15\Project\warehousemodel.ou4    75

**************************************************
*                                    *
*            Refrigerated Warehouse          *
*            RTP Simulation                *
*            Ronald Stoeckle 2000          *
*                                    *
**************************************************
*
*
**automatic RTP controller TYPE 117
*
**SIMULATION TIME CORRESPONDS TO REAL TIME, I.E. TIME 1 IS ONE O'CLOCK IN THE MORNING**
*
*
CONSTANTS 4
N=4
STEP=1/(2**N)
Ton=1
Tend=169

EQUATIONS 1 SIMULATION DURATION
simdur=(time+1)-Ton


SIM Ton Tend STEP
```

```
LOOP 19 REPEAT 20
 89   9    16  14  19   88   105     101   5      107   109 110  2 4     33 34 35 36 37
*read read rad set zone dock product infil infild equip fan fan  control psycho

LIMITS 30 60  ! DEFAULT 20 50
WIDTH 72

CONSTANTS 8
weatherLU=20
LoadDes=450  ! 260 tons for unmassive wall, 200 tons for massive wall
Tupper=0
Tlower=-30
Tcont=-19
ratiocrit=2.2
C1=13.375  ! coeffcients for floating time regression
C2=-0.24472

EQUATIONS 9 RTP CONTROLLER
timeoff=[114,1]
timeon=[114,2]
timefloat4=[114,3]
Thigh=[114,4]
Tlow=[114,5]
ratio=[114,13]
Tavg=[112,1]
Tmax=[112,2]
timefloat=[113,3]


*-----------------------

CONSTANTS 16
price=0.04  ! Dollars/kWh
CPAIR=1.005  ! Kj/Kg-C
RHOAIR=1.394  ! Kg/m^3
VOLUME=88368
*m^3, warehouse A+B
CAPACITY=RHOAIR*VOLUME*CPAIR  ! KJ/Kg-K
ZoneArea=9204  ! m^2, 100000 ft^2
DoorArea=65  ! m^2, 5 doors, 14ft*10ft
```

```
height=4.2  ! height of doors, m, 14ft
E=0.933  ! effectiveness of door protection device 0<E<1, doors 4 min/hr open
mdotmax=1700000  ! Kg/hr
*Tvent=-25
dTevapair=3  ! C
Tcore=-24  ! C
dHvapfus=2660  ! Kj/KG enthalpy of evaporization+fusion for water at 0C
dHfreeze=335  ! Kj/KG enthalpy of fusion for water, 144 BTU/lbm
etadef=0.2  ! effciency of defrost, 20 % from Cole (1989)
NSTK=3  ! number of oscialltions in one timestep the controller interates, afterwards it is set to the last iteration value


*------------------------
EQUATIONS 14
*Controlfunction for pump
CF1=[2,1]
*controlfunction, output of controller
Tzone=[19,1]
Tset=[14,1]  ! 14,1 for new forcing function, 14,2 for old
Tvent=Tzone-dTevapair  ! [23,1]
Tdb=[89,5]
Tdbavg=[112,1]
Tdbmax=[112,2]
TTpcorner=[105,2]
TBmcorner=[105,3]
TFtmid=[105,4]  ! temperature in the middle of front
Twb=[33,2]
mdot=CF1*mdotmax   ! Kg/hr
mdotinf=[101,2]  ! Kg/hr
*\dHinf=[101,3]  ! Kj/Kg
RTPprice=[9,2]  ! $/Kwh

EQUATIONS 12 CONDITIONING EQUIPMENT
peakcap=[107,1]  ! tons, max capacity of one compressor
numbercomp=[107,2]  ! number of compressors
Pelecmax=[107,3]  ! KW, maximum power consumption per compressor
Pelec=[107,4]  ! KW, actual power consumption of equipment
MaxCap=[107,5]  ! Maximum available cooling capacity per compressor, KJ/hr
MaxCaptons=MaxCap*7.89827E-5  ! tons
Cap=[107,6]  ! Actual available cooling capacity of refrigeration equipment, KJ/hr
```

```
Captons=Cap*7.89827E-5  ! tons
fractFLC=[107,7]
fractFLP=[107,8]
Tcond=[107,9]
compuse=[107,11]  ! number of compressors in use

*------------------------
CONSTANTS 11 DOCK
Tdset=0
Tdvent=-4.5
Udock=1.99  !  Kj/hr-m^2-C, minimum value from Todd p.7
Capdock=30000  ! Kj/C, not that important as Tdock constant
SurfDock=2332  ! m^2
VolDock=6733  ! m^3
DockArea=1841  ! m^2
DoordArea=200  ! m^2, 30 doors, 9ft*8ft
heightdock=2.75  ! m, 9ft height of dock doors
Edock=0.966  ! eta of Dock doors, 2 min per hour open
mdockmax=200000  ! Kg/hr

EQUATIONS 3 DOCK
Tdock=MAX([88,1],-1)  ! dock temperature, C, not less than 0, heated in winter
CF2=[4,1]
mdvent=CF2*mdockmax  ! Kg/hr

*------------------------
CONSTANTS 14 PRODUCT PROPERTIES
PRODHEIGHT=7.62
HALFWIDTH=3.05
DEPTH=7.62
XMAX=30
YMAX=60
TINIT=-19
TIMESTEP=STEP
Cpprod=1.850  ! Kj/Kg-C
kprod=0.55  ! W/m-C
rhoprod=700  ! Kg/m^3
htop=4.26  ! W/m^2-C
hbottom=4.26  ! W/m^2-C
Tfloor=-17  ! C, from joys finite-differnce model for Tzone=-18
```

```
Rfloor=0.1656  ! m^2-C/W, for 2 cm of wood, 10 cm of air and 0.5 cm of cardboard

*------------------------
EQUATIONS 22 PSYCHOMETRICS

hamb=[33,3]  ! ambient
hzone=[34,3]  ! zone
hvent=[35,3]  ! vent
hdock=[36,3]  ! dock
*enthalpies of air in Kj/Kg

omegaamb=[89,6]
omegazone=[19,2]   ! KgH20/Kgdryair of zone, either real value or limited to saturation value
omegavent=MIN([35,1],omegazone)  ! rhvent set to 95%, but omegazone should not be > omegazone, which would
*mean humidification
omegadock=[88,2]
omegadvent=[37,1]
*humidity ratios of air in KgH20/Kgdryair

! FOR PLOTTING
oamb=omegaamb*10000
ozone=omegazone*10000
ovent=omegavent*10000
odock=omegadock*10000
odvent=omegadvent*10000

rhamb=[89,10]  ! using TYPE 89 data reader
rhzone=[34,6]
rhvent=[35,6]
rhdock=[36,6]
rhdvent=[37,6]
*relative humdities in %

rhozone=MAX([34,4],0.1)   ! to avoid 0 at beginning of sim
rhoamb=MAX([33,4],0.1)
rhodock=MAX([36,4],0.1)
*densities of water-air mixture in Kg/m^3

*------------------------
UNIT 89 TYPE 89 FORMATED DATA READER READ WEATHER DATA
PAR 2
```

```
-1 weatherLU

*------------------------

**RTP DATA IS READ CORRESPONDING TO TIME, I.E. FROM TIME 1 TO TIME 2 THE RTP DATA FOR HOUR 1 IS
*READ FROM THE FILE.**

**(FILE STARTS AT HOUR 0, WHICH IS FROM TIME 0 TO 1)**

UNIT 9 TYPE 9 DATA READER READ RTP DATA

PAR 9

 -1   1    2    1  -2      1    0   19 -1   ! reading starts in hour 1 of data file, not hour 0

*mode skip Ncol dt readcol mult add LU FRMT

*------------------------

UNIT 33 TYPE 33 PSYCHOMETRICS FOR AMBIENT

PAR 4

4 1 1 1

INPUT 2

Tdb omegaamb

20  0.025

*------------------------

UNIT 34 TYPE 33 PSYCHOMETRICS FOR ZONE

PAR 4

4 1 0 1

INPUT 2

Tzone omegazone

-17.5 0.0004  ! output from TYPE 19

*------------------------

UNIT 35 TYPE 33 PSYCHOMETRICS FOR VENT

PAR 4

2 1 0 1

INPUT 2

Tvent rhvent

-22   95  ! rh set to 95%

*------------------------

UNIT 36 TYPE 33 PSYCHOMETRICS FOR DOCK

PAR 4

4 1 0 1

INPUT 2

Tdock omegadock
```

```
0.5   0.0004

*------------------------
UNIT 37 TYPE 33 PSYCHOMETRICS FOR DOCK VENT
PAR 4
2 1 0 1
INPUT 2
Tdvent 0,0
-0.5   95  ! rh set to 95%

*------------------------
UNIT 16 TYPE 16 RADIATION PROCESSOR
PAR 9
4 1 1 1 43.1 4921 0 2 -1   !  IMPORTANT PAR 4: 1=DAY OF YEAR TO START THE SIMULATION, ADJUST!
INP 13
89,4 89,3 89,99 89,100 0,0 0,0 0,0 0,0 0,0 0,0 0,0 0,0 0,0
0. 0. 0. 0. 0.2 90. 0. 90. -90. 90. 180. 90. 90.
*orient walls:  south    east     north    west

*------------------------
UNIT 14 TYPE 102 NEW SET TEMPERATURE PROFILE
INPUT 4
timeoff timeon Thigh Tlow
12      20     Thigh Tlow
*toff   ton    Thigh Tlow

*\UNIT 14 TYPE 120 NEW SET TEMPERATURE PROFILE uses Tintermediate
*\INPUT 6
*\timeoff timeon 0,0   0,0  0,0       0,0
*\12      20     Thigh Tlow -18       6
*\*toff   ton    Thigh Tlow Tintermed tprecool

*------------------------
UNIT 2 TYPE 116 PROPORTIONAL CONTROLLER FOR ZONE
PAR 2
2 NSTK
INPUT 2
TZONE TSET
-17.5 -18
```

```
*------------------------
UNIT 4 TYPE 116 PROPORTIONAL CONTROLLER FOR DOCK
PAR 2
2 NSTK
INPUT 2
Tdock Tdset
1     0

*------------------------
! Still  in use because of convergence problems with unit 104
EQUATIONS 6 CONTROL AND ADJUSTMENT OF MASS FLOW RATE
Capred=CF1*Cap/(CPAIR*(Tzone-Tvent)+dHvapfus*(omegazone-omegavent)+0.0001)  ! reduced cooling capacity
mdotadj1=GT(mdotmax*(CPAIR*(Tzone-Tvent)+dHvapfus*(omegazone-omegavent)), Cap) * Capred
*units: Kg/hr, +0.00001 to avoid division by zero im first run
mdotadj2=LT(mdotmax*(CPAIR*(Tzone-Tvent)+dHvapfus*(omegazone-omegavent)), Cap) * mdot
*units: Kg/hr
mdotadj3=EQL(mdotmax*(CPAIR*(Tzone-Tvent)+dHvapfus*(omegazone-omegavent)), Cap) * mdot
*units: Kg/hr
mdotadj=MAX(MAX(mdotadj1, mdotadj2), mdotadj3)
*units: Kg/hr
mdotadjtons=mdotadj/1000  ! tons/hr
*control strategy: Maximum possible mass flow rate of air if sufficient cooling capacity of
*refrigeration system. If Qcoolmax= (CPAIR*(Tzone-Tvent)+dHvapfus*(omegazone-omegavent)+0.0001) greater than
*cooling capacity=Cap, mass flow rate is reduced to maximum possible cooling capacity

*------------------------
EQUATIONS 11 COOLING LOAD CALCULATION

Qsenstons=mdotadj*CPAIR*(Tzone-Tvent)*7.89827E-5  ! tons
Qlattons=mdotadj*dHvapfus*(omegazone-omegavent)*7.89827E-5  ! tons
Qtotaltons=Qsenstons+Qlattons  ! tons
Qtotal=Qtotaltons*12660.66  ! Kj/hr
Qinf=[101,1]  ! Kj/hr
Qinftons=[101,1]*7.89827E-5  ! tons, infiltration load ASHRAE
Qcondtons=Qtotaltons-Qinftons  ! tons
Qtotalavg=[24,1]/simdur  ! tons, TOTAL AVERAGE LOAD
Qpz=85*[105,1]  ! KJ/hr, 85 pallettes in warehouse, see EES-program
Qpztons=85*[105,1]*7.89827E-5 ! tons, 85 pallettes from EES
Qpztonsavg=[24,3]/simdur  ! tons
```

```
EQUATIONS 8 DOCK LOAD CALCULATION
Qdsenstons=mdvent*CPAIR*(Tdock-Tdvent)*7.89827E-5  ! tons
Qdlattons= mdvent*dHvapfus*(omegadock-omegadvent)*7.89827E-5  ! tons
Qdtottons=Qdsenstons+Qdlattons  ! tons
Qdexinf=[5,1]  ! KJ/hr
Qdexinft=[5,1]*7.89827E-5  ! tons, infiltration load ASHRAE
Qdinf=Qdexinf-Qinf  !  Kj/hr
Qdinftons=Qdexinft-Qinftons  ! tons
Qdloss=Udock*SurfDock*(Tdb-Tdock)  ! Kj/hr, loss thru walls

*----------------------
CONSTANTS 4 FOR CONDITIONING EQUIPMENT
Twbdes=25
Tventdes=-22.5
dTevapref=1.5
dTcond=10

UNIT 107 TYPE 108 CONDITIONING EQUIPMENT
PAR 23
LoadDes Twbdes Tventdes dTevapref dTcond
21.634 3.7262 0.0014765 -1.3623 -0.019687 0.063796
*6 power coeff
279.6 -1.0101 -0.00468 9.5128 0.089808 -0.023317
*6 capacity coeff
21.5733 0.465983 0.00544201 -5.5343e-6 7.40075e-8 -2.43589e-9
*6 part load coeff
INPUT 3
Tvent Twb Qtotal
*\TVENT TWB QTOTAL
-22 11 1266166

*------------------------
EQUATIONS 3 DEFROST LOAD FOR ZONE
Qlatice=mdotadj*dHfreeze*(omegazone-omegavent)  ! KJ/kg, assuming all dehumidfication in the evaporator leads to
*frost
Qdef=(1/etadef)*(1-etadef)*Qlatice  ! (5 times more defrost needed than frost)*(but 20% of this energy is absorbed by
*melting ice)*Qlatice
Qdeftons=Qdef*7.89827E-5  ! tons

*------------------------
CONSTANTS 5 ADDITIONAL LOADS
```

```
Qlights=17.6*ZoneArea  ! Kj/hr, =0.45 W/ft^2
Qlitons=Qlights*7.89827E-5  ! tons
Plights=Qlights/3600  ! KW
Qforks=230000  ! Kj/hr, value from Kyle for 100000 ft^2
Qpeople=28500  ! Kj/hr

EQUATIONS 5
Qfans=[109,1]
Qfanstons=Qfans*7.89827E-5  ! tons
Qfansmax=[109,3]*7.89827E-5  ! tons
Pfanselec=[109,2]
Qadd=Qinf+Qfans+Qdef+Qlights+Qforks+Qpeople  ! ADDTIONAL LOAD ON ZONE in Kj/hr

*------------------------
CONSTANTS 3 ZONE EVAPORATORS
dP=0.125  ! rated pressure drop over evap fans in KPa, 0.5 inH2O
etafan=0.3
etamotor=0.65

UNIT 109 TYPE 109 FAN POWER FOR ZONE
PAR 5
dP mdotmax etafan etamotor rhoair
INPUT 1
CF1
0.2

*------------------------
EQUATIONS 16 CONDITIONING EQUIPMENT FOR DOCK
*uses T in C, curve fit from Vilter Screw compressor data
*VSS-451 High Stage
*assuming same condesing temperature as for zone equipment

*assumed approach temp of evaporator on refrigerant side, dTevapref same than for zone
Tdsst=Tdvent-dTevapref  !
*electric power curve
pdfact1=21.634
pdfact2=3.7262*Tcond
pdfact3=0.0014765*(Tcond^2)
pdfact4=-1.3623*Tdsst
pdfact5=-0.019687*(Tdsst^2)
```

```
pdfact6=+0.063796*Tcond*Tdsst
Pdelmax=pdfact1+pdfact2+pdfact3+pdfact4+pdfact5+pdfact6
*units: KW

*maximun available cooling capacity curve
cdfact1=279.6
cdfact2=-1.0101*Tcond
cdfact3=-0.00468*(Tcond^2)
cdfact4=9.5128*Tdsst
cdfact5=0.089808*(Tdsst^2)
cdfact6=-0.023317*Tcond*Tdsst
MaxdCaptons=cdfact1+cdfact2+cdfact3+cdfact4+cdfact5+cdfact6

*Simplified power consumption model, neglecting part load behavior:
Pdelec=Qdtottons/MaxdCaptons*Pdelmax  ! KW

*------------------------
EQUATIONS 4 DOCK EVAPORATORS
Qdfans=[110,1]
Qdfanstons=Qdfans*7.89827E-5  ! tons
Qdfansmax=[110,3]*7.89827E-5  ! tons
Pdfanselec=[110,2]

UNIT 110 TYPE 109 FAN POWER
PAR 5
dP mdockmax etafan etamotor rhoair
INPUT 1
CF2
0.2

*------------------------
UNIT 105 TYPE 105 PRODUCT FINITE DIFFERNCE MODEL
PAR 7
PRODHEIGHT HALFWIDTH DEPTH XMAX YMAX TINIT TIMESTEP
INPUT 8
TZONE 0,0    0,0   0,0     0,0  0,0     0,0    0,0
-17.5 Cpprod kprod rhoprod htop hbottom Tfloor Rfloor

*------------------------
EQUATIONS 2
```

```
humdgain=mdotinf*(omegadock-omegazone)+mdotadj*(omegavent-omegazone)  ! humidity gain for zone
Qinflat=mdotinf*(omegadock-omegazone)*dHvapfus ! Latent infiltration load for zone, KJ/hr

*------------------------
UNIT 19 TYPE 19 WAREHOUSE
*ZONE
PAR 9
 2    VOLUME 0. 0  0  CAPACITY 8     -18   .0002 !  value for rh=0.9 at -30 C, 1atm
*mode V       K1 K2 K3 Cap       Nsurf Tinit winit

INP 11
 Tdb 0,0  Tvent mdotadj  omegazone humdgain 0,0      0,0 0,0  Qadd 0,0
 15  0    -22   mdotmax  0         0        0       0   0    0.   0.
*Tdb wamb Tvent mdotvent wvent      humdgain Npeople act Qrad Qadd windsp
* WALLS


PAR 41 MASSIVE WALL U=0.046
 1  1   921.1 .7  .8    4     9.578 8   8   6
*No ext A      rho alpha coeff hin    Nob Noc Nod
*h_in=9.578 Kj/hr-m^2-C
*coeff for massive wall, 8b, 8c, 6d
   0.0000001   0.0001494   0.0022773   0.0043866   0.0016935   0.0001356   0.0000019   0.0000000
   8.5241165 -18.1708202  13.0176859  -3.7198770   0.3676971  -0.0101863   0.0000284   0.0000000
  -2.0430372   1.3970983  -0.3775299   0.0345480  -0.0007885   0.0000007
*other 3 walls the same
2 -1 921.1 3 -1 460.5 4 -1 921.1


*\PAR 32 LIGHTWEIGHT WALL U=0.046
*\1 1 921.1 .7 .8 4 9.578 5 5 3
*\*h_in=9.578 Kj/hr-m^2-C
*\*coeff for massive wall, 5b, 5c, 3d
*\   0.0746738   0.4014888   0.1136849   0.0015850   0.0000003
*\   4.6777782  -4.5567904   0.4710865  -0.0006418   0.0000000
*\  -0.3241392   0.0134808  -0.0000051
*\*other 3 walls the same
*\2 -1 921.1 3 -1 460.5 4 -1 921.1
```

```
INP 4
16,7 16,12 16,17 16,22
0. 0. 0. 0.
*ROOF


PAR 32 MASSIVE ROOF U=0.046
 5  1   9204  0.8 0.7   4     9.578 8   8   6
*No ext A     rho alpha coeff hin   Nob Noc Nod
*coeff for massive roof, same as for wall
   0.0000001   0.0001494   0.0022773   0.0043866   0.0016935   0.0001356   0.0000019   0.0000000
   8.5241165 -18.1708202  13.0176859  -3.7198770   0.3676971  -0.0101863   0.0000284   0.0000000
  -2.0430372   1.3970983  -0.3775299   0.0345480  -0.0007885   0.0000007


*\PAR 23 LIGHTWEIGHT ROOF U=0.046
*\5 1 9204 0.8 0.7 4 9.578 5 5 3
*\*coeff for massive roof, same as for wall
*\   0.0746738   0.4014888   0.1136849   0.0015850   0.0000003
*\   4.6777782  -4.5567904   0.4710865  -0.0006418   0.0000000
*\  -0.3241392   0.0134808  -0.0000051


INP 1
16,4
0.
*HEATED FLOOR
PAR 5
 6  4          9290 .7  33.73
*No non-Ashrae A     rho hin
*floor area in m^2, h_inside in Kj/hr-m^2-C
INP 1
0,0
*\250000  ! 20 tons
379820  ! 30 tons
*\0
*units: KJ/hr
*REFRIGERATED PRODUCT
PAR 5
 7  4          17748 .7  15.33
```

```
*No non-Ashrae A      rho hin
*units: area in m^2, h in KJ/hr-m^2-R (0.75 BTU/hr-ft^2-F)
INP 1
Qpz
*\Qpztot
*\0,0
0

*INTERIOR WALL B TO DOCK
PAR 26
 8  3   450.5 .7  .8     4     9.578 6   6   4
*No int A     rho alpaha coeff hin   Nob Noc Nod
*h_in=9.578 Kj/hr-m^2-C
*coeff for wallB, 6b, 6c, 4d
   0.0028776   0.0828556   0.1075742   0.0151226   0.0001932   0.0000001
   4.5339980  -6.2018962   1.9650815  -0.0887716   0.0002116   0.0000000
  -0.7118529   0.0961851  -0.0022979   0.0000026
INPUTS 3
Tdock Tdock 0,0
0.0 0.0 0.0

* VIEW FACTORS
PAR 1
0
*OPTIONAL OUTPUT PARAMETERS
PAR 15 Qconv FOR 5 WALLS, ROOF AND FLOOR AND COMMOM WALL WITH DOCK
7
4 1 !Wall1
4 2 !Wall2
4 3 !Wall3
4 4 !Wall4
4 5 !Roof
4 6 !Floor
4 8 !dockwall

*INFILTRATION CONSTANTS FOR MODIFIED TYPE19 FROM DAVE BRADLEY, NOT IN USE
INPUTS 3
*k1 k2  k3
0,0 0,0 0,0
0.0 0.0 0.0
```

```
EQUATIONS 2 Qconv from surfaces
Qdcom=-[19,17]  ! Kj/hr, heat flow to dock from zone thru common wall
Qdcomtons=-[19,17]*7.89827E-5 ! tons

*------------------------
UNIT 101 TYPE 101 INFILTRATION LOAD ZONE
PAR 3
DoorArea height E
INPUT 4
hdock hzone rhodock rhozone
273   255   1       1.1
*output: 1 Qinf, 2 mdotinf, 3 dHinf

*------------------------
EQUATIONS 3 HUMIDITY GAIN FOR DOCK
mdinf=[5,2]  ! Kg/hr
dhumdgain=mdinf*(omegaamb-omegadock)+mdotinf*(omegazone-omegadock)+mdvent*(omegadvent-omegadock)  !
*Kg/hr, gains from exterior+zone
Qdinflat=(mdinf*(omegaamb-omegadock)+mdotinf*(omegazone-omegadock))*dHvapfus  ! lat infiltration load on dock,
*Kj/hr

*------------------------
CONSTANTS 3 ADDITIONAL DOCK LOADS
Qdlights=97*DockArea  ! Kj/hr, =2.5 W/ft^2
Qdlitons=Qdlights*7.89827E-5  ! tons
Pdlights=Qdlights/3600  ! KW

EQUATIONS 2
Qdadd=Qdcom+Qdinf+Qdfans+Qdlights
Qdaddtons=Qdadd*7.89827E-5  ! tons

UNIT 88 TYPE 88 DOCK
PAR 10
Udock CapDock CPAIR RHOAIR SurfDock VolDock 1     0     0.004 2500
*U    Cap     cp    rho    A        V        wmult Tinit winti hfg
INP 10
Tdvent  omegadock mdvent Tdb omegaamb 0,0  0,0     Qdadd  0,0     dhumdgain
-0.5    0.0004    5000   10  0.007    0    0       0      0       0
*Tdvent wdvent    mdvent Tdb wamb     minf Qlights Qequip Qpeople wgain
```

```
*-----------------------
UNIT 5 TYPE 101 INFILTRATION LOAD DOCK
PAR 3
DoorDArea heightdock Edock
INPUT 4
hamb hdock rhoamb rhodock
280  273   1      1.1
*output: 1 Qinf, 2 mdotinf, 3 dHinf

*-----------------------
EQUATIONS 8 ELECTRICITY DEMAND
Ptotelec=Pelec+Pfanselec+Plights
Ptotavg=[24,4]/simdur  ! KW
Cost=Ptotelec*RTPprice  ! Dollars/hour
Pdtotelec=Pdelec+Pdfanselec+Pdlights
Pdelavg=[24,11]/simdur
dcost=Pdtotelec*RTPprice  ! Dollars/hour
totCost=Cost+dCost  ! Dollars/hour
Pelwrhse=Ptotelec+Pdtotelec  ! total power consumption od warehouse

*-----------------------
EQUATIONS 3 COP
COP=Qtotaltons*3.513725/(Pelec+0.0000001)*100  ! %, avoid division by 0 in first run, for dock
COPavg=Qtotalavg*3.513725/(Ptotavg+0.000001)*100  ! %, convert tons into KW
COPtot=(Qtotaltons+Qdtottons)*3.513725/(Pelec+Pdelec+0.000001)*100  ! %, total COP for warehouse

*-----------------------
UNIT 24 TYPE 24 QUANTITY INTEGRATOR
*integrates over whole period
INPUT 14
Qtotaltons Qinftons Qpztons Ptotelec cost Qsenstons Qlattons
Qdtottons Qdsenstons Qdlattons Pdtotelec dcost totCost Qdeftons
0          0       0       0       0   0         0
0         0          0         0         0     0       0
*units: tonhours tonhours tonhours tonhours kwh dollars tonhours
*tonhours tonhours tonhours tonhours kwh dollars dollars tonhours

*-----------------------
UNIT 28 TYPE 24 QUANTITY INTEGRATOR
*integrates over 24hrs
```

```
PAR 1
24
INPUT 20
*Cooling Load                                          *Gains: *Freezer
Qsenstons Qlattons Qdsenstons Qdlattons Qlights Qpeople Qforks Qfans Qdef Qinf Qinflat 19,3
*Dock                                                   **Electric
Qdlights Qdfans Qdexinf Qdinflat Qdloss    Ptotelec Pdtotelec Pelwrhse
0 0 0 0 0 0 0 0 0 0 0 0 0 0 0 0 0 0 0 0

UNIT 72 TYPE 25 PRINT DAILY LOAD SUMMARY
PAR 4
24 Ton Tend 27 !out
INPUT 20
28,1     28,2     28,3      28,4     28,5    28,6    28,7    28,8  28,9 28,10 28,11   28,12
28,13    28,14  28,15   28,16    28,17     28,18    28,19     28,20
Qsenstons Qlattons Qdsenstons Qdlattons Qlights Qpeople Qforks  Qfans Qdef Qinf  Qinflat Qtrans
Qdlights Qdfans Qdexinf Qdinflat Qdloss    Wtotelec Wdtotelec Welwrhse

*------------------------
UNIT 26 TYPE 24 QUANTITY INTEGRATOR
*integrates over every hour
PAR 1
1
INPUT 5
Qtotaltons cost dcost totCost Pelwrhse
0         0    0     0       0
*units: tonhours dollars dollars dollars kwh

*------------------------
UNIT 112 TYPE 119 AVERAGE AND MAX TEMPERATURE
PAR 1
200
*weatherLU
*----------------------
UNIT 113 TYPE 113 POSSIBLE FLOATING TIME
PAR 2
C1 C2
INP 2
Tavg 0,0
0    16
```

```
*Tdep centertime

*----------------------
UNIT 114 TYPE 118 BEST WINDOW
PAR 5
201    ratiocrit Tupper Tlower Tcont
*RTPLU ratiocrit Tupper Tlower Tcont
INP 1
timefloat
5

*------------------------
UNIT 55 TYPE 55 7th DAY PERIODIC INTEGRATOR
PAR 42
1 0 24 24 24 1 8760
2 0 24 24 24 1 8760
3 0 24 24 24 1 8760
4 0 1  1  1  1 8760
5 0 1  1  1  1 8760
6 0 1  1  1  1 8760

INPUT 6
Ttpcorner Tftmid totcost COP COPtot Tzone
0         0   0             0   0      0


UNIT 30 TYPE 25 PRINT PERIODIC RESULTS
PAR 4
24 0 Tend 75 !ou4
INPUT 5
Tavg Tmax 55,9   55,19  55,21
Tavg Tmax Ttpmax Tftmax totcost

*------------------------
UNIT 25 TYPE 25
PAR 4
1 Ton Tend 28 !ou1
INPUT 6
Tdb 55,53    26,5     55,33    55,43       ratio
Tdb Tzoneavg Welwrhse COPavghr COPtotavghr ratio
```

```
*-----------------------
UNIT 65 TYPE 65 ONLINE
PARAMETERS 10
  9 10 -40 40 -100  250   1  20    0 -1
INPUTS 19
Tdb Twb Tzone Tset Tvent Tdock RTPprice numbercomp compuse
 Qtotaltons Captons MaxCaptons Ptotelec Pdtotelec Qfanstons Qfansmax Qdeftons Qlitons mdotadjtons
Tdb Twb Tzone Tset Tvent Tdock RTPprice numbercomp compuse
 Qtotaltons Captons MaxCaptons Ptotelec Pdtotelec Qfanstons Qfansmax Qdeftons Qlitons mdotadjtons
LABELS 5
C MJ/hr
Out, Zone and Set Temperature, CF
Cooling Load, mass flow in tons
EQUIPMENT

UNIT 66 TYPE 65 ONLINE
PARAMETERS 10
  5 5 -0.1 1.1 -100 250   1  20    0 -1
INPUTS 10
Tdb Tzone Tset Tdock CF1 Qinftons Qsenstons Qlattons Qpztons Qpztonsavg
Tdb Tzone Tset Tdock CF1 Qinftons Qsenstons Qlattons Qpztons Qpztonsavg
LABELS 5
C tons
temperature
Cooling Load
ZONE

UNIT 67 TYPE 65 ONLINE
PARAMETERS 10
  5 8 -40 40  -100  250   1  20    0 -1
INPUTS 13
Tdb Tzone Tset Tdock CF2 Qdtottons Qinftons Qdexinft Qdinftons Qdfanstons Qdfansmax Qdlitons Qdaddtons
Tdb Tzone Tset Tdock CF2 Qdtottons Qinftons Qdexinft Qdinftons Qdfanstons Qdfansmax Qdlitons Qdaddtons
LABELS 5
C tons
temperature
Cooling Load
DOCK
```

UNIT 68 TYPE 65 ONLINE

PARAMETERS 10

5 10 -40 40 0 100 1 20 0 -1

INPUTS 15

oamb ozone ovent odock odvent omegazone omegavent omegadock omegadvent omegaamb rhamb rhzone rhvent rhdock rhdvent

oamb ozone ovent odock odvent omegezone omegavent omegadock omegadvent omegaamb rhamb rhzone rhvent rhdock rhdvent

LABELS 5

C tons

temperature

Cooling Load

PSYCHOMETRICS

UNIT 69 TYPE 65 ONLINE

PARAMETERS 10

6 2 -40 40 -100 100 1 20 0 -1

INPUTS 8

Tdb Tzone Tset TTpcorner TBmcorner TFtmid Qpztons Qpztonsavg

Tdb Tzone Tset TTpcorner TBmcorner TFtmid Qpztons Qpztonsavg

LABELS 5

C tons

temperature

Cooling Load

PRODUCT

END

References

(1990). ASHRAE Handbook Refrigeration. Atlanta, GA, ASHRAE.

(1993). ASHRAE Handbook fundamentals. Atlanta, GA, ASHRAE.

(1998). ASHRAE Handbook Refrigeration. Atlanta, GA, ASHRAE.

Altwies, J. (1998). Electrical Demand Reduction in Refrigerated Warehouses. Solar Energy Laboratory. Madison, WI, University of Wisconsin-Madison.

Braun, J., N. Chaturvedi, et al. (2000). Implementation of thermal storage in building mass. W. Lafayette, IN, Purdue University.

Brownell, K. A. (1998). Investigation of field performance of industrial refrigeration systems. Solar Energy Laboratory. Madison, WI, University of Wisconsin-Madison.

Cleland, A. C. (1990). Food refrigeration processes: analysis, design and simulation. London, New York, Elsevier Applied Science.

Dellino, C. V. J. (1997). Cold an Chilled Storage Technology. London, New York, Blackie Academic & Professional.

Downing, C. C. and W. A. Meffert (1993). "Effectiveness of cold-storage door infiltration protective devices." ASHRAE transactions **99 part 2**: 356-366.

EPRI (1995). Real-time pricing quick start guide. Palo Alto, CA, Electric Power Reasearch Institute.

Gabel, S. D., L. Carmichael, et al. (1998). Automated Controls in Response to Real-Time Pricing. ASHRAE Journal **40**(11): 26-29.

Henze, G. P., R. H. Dodier, et al. (1997). "Development of a predictive optimal controller for thermal energy storage systems." HVAC&R Research **3**(3): 233-264.

Hoffmann, S. and R. Renner (1997). "Taking Advantage of Real-Time Pricing." EPRI Journal **22**(2): 16-23.

Incropera, F. P. and D. P. DeWitt (1996). Introduction to Heat Transfer, 3rd edition.

Jekel, T. B. and D. T. Reindl (2000). Energy Efficiency Opportunities at Supervalu. Madison, WI, University of Wisconsin, HVAC&R Center.

Klein, S. A. and F. L. Alvarado (2000). Engineering Equation Solver. Middleton, WI, F-Chart Software.

Lovatt, S. J., P. Q. T., et al. (1993). "New method of predicting the time-variability of product heat load during food cooling - Part 1: Theoretical considerations." Journal of Food Engineering **18**(1): 13-36.

Lovatt, S. J., P. Q. T., et al. (1993). "New method of predicting the time-variability of product heat load during food cooling - Part 2: Experimental testing." Journal of Food Engineering **18**(1): 37-62.

Manske, K. A. (1999). Performance optimization of industrial refrigeration systems. Solar Energy Laboratory. Madison, WI, University of Wisconsin.

Mitalas, G. P. and J. G. Arsenault (1970). Fortran IV program to calculate z-transfer functions for the calculation of transient heat transfer through walls and roofs.

Mitalas, G. P. and D. G. Stephenson (1967). "Room Thermal Response Factors." ASHRAE Transactions **73, part 1**: III 2.1 - III 2.10.

Pawelski, M. J. (1976). Development of Transfer Function Models and their use in modeling the CSU Solar House 1. Solar Energy Laboratory. Madison, WI, University of Wisconsin-Madison.

Popper, K. R. (1959). The logic of scientific discovery. London, Hutchinson.

Rao, M. A. and S. S. H. Rizvi Engineering properties of foods.

Sanz, P. D. and M. D. Alonso (1986). "Time-Temperature Prediction Curves of food stuffs by means of the z-transfer function method." International Journal of Refrigeration **9**: 92-98.

Seem, J. E. (1987). Modeling of Heat Transfer in Buildings. Solar Energy Laboratory. Madison, University of Wisconsin.

SEL (2000). TRNSYS - A transient system simulation program. Madison, WI, Solar Energy Laboratory.

Stephenson, D. G. and G. P. Mitalas (1967). "Calculation of Heat Conduction Transfer Functions for Multi-Layer Slabs." ASHRAE Transactions **78**: 117-126.

Stephenson, D. G. and G. P. Mitalas (1967). "Cooling Load Calculations by Thermal Response Factor Method." ASHRAE Transactions **73, part 1**: III 1.1 - III 1.7.

USDA (2000). Capacity of Refrigerated Warehouses, 1999 Summary, United States Department of Agriculture.